STRUCTURAL RESPONSE OF PRESTRESSED CONCRETE MEMBERS SUBJECTED TO ELEVATED TEMPERATURES

By

WILLIAM J. MBWAMBO

A DISSERTATION PRESENTED TO THE GRADUATE SCHOOL
OF THE UNIVERSITY OF FLORIDA IN PARTIAL FULFILLMENT
OF THE REQUIREMENTS FOR THE DEGREE OF
DOCTOR OF PHILOSOPHY

UNIVERSITY OF FLORIDA

1995

ACKNOWLEDGMENTS

The author expresses sincere appreciations to his advisor and committee chairman, Dr. Fagundo F.E, for devoting much patience and guidance throughout the course of this study. He also give thanks to Dr. Hoit M.I., Dr. Cook R.A., Dr. Tia M. and Dr. Chang W. for their help in various ways and for serving as members of his committee.

The author also acknowledges the help and services of Prof.Thompson P.Y., Chairman of the CE Department, UF, and Mrs. Micha M., Asst. Director, International Student Services, UF, during the critical times of his studies.

He also expresses deepest gratitude to his wife Stella and his son John for their understanding, patience and encouragement during the whole period of the study.

The author was awarded a scholarship to study in the United States by the University of Dar es Salaam through the German Academic Exchange Services (GTZ).

TABLE OF CONTENTS

page

ACKNOWLEDGMENTS ii

ABSTRACT vi

CHAPTERS

1 INTRODUCTION 1

1.1. General Remarks 1
1.2. The Problem 1
1.3. Research Objectives 3
1.4. Scope of the Study 4
1.5. Problems and Solution Schemes 5
1.5.1. Problem environment 5
1.5.2. Solution Strategy 8
1.6. Previous Research. 12
1.6.1. Material Property Behavior. . . . 13
1.6.2. Structural Response-Experimental 17
1.6.3. Structural Response-Numerical . . 18

2 THERMAL ANALYSIS 22

2.1. Introduction 22
2.2. Heat Transfer Models 22
2.2.1. Heat Flow Models 22
2.2.2. Finite Element Formulations . . . 24
2.2.3. Matrix Equations 25
2.2.4. Time Integration of Temperature . 28
2.3. Evaluation of Thermal Matrices and Load Vector 30
2.3.1. Interpolation Functions 31
2.3.2. Conductivity Matrix 31
2.3.3. Thermal Capacitance Matrix . . . 32
2.3.4. Thermal Load Vector 33
2.4. Solution Algorithm 33

3 MODELING OF TEMPERATURE DEPENDENT MATERIAL PROPERTIES 35

3.1. Introduction 35

3.2. Modeling Procedures 35
3.3. Concrete 37
3.3.1. Thermal Properties 37
3.3.2. Mechanical Properties 40
3.3.3. Deformation Properties 44
3.4. Prestressing Steel 48
3.4.1. Mechanical Properties 48
3.4.2. Deformation Properties 49
3.5. Remarks 53

4 MODELING OF PRESTRESSED CONCRETE FRAME MEMBER 54

4.1. Introduction 54
4.2. Basic Finite Element Equations for a 2D Beam Element 54
4.3. Evaluation of Displacement Functions for a Beam Element . . . 57
4.4. Idealization of a Prestressed Concrete Member 59
4.5. Evaluation of Element Stiffness Matrix . 61
4.6. Incremental Strains in Concrete and Prestressing Steel 64
4.6.1. Concrete Deformations 64
4.6.2. Prestressing Steel Strains . . . 67
4.7. Load Vector due to Prestress Force . . . 67
4.8. Remarks 69

5 SOLUTION METHOD FOR STRUCTURAL RESPONSE . . . 70

5.1. Introduction 70
5.2. Induction Forces 71
5.2.1. Thermal and shrinkage strain . . 71
5.2.2. Strength degradation 72
5.2.3. Shift in stress 73
5.3. Effective Prestress Action 74
5.4. Evaluation of Action Load Vector 76
5.5. Solution of Displacement Response . . . 77
5.7. Local and Global Values 82
5.8. Computation of Moment Capacity Response 84

6 COMPUTER IMPLEMENTATION 85

6.1. Introduction 85
6.2. Main Program PRECET 85
6.3. Program TEDIAN 85
6.4. Program STREAN 85
6.5. Program MAPRAN 85

7 NUMERICAL ANALYSIS 92

7.1. Introduction 92
7.2. Analysis of Prestressed Concrete Beams . 92

7.2.1. Description of Test Specimen . . 92
7.2.2. Beam Testing 93
7.2.3. Design Details 95
7.2.4. Numerical Model 96
7.2.5. Numerical and Test Result 97
7.3. Prestressed Concrete Slabs 108
7.3.1. Description of Test Specimen . . 108
7.3.2. Material Specifications 111
7.3.3. Testing Procedures 111
7.3.4. Finite Element Model 112
7.3.5. Comparison of Numerical and Test Result 112
7.4. Evaluation of Influences of Material Properties 119
7.4.1. Effect of Thermal Properties on Temperature Distribution . . . 120
7.4.2. Effect of other Material Properties on Deflection . . . 122
7.4.3. Effect of Thermal Properties on Structural Response 124
7.5. Method of Estimating Fire Endurance of Beams 126
7.5.1. Effects of Exposure Conditions . 126
7.5.2. Specimen for Analysis 126
7.5.3. The Analysis Procedure and Results 127

8 SUMMARY AND CONCLUSIONS 134

8.1. Summary 134
8.2. Conclusions 136
8.3. Recommendations 138

REFERENCES 139

APPENDICES

A INSTRUCTIONS FOR THE PREPARATION OF THE INPUT DATA FILE FOR THE PRECET PROGRAM 144

B EXAMPLE OF INPUT DATA FILE 152

BIOGRAPHICAL SKETCH 161

Abstract of Dissertation Presented to the Graduate School of the University of Florida in Partial Fulfillment of the Requirements for the Degree of Doctor of Philosophy

STRUCTURAL RESPONSE OF PRESTRESSED CONCRETE MEMBERS SUBJECTED TO ELEVATED TEMPERATURES

By

William J. Mbwambo

May, 1995

Chairperson: Fernando E. Fagundo
Major Department: Civil Engineering

A numerical procedure is developed for the nonlinear analysis of the structural response of prestressed concrete members subjected to fire. The fire environment is simulated by the time-temperature relationship of the standard fire test (SFT). The procedure computes temperature distributions, mid-span deflection and moment capacity of a member supporting its design service loads throughout the simulated fire exposure period.

The formulation of the numerical model and the solution of the equilibrium equations is based on the displacement finite element method. The member cross section is idealized into triangular elements for temperature distribution analysis and for evaluation of variation in material properties within the section. Beam elements are used to model the member for both deflection and moment

capacity analysis. The transient heat transfer mechanisms of the SFT is modeled by dividing the time scale into discrete number of time steps. At each time step equilibrium equations are set and solved iteratively for temperature distribution and structural response. Incremental deflections within a time step are added cumulatively to determine the total deflection at the end of each time step.

A series of numerical analyses of prestressed concrete beams and slabs, and the evaluation of the influences of temperature-dependent properties of concrete and steel on temperature distribution, deflection and moment capacity is presented. Numerical results show good agreement with corresponding test results. Temperature distribution is more sensitive to thermal capacity properties for normal weight concretes and to thermal conductivity properties for lightweight concretes. Deflection is mostly influenced by the effects of temperature on the relaxation properties of prestressing steel. Thermal properties of concrete influence both the deflection and moment capacity.

Graphs for predicting fire endurance of prestressed concrete beams exposed to fire have been developed both for normal and lightweight concretes.

CHAPTER 1
INTRODUCTION

1.1. General Remarks

The determination of the behavior of prestressed concrete members subjected to high temperatures has been mostly experimental. The experiments are based on the standard fire tests (SFT). In the United States the SFT procedures are defined by ASTM E-119 [1]. Results from the standard fire tests have been used to develop numerical procedures for fire safety designs.

1.2. The Problem

The main objective of the Standard Fire Test (SFT) is to predict the fire endurance of building components. The parameters measured during the test of prestressed concrete members are temperature distribution within the member, and the mid-span deflection of the member [2,3]. The variables considered are concrete cover and type of concretes. These variables affect the temperature distribution within a member.

Numerical methods developed for fire safety design of prestressed concrete also estimate the fire endurance time. The parameter used is the moment capacity [3,4,5]. The

retained moment capacity is taken as a function of the temperature-dependent tensile strength of prestressing steel. The temperature of steel is derived from temperature distribution curves for a given exposure period and concrete cover. However, since beams are exposed to fire on three sides, these curves do not give a good estimate of temperature of steel in beams [3]. The variables considered are the same as those of fire tests.

Many studies show that almost all the physical and mechanical properties of concrete and prestressing steel undergo considerable changes at high temperatures [6,7,8,9,10]. The procedures of the standard fire test does allow for the evaluation of the influence of these properties in the measured temperature and deflection behavior. A similar problem is experienced with the existing numerical fire design methods.

The fire tests are not designed to measure changes in moment capacity. On the other hand, the numerical methods are not developed for predicting changes in member deflection.

Based on these observations, it is paramount to develop a method that will address all the above short comings. The procedures should be comprehensive enough to incorporate the changes in properties of concrete and steel, and predict the history of temperature distribution, member deflection, and moment capacity.

1.3. Research Objectives

The objectives of this study are as follows:

1. Develop a numerical procedure for determining temperature distribution and structural response of prestressed concrete members exposed to fires. The procedure will incorporate the nonlinearity of temperature-dependent material properties of concrete and prestressing steel.

2. Use the procedure developed in (1) to evaluate the degree of influence of temperature-dependent properties of concrete and prestressing steel on the computed temperature distribution, and the structural response.

The histories of structure deformation and strength capacity are considered as main functions for defining structure response. The numerical model developed will evaluate these parameters for a prestressed concrete structure exposed to a simulated fire environment, while supporting its designed service load.

The resulting model could be used to

(a) estimate temperature distribution and deformation status of a loaded prestressed concrete member exposed to fire. This application will reduce dependence on experiments,

(b) evaluate strength status of a prestressed concrete member after a prolonged exposure to fire and

(c) show influence of temperature-dependent material properties of concrete and prestress steel on temperature distribution and structural behaviors.

1.4. Scope of the Study

The temperature-dependent material properties considered in this study are

(a) compressive and tensile strength of concrete,

(b) stress-strain relationship of both concrete and prestressing steel,

(c) tensile strength of prestressing steel,

(d) thermal strain of concrete and steel,

(e) shrinkage strain of concrete and

(f) accelerated relaxation of prestressing steel.

Concrete members are analyzed on the assumption that the moisture content is within the equilibrium relative humidity of 70 percent or less. This state simulates the common conditions attained in service [11].

The fire environment for the numerical model is simulated by the time-temperature relationship defined for the SFT. The imposed service load is assumed to be constant during exposure to fire.

Mathematical models of temperature-material property relationships are derived from temperature test results published in the literature.

The types of construction materials considered are normal weight (silicon aggregate and carbonate aggregate) and lightweight (expanded shale) concretes and cold drawn prestressing steel (wire or tendon).

1.5. Problems and Solution Schemes

1.5.1. Problem Environment

The problem involves both temperature distribution and structure response analyses. The main components of analysis are

(a) temperature distribution within a member,

(b) temperature-dependent structural displacements and

(c) temperature-dependent moment capacity.

1.5.1.1. Temperature distribution problem

The temperature distribution problem is defined graphically in Fig. 1.1. Exposure conditions for a typical beam element are shown in (a). The problem is to find the temperature distribution function T(t) under the transient heat transfer condition of the SFT shown in (b).

Heat is transferred from the source to the element's exposed surfaces and then distributed within the element. Heat transfer modes involved are

(a) radiation and convection ($Q_{hc,hr}$): from heat source to the exposed surfaces of an element and

(b) conduction ($Q_{k,\rho c}$): within the element.

The quantity and rate of heat transferred has the following dependencies:

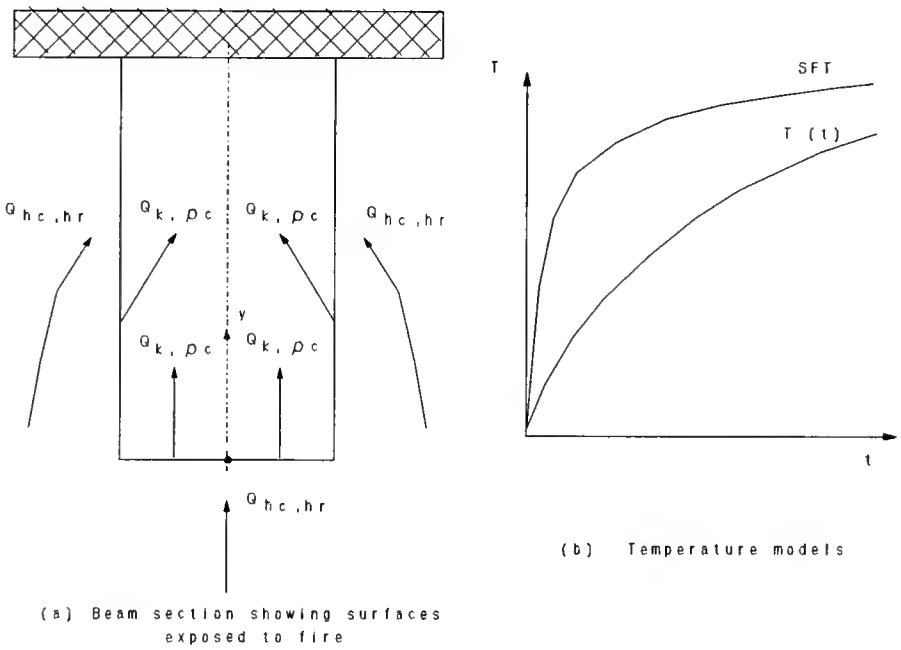

Fig. 1.1. Temperature distribution problem environment

(a) $Q_{hc,hr}$ is a function of heat transfer coefficients of convection (h_c) and radiation (h_r).

(b) $Q_{k,\rho c}$ is a function of thermal conductivity (k) and thermal capacity (ρc). Higher k and lower ρc values result in higher temperatures for a given heat transferred.

The above variables and their interrelation have to be computed continuously in the process of solving for the

temperature distribution. Detailed procedures for the solution of temperature distribution are discussed in Chapter 2.

1.5.1.2. Structure response problem

Fig.1.2 (a) depicts the typical system configuration to be analyzed for structural response. The system is under constant service load. However, due to effect of temperature on material properties, there is a continuous redistribution of internal stresses within an element. The core of the problem is the determination of changes in the internal load function F, and the response function r, under the constant load function L, as shown in Fig.1.2 (b).

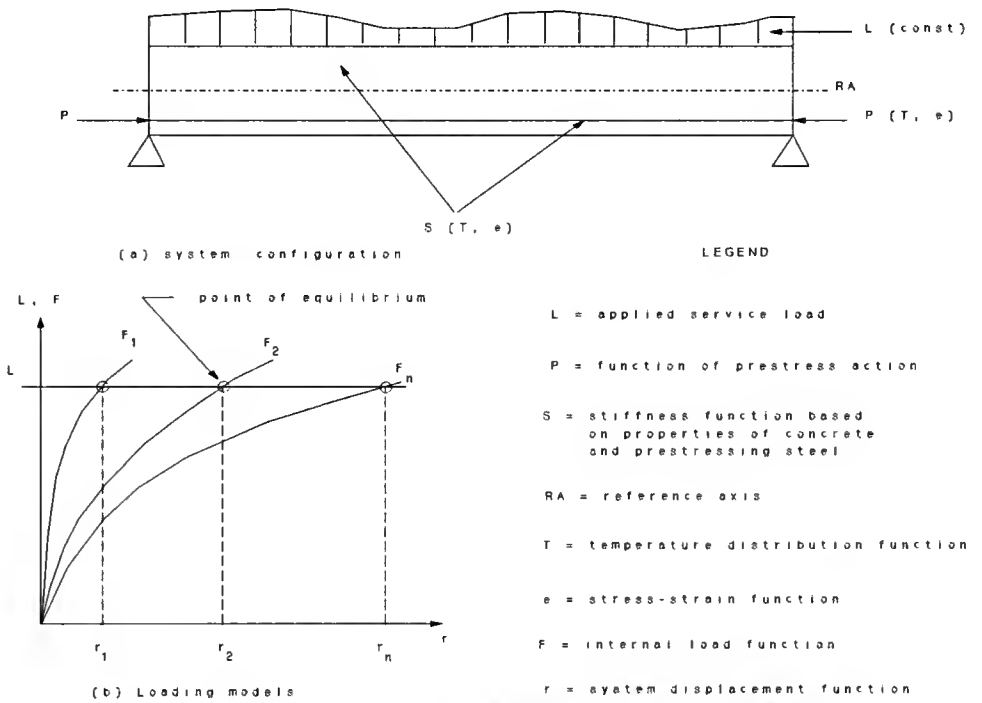

Fig. 1.2. Structural system configuration

The hypothetical characteristics of the main parametric functions of the analysis are illustrated qualitatively in Fig.1.3. Fig.1.3 (a) shows the decline in effective prestress action with exposure time due to effects shown in Fig.1.3 (b), and Fig.1.3 (c) shows variations of stiffness parameter S and displacement r, as temperature T increases. The procedure for evaluating these parameters is discussed in detail in Chapters 4 and 5.

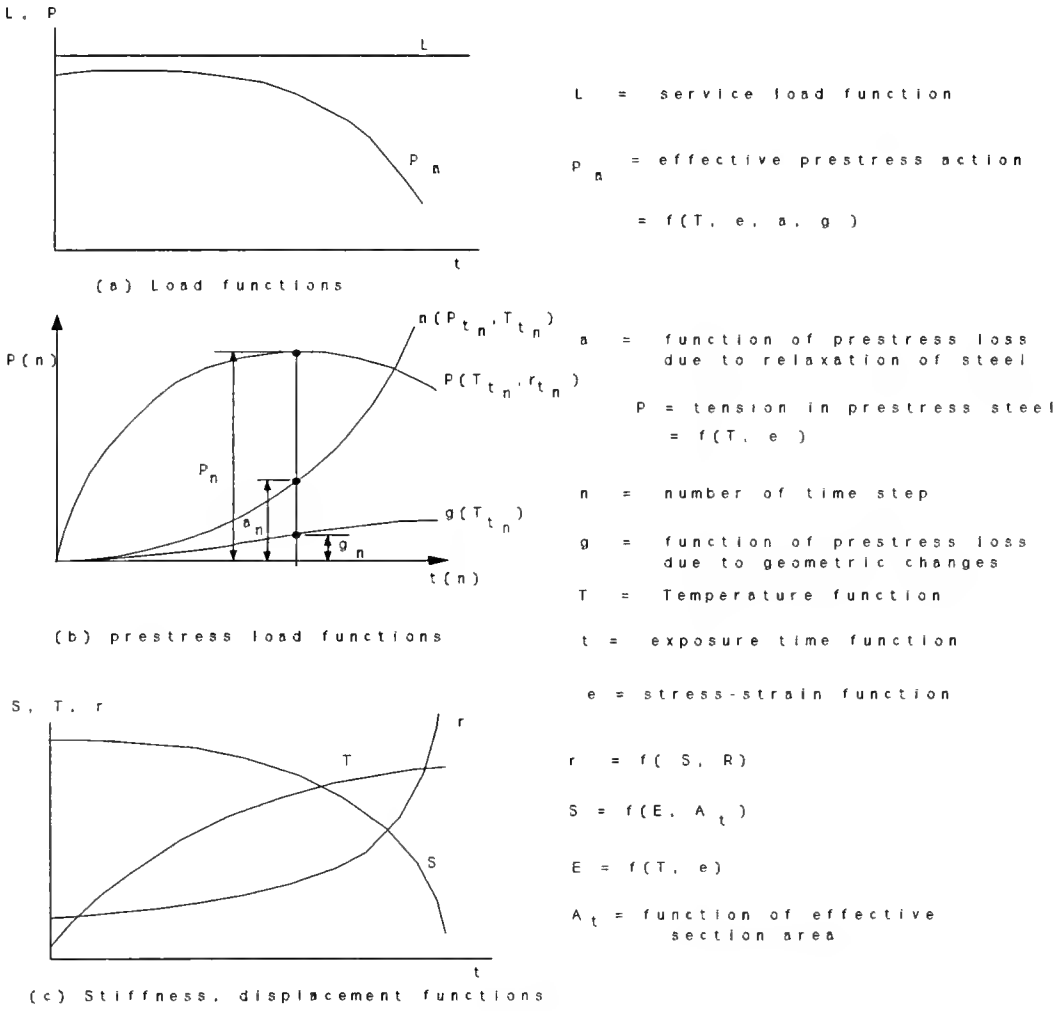

Fig. 1.3. Loading, stiffness, and deformation behavior

1.5.2. Solution Strategy

The entire problem involves both temperature distribution and structure response analysis. The problem is formulated and solved using standard finite element techniques. The techniques are then implemented in computer programs.

The prestressed concrete member is idealized into finite beam elements for structural response analysis. The cross section of each beam element is modeled into triangular sub-elements. The cross section model is utilized for temperature distribution analysis, evaluation of the variation of material properties across the section and for summation of the overall cross section properties. This approach is illustrated graphically in Fig. 1.4.

The time-temperature relation of the SFT is divided into a number of thermal time segment. The time boundaries of the segment are called time step points. Solutions of equilibrium equations are performed at these time steps for both temperature distribution and structure response.

The solution process begins with solution of the temperature distribution problem. Obtained temperature values are used to compute active material properties for each concrete sub-element and prestressing steel segments, of the beam element section. Based on the variation of temperature across the section and the temperature-material

properties relationship, each concrete sub-element and steel segment may have different set of properties.

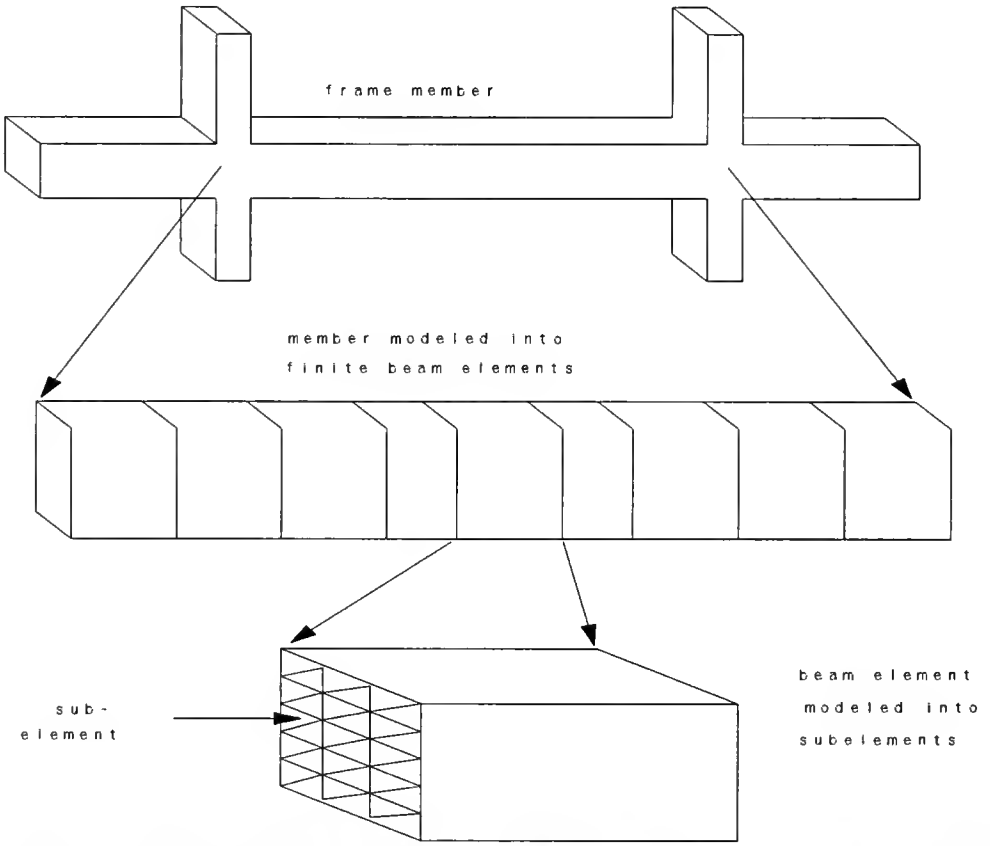

Fig. 1.4. Finite element idealization for temperature and structure response analysis

The stiffness parameters of concrete sub-elements and steel segments are integrated across the cross section of each beam element to determine the overall element stiffness characteristics. The strength parameters of the prestressing steel are added across the section to determine

the overall effective prestressing effect on each beam section. The computed functions for each beam element are assembled to configure the structure model. The solution process is then continued to solve for structure response.

The whole procedure is implemented in a computer program named PRECET (PRestressed Concrete at Elevated Temperature). The program consists of the following sub-programs:

(a) TEDIAN (TEmperature DIstribution ANalysis),

(b) STREAN (STructure REsponse ANalysis) and

(b) MAPRAN (MAterial PRoperty ANalysis).

Discussion on the development of the computer implementation is presented in Chapter 6. The program is used to run a number of examples which have been tested in laboratories according to Standard Fire Tests (SFT). The numerical procedure developed in this study is validated by comparing the test results with numerical results. The example problems investigated and the comparison of results, are presented in Chapter 7.

1.6. Previous Research

Much of the previous research related to structural response of prestressed concrete members subjected to building fires have been devoted to studying the effects of high temperature on the properties of concretes and steels used in prestressed concrete structures and in determining

the temperatures within a concrete member during the laboratory standard fire tests [3,5].

Behavior of concrete and prestressing steel under varying temperatures have been studied extensively [5]. Results from these studies show common qualitative behaviors, though may differ quantitatively depending on the nature of materials used and the testing procedures. This section presents a summary of findings from some of these studies. More information regarding material properties behavior will be given in Chapter 3.

1.6.1. Material Property Behavior.

1.6.1.1. Tensile strength of prestressing steel

Day et al. [3], Abram et al. [1] and Podolny [10] have studied the effect of temperature on the tensile strength of prestressing steel. Results show that the strength of prestressing steel decreases by more than 50% at 800 °F. At 1200°F the strength is down to 5% of its original value.

1.6.1.2. Loss of prestress force

Abram and Cruz [1] observed that loss of prestressing amounted to 15% at 600 °F, 23% at 700 °F and between 70% and 80% at 1000 °F, depending on the initial prestressing force. Only about 12% of the loss at temperatures above 700 °F is recovered on cooling. The test was performed on bare wire, that is, not embedded in concrete. The report from the study did not isolate the parameters that caused the losses.

1.6.1.3. Compressive strength of concrete

Three types of tests have been used to determine the relationship between the compressive strength of concrete and temperature changes. The resulting strength categories are as follows:

(a) 'unstressed' strength which is determined by heating the specimen with no superimposed loads. When the desired test temperature is reached, the specimen is then tested for compressive strength.

(b) 'stressed' strength which is determined by first loading the concrete specimen with a desired test load. The stressed specimen is heated to a certain temperature and then tested for compressive strength.

(c) 'unstressed residual' strength which is for specimens which have been heated to any desired temperature, cooled to room temperature and then tested for compressive strength.

Results from compressive strength studies by Abrams [9] and Malhorta [7] show that most concrete types retain their near full strength at temperatures below 700 °F. Siliceous aggregate concretes start loosing appreciable amount of strength at temperatures above 700 °F, whereas lightweight and carbonate concrete losses increase at temperatures above 1000 °F. However, most concretes will retain only about 20% of their room temperature strength at 1600 °F. It was observed that type of aggregate and aggregate/cement ratio

have the most significant effect on the strength behavior. Specimen tested while under stress showed higher values of compressive strength than for unstressed specimen.

1.6.1.4. Elastic properties

Elastic properties of concrete have been studied by Cruz [12] and Harada [13], among others. Results from Cruz show that the elastic modulus of concrete drops to 40-50% at 750°F, and below 30% of its room temperature value at 1200°F.

Cruz [12] shows that the modulus of elasticity of concrete is affected primarily by the same factors which influence the compressive strength. The aggregate type and concrete strength do not have significant effect. However, as for compressive strength, the elasticities from stressed tests show higher values than the unstressed ones. According to report by Harada [13], original room temperature values of elastic modulus are not regained upon cooling.

The effects of temperature on the elastic modulus of prestressing steel have been reported in Ref.[5]. At lower temperatures, the modulus of elasticity decreases at a slow rate with steel temperatures. The modulus is reduced by about 6% at 400 °F and by approximately 20% at 600 °F. Above 900°F, the modulus of elasticity decreases at higher rates to almost zero at 1400 °F.

1.6.1.5. Concrete bond

The effect of temperature on bond strength has been studied by Morley [14], Morley and Royles [15] and Diederichs and Schneider [16]. Results show that at 900 °F the maximum bond strength is reduced to 50% and to less than 20% at 1300 °F. Effective bond between concrete and prestressing steel is also reduced at high temperature resulting to the extension of development length [17,18] due to bond slip. Fagundo and Richardson [19] also studied the effects of temperature on bond slip of epoxy-coated prestressing strands. Results of the study shows a bond slip of 0.02 in. when the strand temperature reached of 220°F. The strands were initially stressed to 75% of their ultimate strength.

1.6.1.6. Deformation and thermal properties

Characteristics of nonmechanical deformation properties, such as concrete shrinkage and thermal strains of concrete and prestressing steel, at high temperatures have been reported in various studies. Relationship of thermal properties of concrete with temperature have also been studied. This information is presented in Chapter 3.

1.6.1.7. Application to this study

The models of temperature-material property relationships used in this study have been derived from the results published in the literature. Strength properties,

nonmechanical deformation and thermal properties of concrete and prestressing steel are used as reported.

Information on loss of prestress is not used, however, the loss of prestress is derived from effects of concrete shrinkage, thermal strains of concrete and steel, and relaxation properties of prestressing steel at high temperatures. Modulus of elasticity data is also not applied directly. Elastic properties are derived from information on influence of temperature on stress-strain relation of concrete and prestressing steel. Due to lack of sufficient data on bond slip of prestressing steel in relation to temperature changes, bond properties are not included in this study. Therefore a perfect bond between concrete and prestressing steel is assumed at all temperature levels.

1.6.2. Structural Response-Experimental

Fire tests have been the main procedure for studying structural response of prestressed concrete in fire environment. Most of the test data reported come from (a) Portland Cement Association PCA), Skokie, and (b) Underwriters' Laboratories, Chicago. The main objective of these tests was to determine the fire endurance of prestressed concrete members while supporting their full service loads [2,20,21,22].

Fire tests of building components are conducted under the specifications of the ASTM Standard Methods of Fire Tests of Building Construction and Materials [1]. The test sample is placed in a furnace and loaded at the desired service stage. The applied load is the maximum permissible superimposed load as required or permitted by recognized building codes. The furnace is then fired by natural gas burners from each side of the sample. The heating of the furnace is controlled by using thermocouples so that the temperature conforms to the standard time-temperature curve shown in Fig.1.5.

Temperature distribution within the specimen is measured through thermocouples located at various points in the specimen. Test on a specimen is conducted until an arbitrary selected deflection limit or a defined end point is reached. Some of the end point criteria [1] are

(a) Structural end point: when collapse occurs for load bearing specimens while supporting the applied loading and

(b) Heat transmission end point: when the temperature of the unexposed surface of floors, roofs or walls reach an average of 250 °F or a maximum of 325 °F at any one point.

1.6.3. Structural Response-Numerical

Research areas for developing numerical procedures have included heat transfer and structural response analysis [23]. Numerical methods developed for temperature

distribution include the use of finite difference techniques [13,24], multi-degree polynomials [25], and finite element [26,27]. Finite element techniques have also been used to develop numerical methods for structural response analysis of steel structure.

Jeanes [28] developed a rational method and computer implementation, FABUS II, for determining the structural response of steel buildings subjected to fire. Temperature distribution was analyzed using FIRES-T3 [27]. Temperature-dependent properties of steel considered in the model were the yield strength, modulus of elasticity and coefficient of expansion. Structural responses studied were deflections, beam elongation and changes in stress levels across beam sections.

Anderberg et al. [29] also developed numerical procedures for predicting behavior of steel structures subjected to fire and implemented in a FE computer program STEELFIRE. Structure responses are determined by the analysis of plane steel frames subjected to in-plane loading. Measured temperature values were part of the input to the model. Main response computed was deflection.

Other developments of numerical methods for response of steel structures in fire include those of Bresler and Iding [30] and Nakamura et al. [31].

Numerical methods for structural response of prestressed concrete structures have been limited to the

determination of fire endurance. The procedures determine the end point moment capacity of a prestressed concrete member subjected to elevated temperatures [3,4,5,21].

The residual moment capacity is computed using the rectangular beam formula given in the concrete building code [32]. The basic equation is

$$M_{u\theta} = \phi A_{ps} f_{ps\theta} (d - a_\theta/2) = \phi M_{n\theta}$$

$$a = \frac{A_{ps} f_{ps\theta}}{0.85 f'_{c\theta} b} \qquad (1.1)$$

$$f_{ps\theta} = f_{pu\theta}\left(1 - \frac{0.5 A_{ps} f_{pu\theta}}{b d f'_{c\theta}}\right)$$

where

ϕ = capacity reduction factor for flexure

A_{ps} = the cross sectional area of the prestressing steel, in.^{2}

f_{ps} = the stress in the prestressing steel at the ultimate load, ksi

f_{pu} = the ultimate tensile strength of the prestressing steel, ksi, (temperature dependent)

M_n = nominal moment strength, in.-k

d = effective depth, in.

a = the depth of the equivalent rectangular stress block at ultimate load, in.

θ = indicates temperature dependence

Fire safety designs aids have been developed based on the results of experimental studies on temperature

distribution and material behavior. The aids are in the form of graphs for temperature distribution within beams and slabs, and for temperature and strength relationship for both concrete and prestressing steel [3,4,5,22,33,34].

Steel temperature within the concrete at certain distances from fire exposed surfaces of beams or slabs, and at various times of exposure, can be estimated from the temperature distribution curves. The steel strength, f_{pu}, in Eq. (1.1), is then computed according to the relationship between the temperature and strength of prestressing steel given in strength-temperature curves. The data is used to compute the moment capacity at various exposure times.

Flexural failure is assumed to occur when the retained moment capacity, $M_{n\theta}$, is reduced to the level of the applied moment M. This condition is demonstrated in Fig. 1.5. From Eq. (1.1) it can be seen that the fire endurance depends on the applied loading, and on the strength-temperature characteristics of the prestressing steel.

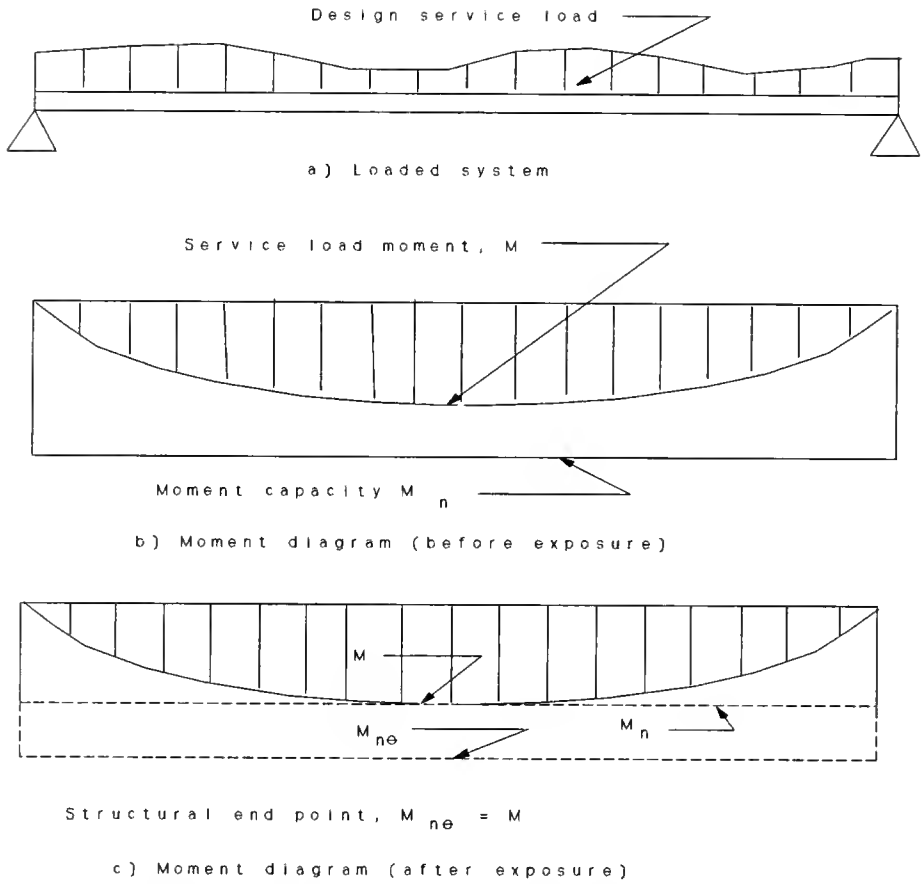

Fig. 1.5. Moment capacity of a beam exposed to fire

CHAPTER 2
THERMAL ANALYSIS

2.1. Introduction

This chapter presents the development of the procedure for the analysis of temperature distribution history of members in a fire environment. It is based on the general approach introduced by Wilson [35,36] and Zienkiewicz [37], and simplified for the needs of this study.

The members are idealized by a systems of two-dimensional triangular elements. The thermal boundary conditions, represented by the time-temperature relationship of the Standard Fire Test (SFT), consists of convective and radiative heat transfer mechanisms. Development of a computer program (TEDIAN) is also discussed.

2.2. Heat Transfer Models

2.2.1. Heat Flow Models

The general transient heat transfer equation is

$$\frac{\partial}{\partial x}\left(k\frac{\partial T}{\partial x}\right) + \frac{\partial}{\partial y}\left(k\frac{\partial T}{\partial y}\right) = \rho c\frac{\partial T}{\partial t} \qquad (2.1)$$

where

x,y = spatial coordinates

T = temperature distribution history

t = time

k = isotropic conductivity (temperature dependent)

c = specific heat capacity (temperature dependent)

ρ = material density (temperature dependent)

Initial condition is specified as

$$T(x,y,t=o) = T_0(x,y) \tag{2.2}$$

where T_0 is the specified uniform temperature for every point in the structure before analysis begins. In this study its value is taken as 68 °F. Using the mathematical formulation described by Segerlind [38], the convective and radiative boundary conditions are expressed as

$$k\left(\frac{\partial T}{\partial x}\right)l_x + k\left(\frac{\partial T}{\partial y}\right)l_y + h_c(T_s - T_f) + h_r(T_s - T_f) = 0 \tag{2.3}$$

where

l_x, l_y = directional cosine along x- and y-coordinates, respectively

h_c = convective heat transfer coefficient

h_r = radiative heat transfer coefficient

T_s = surface temperature of concrete member

T_f = furnace temperature

The dependence of convective heat transfer coefficient on temperature has minimal effect on the heat transfer process

of the standard fire test. As temperature increases the process becomes more and more dependent on radiation. For numerical computations h_c is assumed constant [39,40], and approximated as

$$h_c = 4.4 \quad (Btu/hr.ft^2{}^\circ F) \tag{2.4}$$

The radiative heat transfer coefficient is expressed as

$$h_r = \sigma\epsilon[(T_s + 460)^2 + (T_f + 460)^2](T_s + T_f + 920) \tag{2.5}$$

where

σ = Stefan-Boltzmann constant

= $0.119 * 10^{-10}$ Btu/hr.in^2.°R)

ϵ = resultant emissivity of the flames, combustion gases and the boundary surface.

For furnace conditions of the standard fire test, the value of resultant emissivity is taken as 0.5 [39,40].

2.2.2. Finite Element Formulations

Based on variational principles [36,38,41], Eqs.(2.1) and (2.3) are expressed, respectively, as

$$I = \frac{1}{2}\int_v \left[k\left(\frac{\partial\phi}{\partial x}\right)^2 + k\left(\frac{\partial\phi}{\partial y}\right)^2 + \rho c\phi^2 - 2\rho c\phi_0\phi\right]dV \tag{2.6}$$

$$\frac{1}{2}\int_s h_c(\phi_s - \phi_f)^2 dS + \frac{1}{2}\int_s h_r(\phi_s - \phi_f)^2 dS \tag{2.7}$$

where

$\Phi(x,y,t)$ = unknown temperature function

Φ_o = initial temperature field

Φ_s = temperature field of surface exposed to heat source (unknown)

Φ_f = temperature field of medium of heat source (known)

The above functional are combined so that the boundary conditions are satisfied automatically after minimization of the integral I [42]. The resulting functional is

$$I = \frac{1}{2}\int_v \left[k\left(\frac{\partial\phi}{\partial x}\right)^2 + k\left(\frac{\partial\phi}{\partial y}\right)^2 + \rho c\phi^2 - 2\rho c\phi_0\phi\right]dV \qquad (2.8)$$
$$+ \frac{1}{2}\int_s h_c(\phi_s - \phi_f)^2 dS + \frac{1}{2}\int_s h_r(\phi_s - \phi_f)^2 dS$$

2.2.3. Matrix Equations

Thermal matrices are formulated using standard displacement finite element procedures. Following relations are assumed:

$$\phi(x,y,t) = N(x,y)\,T(t) \qquad (2.9)$$

where

T(t) = nodal temperature vector

N(x,y) = interpolation function

$$(H)^T = \left(\frac{\partial \phi}{\partial x} \quad \frac{\partial \phi}{\partial y}\right) \tag{2.10}$$

$$[D] = \begin{bmatrix} k & 0 \\ 0 & k \end{bmatrix} \tag{2.11}$$

$$[B]^T = \left[< \frac{\partial N}{\partial x} > \quad < \frac{\partial N}{\partial y} > \right] \tag{2.12}$$

$$[H] = [B(x,y)] \ (T(t)) \tag{2.13}$$

Making substitutions of Eqs.(2.10) to (2.13) in Eq.(2.8) results in

$$\begin{aligned} I = & \int_v \frac{1}{2} (T)^T [B]^T [D] [B] (T) \, dV \\ & + \int_v \frac{1}{2} \rho c \ (T)^T [N]^T [N] (T) \, dV \\ & - \int_v \rho c (T)^T [N]^T [N] (T_0) \, dV \\ & + \int_s \frac{1}{2} h (T)^T [N]^T [N] (T) \, dS \\ & - \int_s h T_f [N] (T) \, dS + \int_v \frac{1}{2} h T_f^2 \, dS \end{aligned} \tag{2.14}$$

where h represents the heat transfer coefficient, convective or radiative. Eq.(2.14) is differentiated with respect to temperature T, and equated to zero. The minimized function is

$$\int_v \left([B]^T [D]\ [B]\ dV + \int_s h\,[N]^T [N]\ dS \right) (T) + \int_v \rho c\,[N]^T [N] ((T) - (T_0))\, dV - \int_s h T_f\,[N]\ dS = 0 \tag{2.15}$$

For an integration step Δt, temperature rate is given as

$$(T) - (T_0) = (T_{t+\Delta t}) - (T_t) = (T') \tag{2.16}$$

where

$(T_o) = (T_t)$ = initial spatial temperature

The terms in Eq. (2.15) are defined as follows:

$$[K_1] = \int_v [B]^T [D]\ [B]\ dV \tag{2.17}$$

$$[K_2] = \int_s h_c\,[N]^T [N]\ dS \tag{2.18}$$

$$[K_3] = \int_s h_r\,[N]^T [N]\ dS \tag{2.19}$$

$$[C] = \int_v \rho c\,[N]^T [N]\ dV \tag{2.20}$$

$$[R_1] = \int_s h_c T_f\,[N]\ dS \tag{2.21}$$

$$[R_2] = \int_s h_r T_f\,[N]\ dS \tag{2.22}$$

Eqs.(2.16) to (2.22) are lumped into a matrix form of the following transient heat equation:

$$[C]\,(T') + [K]\,(T) = (R) \tag{2.23}$$

where

[K] = $[K_1] + [K_2] + [K_3]$ (conductivity matrix, temperature-dependent)

[R] = $[R_1] + [R_2]$ (thermal load matrix, due to pseudo fire boundary conditions, temperature-dependent)

[C] = thermal capacitance matrix, temperature-dependent.

2.2.4. Time Integration of Temperature

Over a time interval (t+ Δt,t), the rate of temperature change, (T'), is approximated based on following assumptions [42,43]:

$$T'_{t+\alpha\Delta t} = \frac{1}{\Delta t}(T_{t+\Delta t} - T_t) \tag{2.24}$$

$$T_{t+\alpha\Delta t} = (1 - \alpha)\,T_t + \alpha T_{t+\Delta t}$$

where $0 \le \alpha \le 1$. Then, for a time instant (t+ αΔt), Eq.(2.23) is rewritten as

$$[C]_{t+\alpha\Delta t}(T')_{t+\alpha\Delta t} + [K]_{t+\alpha\Delta t}(T)_{t+\alpha\Delta t} = (R)_{t+\alpha\Delta t} \tag{2.25}$$

which upon substituting in Eq. (2.24) results in

$$\left[\frac{1}{\Delta t}[C]_{t+\alpha\Delta t} + \alpha[K]_{t+\alpha\Delta t}\right](T)_{t+\alpha\Delta t} = (R)_{t+\alpha\Delta t} + \frac{1}{\Delta t}[C]_{t+\alpha\Delta t}(T)_t - (1-\alpha)[K]_{t+\alpha\Delta t}[T]_t \tag{2.26}$$

For conditionally stable solution of Eq.(26) implicit algorithm obtained for $\alpha \neq 0$ are more preferred. Using the algorithm of $\alpha = 1/2$, [35,42], the transient heat transfer equation becomes

$$\left[\frac{2}{\Delta t}[C]_{t+\Delta t} + [K]_{t+\Delta t}\right](T)_{t+\Delta t} = (R)_{t+\Delta t} + (R)_t + \left[\frac{2}{\Delta t}[C]_{t+\Delta t} - [K]_{t+\Delta t}\right](T)_t \tag{2.27}$$

Implementing and trying other algorithms, Eq.(2.27) required more computation effort for the same level of accuracy than for $\alpha = 1$. Thus, the form of equation used in this development is

$$\left[\frac{1}{\Delta t}[C]_{t+\Delta t} + [K]_{t+\Delta t}\right](T)_{t+\Delta t} = (R)_{t+\Delta t} + \frac{1}{\Delta t}[C]_{t+\Delta t}(T)_t \tag{2.28}$$

The more convenient form for solution is

$$[KC](T)_{t+\Delta t} = (RC) \tag{2.29}$$

where the effective conductivity matrix, [KC], is given by

$$[KC] = \left[\frac{1}{\Delta t}[C]_{t+\Delta t} + [K]_{t+\Delta t}\right] \tag{2.30}$$

and the effective thermal load vector, [RC], is

$$[RC] = (R)_{t+\Delta t} + \frac{1}{\Delta t}[C]_{t+\Delta t}(T)_t \tag{2.31}$$

2.3. Evaluation of Thermal Matrices and Load Vector

The evaluation of thermal matrices of Eq.(2.29) is based on the characteristics defined for the two dimension triangular element presented in Fig. 2.1. The element has one temperature degree of freedom per node.

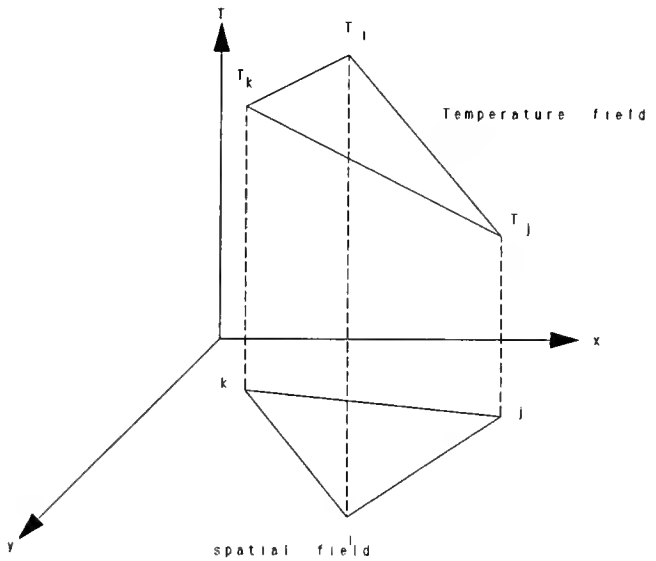

Fig.2.1. Plane triangular element

2.3.1. Interpolation Functions

The area of triangular element of Fig. 2.2. is given by

$$A_{ijk} = \frac{1}{2}[(x_i y_j - x_j y_i) + (x_j y_k - x_k y_j) + (x_k y_i - x_i y_k)] \quad (2.32)$$

The three shape functions are defined as follows:

$$N_i = \frac{1}{2A}[(x_j y_k - x_k y_j) - (y_j - y_k)x - (x_k - x_j)y] \quad (2.33)$$

$$N_j = \frac{1}{2A}[(x_k y_i - x_i y_k) + (y_k - y_i)x + (x_i - x_k)y] \quad (2.34)$$

$$N_k = \frac{1}{2A}[(x_i y_j - x_j y_j) + (y_i - y_j)x + (x_j - x_i)y] \quad (2.35)$$

Substituting Eqs.(2.33), (2.34) and (2.35) in Eq. (2.12) we get matrix [B]:

$$[B] = \frac{1}{2A}\begin{bmatrix} BI & BJ & BK \\ CI & CJ & CK \end{bmatrix} \quad (2.36)$$

where,

$BI = (y_j - y_k)$ $\qquad$ $CI = (x_k - x_j)$
$BJ = (y_k - y_i)$ $\qquad$ $CJ = (x_i - x_k)$
$BK = (y_i - y_j)$ $\qquad$ $CK = (x_j - x_i)$

2.3.2. Conductivity Matrix

For an element of unit thickness, Eq.(2.17) becomes

$$[K_1] = \frac{k}{4A}\begin{bmatrix} (BI^2 + CI^2) & (BIBJ + CICJ) & (BIBK + CICK) \\ & (BJ^2 + CJ^2) & (BJBK + CJCK) \\ & SYM & (BK^2 + CK^2) \end{bmatrix} \quad (2.37)$$

Assuming dS = 1.dL and using area coordinate method of integration [44], Eq. (2.18) takes the following form:

$$[K_2] = \frac{h_c L_{ij}}{6}\begin{bmatrix}2 & 1 & 0\\ 1 & 2 & 0\\ 0 & 0 & 0\end{bmatrix} + \frac{h_c L_{jk}}{6}\begin{bmatrix}0 & 0 & 0\\ 0 & 2 & 1\\ 0 & 1 & 2\end{bmatrix} \qquad (2.38)$$

where i-j denote the end nodes of exposed edge. The length L_{ij} is defined as

$$L_{ij} = \sqrt{(x_j - x_i)^2 + (y_j - y_i)^2} \qquad (2.39)$$

Eq.(2.19) takes the same form as Eq.(3.38), replacing h_c by h_r.

2.3.3. Thermal Capacitance Matrix

Applying the area coordinate method [42], the capacitance Eq.(2.20) becomes

$$[C] = \frac{\rho c A}{12}\begin{bmatrix}2 & 1 & 1\\ & 2 & 1\\ SYM & & 2\end{bmatrix} \qquad (2.40)$$

When the implementation of Eq.(2.40) was used temperature values of certain nodes diminished below zero before rising. The reason for this characteristic is not clear. To avoid this problem an alternative approach is utilized in this study. The capacitance matrix is computed by delineating part of element volume to a node. For element m of unit thickness the volume contribution to node i is given by

$$C_{m,i} = \frac{1}{3} A_m \rho(T)\, c(T) \qquad (2.41)$$

The matrix form of Eq.(2.41) is

$$[C] = \frac{\rho CA}{3}\begin{bmatrix} 1 & & \\ & 1 & \\ & & 1 \end{bmatrix} \tag{2.42}$$

The approach produced results with the expected characteristics.

2.3.4. Thermal Load Vector

The load matrices are evaluated using line integrals. For an element of unit thickness with two sides, (i-j) and (j-k), exposed to fire, the evaluation of Eqs. (2.21) and (2.22) result to a complete thermal load vector expressed as

$$(R) = \frac{h_c T_f L_{ij}}{6}\begin{pmatrix}1\\1\\0\end{pmatrix} + \frac{h_c T_f L_{jk}}{6}\begin{pmatrix}0\\1\\1\end{pmatrix} + \frac{h_r T_f L_{ij}}{6}\begin{pmatrix}1\\1\\0\end{pmatrix} + \frac{h_r T_f L_{jk}}{6}\begin{pmatrix}0\\1\\1\end{pmatrix} \tag{2.43}$$

2.4. Solution Algorithm

At time $(t+\Delta t)$, temperature dependent thermal matrices [C], and [K], of Eq.(2.28), are not known. Thus, for each time step increment Δt, the following iterative scheme is used to obtain an acceptable solution:

$$\left[\frac{1}{\Delta t}[C]_{t+\Delta t}^{(i-1)} + [K]_{t+\Delta t}^{(i-1)}\right](T)_{t+\Delta t}^{(i)} = (R)_{t+\Delta t}^{(i-1)} + \frac{1}{\Delta t}[C]_{t+\Delta t}^{(i-1)}\,(T)_t \tag{2.44}$$

where the superscript (i-1) denotes iteration number. The initial values are expressed as

$$\begin{aligned} [C]_{t+\Delta t}^{(0)} &= [C]_t \\ [K]_{t+\Delta t}^{(0)} &= [K]_t \\ (R)_{t+\Delta t}^{(0)} &= (R)_t \end{aligned} \tag{2.45}$$

Convergence of solution is governed by both the system temperature and the boundary condition criteria. For any two successive iterations the temperature convergence is achieved by

$$\frac{\left|T_{t+\Delta t}^{(i)} - T_{t+\Delta t}^{(i-1)}\right|}{\frac{1}{2}\left|T_{t+\Delta t}^{(i)} + T_{t+\Delta t}^{(i-1)}\right|} \leq \epsilon_T \tag{2.46}$$

and that of boundary condition by

$$\frac{\left|h_{r_{t+\Delta t}}^{(i)} - h_{r_{t+\Delta t}}^{(i-1)}\right|}{\frac{1}{2}\left|h_{r_{t+\Delta t}}^{(i)} + h_{r_{t+\Delta t}}^{(i-1)}\right|} \leq \epsilon_r \tag{2.47}$$

CHAPTER 3
MODELING OF TEMPERATURE DEPENDENT MATERIAL PROPERTIES

3.1. Introduction

Both concrete and prestress steel experience certain degree of degradation when exposed to high temperatures [6,7,8,9]. It is, therefore, important to understand the behavior of these properties at elevated temperatures.

The objective of this chapter is to present the mathematical relation of material properties to temperature. Most of the models are derived directly from test data and results published in the literature and summarized in references [45,5,46].

It is expected that the data used and the models developed represent the acceptable behaviors of concrete and prestress steel as related to temperature and, therefore, provide reasonable accurate basis for evaluating the structural response of prestressed concrete elements in fire.

3.2. Modeling Procedures

Most properties of concrete and steel are affected by high temperature. In this study the temperature-dependent behavior of material property curves is estimated by a

series of discrete points connected by by linear segments as shown in Fig. 3.1. Then the parameter value, p, at a given temperature, T_i, is computed by

$$p(T_i) = p(T_n) + (T_i - T_n) S_n$$

$$S_n = \frac{p(T_{n+1}) - p(T_n)}{T_{n+1} - T_n} \qquad (3.1)$$

$$T_n \leq T_i \leq T_{n+1}$$

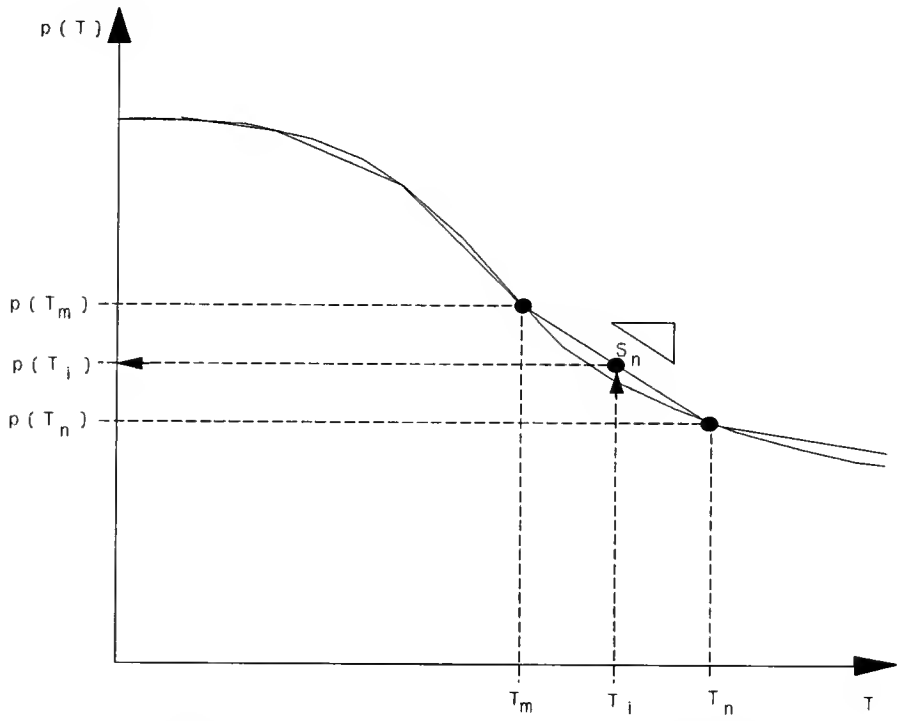

Fig.3.1. Mathematical Modeling of Material Properties from Test Results

3.3. Concrete

3.3.1. Thermal Properties

The parameters which influence the characteristics of heat transfer in solids are the thermal conductivity and thermal capacity.

3.3.1.1. Thermal conductivity

Thermal conductivity of concrete measures the ability of concrete to transfer heat by conducting heat from particles at high temperature to those at low temperature. The variation of thermal conductivity of concrete with temperature is primarily determined by the conductivity of the aggregates used [47,48]. High temperatures increases the disorder of particles in aggregates. This causes the scattering of heat in all directions, hindering effective transmission of heat towards low temperature regions. As a consequence, thermal conductivity of concrete decrease with increase in temperature.

The generic model relating thermal conductivity of concrete to its temperature is expressed as

$$k_c(T) = a_k + b_k T_e \tag{3.2}$$

where

T_e = element temperature (from thermal analysis)

a, b = constants derived from experimental data (according to Fig. 3.2.)

The variation of thermal conductivities with temperature for the three types of concrete is shown graphical Fig. 3.2.

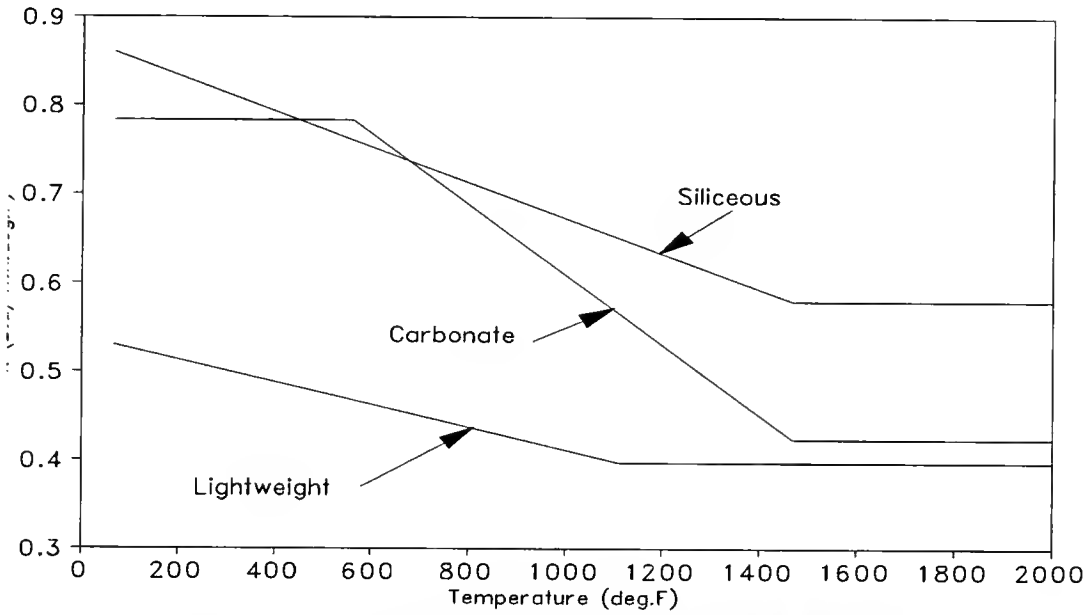

Fig. 3.2. Conductivity of concrete as a function of temperature (Source: Ref. [49])

3.3.1.2. Thermal capacity

Thermal capacity of a material refers to the amount of heat required to raise a unit volume of the material by one degree. It is a product of material density ρ and the specific heat of the material c.

The character of the cement paste and water in the concrete have the most pronouncing effect on the behavior of thermal capacity of concrete [47]. In the case of water most of the supplied heat energy will be used to remove pore

waters in temperatures near 212 °F. Crystalline water is removed at higher temperatures. When removal of water takes place, the thermal capacity of concrete shows substantially higher values. The dependence of thermal capacity of concrete on temperature is shown graphically in Fig. 3.3.

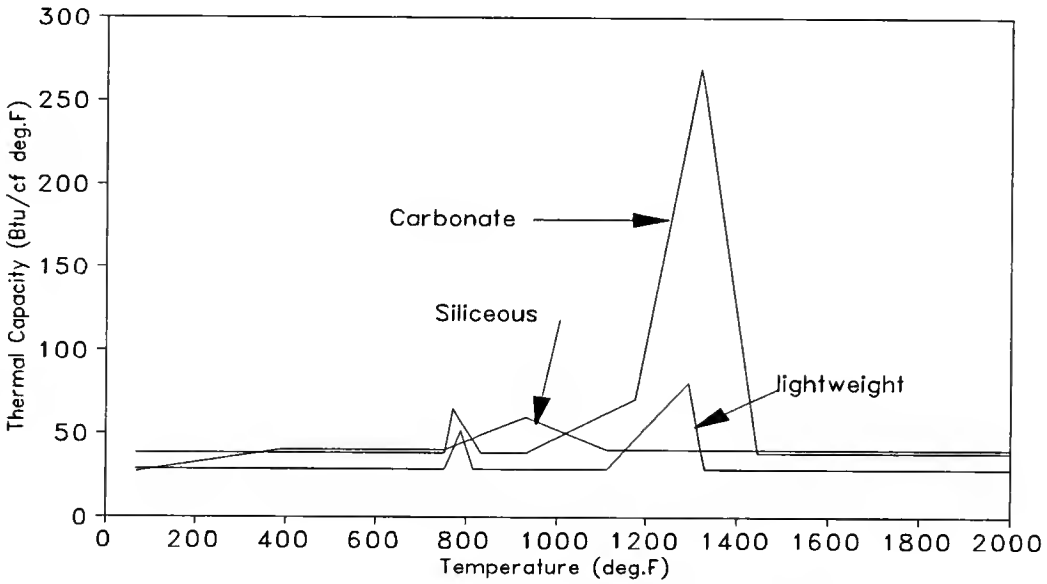

Fig. 3.3. Variation of thermal capacity of concrete with temperature (Source: Ref. [49])

The thermal capacity of the various types of concrete considered in this study are modeled for various ranges of temperatures. The models takes the following form:

$$\rho c(T) = a_{\rho c} + b_{\rho c} T_e \tag{3.3}$$

3.3.2. Mechanical Properties

Mechanical properties are those describing the characteristic of material under stress. Considered in this section are stress-strain relation, compressive strength and modulus of rupture.

3.3.2.1. Stress-strain relation

High temperatures increases deformation properties of concrete. Thus there is a continuous variation of stress-strain relation with temperature resulting to a number of strain-curves. The relationship between stress-strain law and temperature is shown in Fig. 3.4 for some selected temperature ranges.

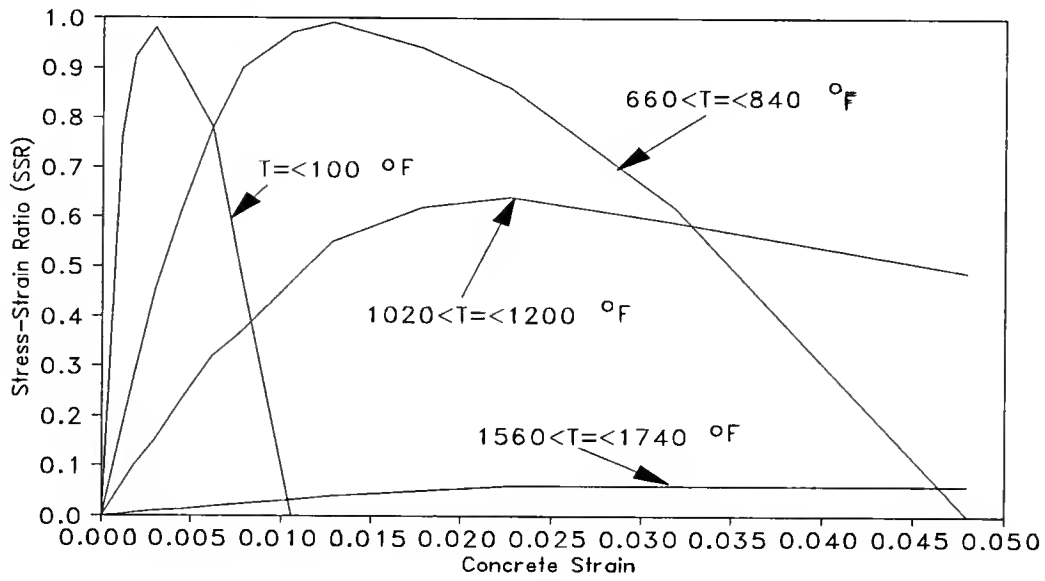

Fig. 3.4. Stress-strain relationship as function of temperature (Source: Ref. [49])

For each temperature range, modulus of elasticity E is computed for a given range m-n. The expression is

$$\Delta\sigma_{mn}(T) = \sigma_n(T) - \sigma_m(T)$$
$$\Delta\epsilon_{mn} = \epsilon_n - \epsilon_m \qquad (3.4)$$
$$E_{mn}(T,\epsilon) = \frac{\Delta\sigma_{mn}(T)}{\Delta\epsilon_{mn}}$$

The mechanical stress for time step j+1, temperature range T_{k+1} and mechanical strain ϵ_i is given by

$$\Delta\epsilon_{mi}^{j+1} = \epsilon_i^{j+1} - \epsilon_m^{j+1} \qquad (3.5)$$
$$\sigma_i^{j+1}(T_{k+1},\epsilon_i) = \sigma_m^{j+1}(T_{k+1},\epsilon_m) + E_{mn}^{j+1}\Delta\epsilon_{mi}^{j+1}$$

The stress-strain curves used in this study have been reported by Lie [49]. They have been adjusted to account for creep by moving the maxima to higher strains with higher temperatures. In addition, the curves give the whole characteristic of stress-strain relation which include the post peak behavior.

From reported data [13], aggregate type and strength have no significant effect on stress-strain relation at high temperatures. As such the set of stress-strain curves represents both normal weight and lightweight concretes.

3.3.2.2. Compressive strength

Type of aggregates, degree of loading and conditions of loading-when hot or cooled are among the important factors which influence the behavior of concrete strength at elevated temperatures.

As temperature of concrete increases the aggregates and the cement matrix expands. At the same time pore and crystalline waters are evaporated, which causes shrinkage of concrete matrix. The resulting expansion differentials cause internal cracking of concrete which results to reduction of stiffness of concrete. The extent of this phenomenon differs considerably with the type of aggregate used in concrete.

Concretes with silicious aggregates are mostly affected since at temperatures above 1000 °F the aggregates also undergo physical changes accompanied by sudden expansion in volume [50]. Carbonate aggregate do not normally undergo physical changes during heating, hence carbonate aggregate concretes are free from severe internal cracks. However, at very high temperatures chemical changes take place when lime is liberated from calcium carbonate. The process is beneficial in retarding temperature rises, but during cooling the lime combines with atmospheric moisture and expands in volume causing cracks and damages to the concrete [50]. Lightweight aggregates normally undergo various heating processes during manufacture, hence they provide a better physical compatibility between the matrix and the aggregate with regard to deformation. In this study experimental data used to derive mathematical models are for 'stressed tests' in which concrete is tested hot while stressed to 40 percent of its room temperature strength.

These results are meaningful in structural response analysis since any prestressed concrete member will be subjected to some stress from external load, prestress or both. According to Abrams [9], the compressive strength values for specimens stressed at 25 to 55 percent of their original compressive strength show no significant variation in behavior.

The graphic models of the variation of concrete strength with temperature are shown in Fig. 3.5.

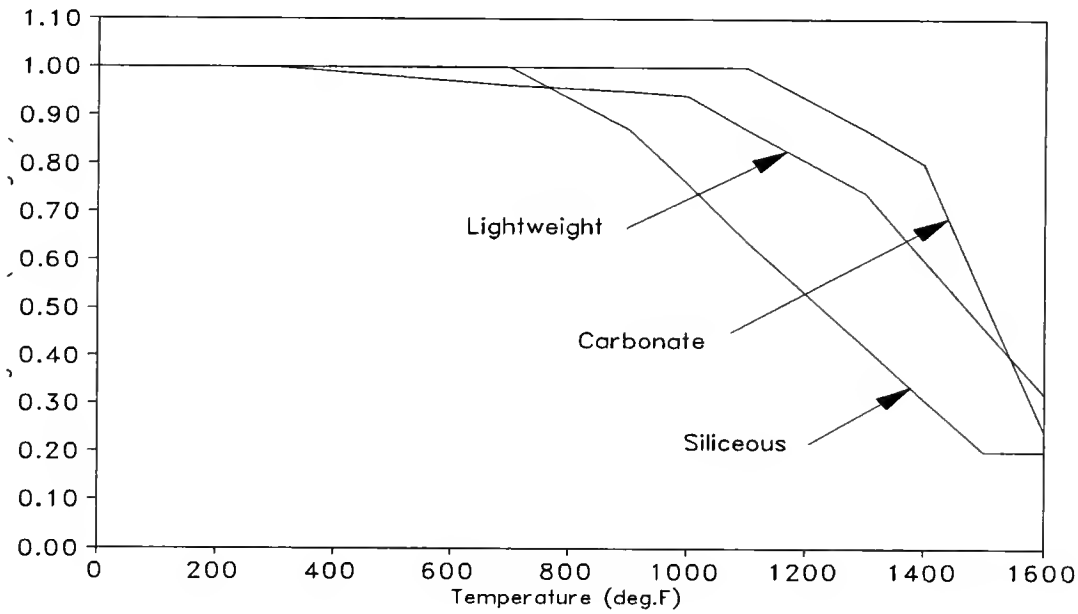

Fig. 3.5. Compressive strength of concrete versus temperature (Source: Ref. [5])

The mathematical expression for the compressive strength ratio is given by the following expression:

$$CSR(T_i) = CSR(T_m) + \Delta T_i S_n \qquad (3.6)$$

where

CSR = concrete strength ratio (percentage of original)

The compressive strength is then computed by

$$FC(T_i) = CSR(T_i)\, FC(T_{68}) \qquad (3.7)$$

3.3.2.3. Tensile strength

Reported test results of tensile strength of concrete at high temperature are very sketch. However, these reports indicate that the deterioration in tension is greater than that in compression [51]. For lack of adequate information, tensile strength of concrete is taken as a function of compressive strength. The relationship is expressed as

$$f_{rT} = 7.5\sqrt{f'_{cT}}$$
$$f_{rT} = 5.6\sqrt{f'_{cT}} \qquad (3.8)$$

where the equations are for normal weight and lightweight concrete, respectively [32].

3.3.3. Deformation Properties

Deformation properties considered are those causing changes in the dimension of a member due to non-mechanical means. These are thermal and shrinkage strains. The thermal strain is due to thermal expansion after making allowance for drying shrinkage. This is only an assumptionsince according to Bazant [52], it is difficult to

separate thermal strain from shrinkage strain under transient temperature conditions. Creep strain, which is both stress and time dependent, has been incorporated in the derivation of stress-strain relations.

3.3.3.1. Thermal expansion

Thermal expansion of concrete increases with increasing temperature. The variations are influenced by the aggregate type, cement content, water content and heating rate [51]. For unstressed specimen the increase in temperature causes the increase of thermal strain to a point of disintegration. At very high temperatures around 1100 °F to 1500°F range most concretes indicate no expansion. In some cases the concrete shrinks due to chemical or physical reactions in the aggregates.

The coefficient of expansion is derived from test results of thermal strain versus temperature. The relation is shown in Fig. 3.6. For a temperature range T_m, T_n, the coefficient of thermal expansion is given by the following model:

$$\alpha_{mn}(T) = \frac{\Delta \epsilon_{th}(T_{mn})}{\Delta T_{mn}} \tag{3.9}$$

Then the incremental and total thermal strain at temperature T_i is computed from

$$\begin{aligned} \Delta \epsilon(T_{mi}) &= \alpha_{mn}(T_i - T_m) \\ \epsilon_{th}(T_i) &= \epsilon_{th}(T_m) + \Delta \epsilon(T_{mi}) \end{aligned} \tag{3.10}$$

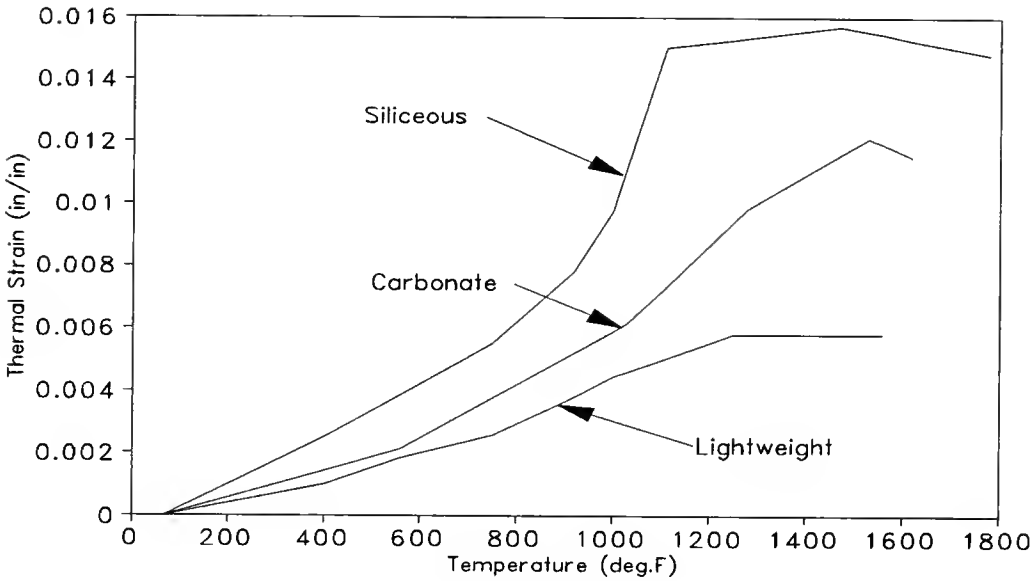

Fig. 3.6. Thermal strain of concrete as function of temperature (Source: Ref. [5])

3.3.3.2. Shrinkage strain

Shrinkage strain in concrete is due to loss of moisture in the cement paste [52]. The amount of shrinkage that occur and the rate of its occurrence are thus dependence on the moisture content in the concrete before heating. In this study the concrete members are assumed to be at normal service condition of relative humidity of 70 percent. In addition the shrinkage strain considered is that caused by loss of free water from the pores of concrete. Based on this criteria all the shrinkage is assumed to take place within 68 to 212 °F temperature range.

The incremental shrinkage strain within a time step n is computed by the following models:

$$\Delta\epsilon_{sh}(T_i) = a(T_i)\,(\epsilon_\infty(T_i) - \epsilon_s(T_n))\,\Delta t_n \qquad (3.11)$$

$$a(T_i) = 0.001 + \left[\frac{T_i - 68}{144}\right]^2 \qquad (3.12)$$

$$\epsilon_\infty(T_i) = 0.0005\left(1 + \frac{T_i - 68}{144}\right) \qquad (3.13)$$

where

$\epsilon_s(T_n)$ = cumulative shrinkage strain (at beginning of current time step)

$\epsilon_\infty(T)$ = total potential shrinkage due to loss of free water

a(T) = shrinkage rate (in/in per hour)

$\Delta\epsilon_{sh}$ = incremental shrinkage strain

Δt = duration of current time step (hour)

As mentioned earlier, both Eqs. (3.12) and (3.13) are valid within the temperature range of 68 °F to 212°F. From Eq. (3.13) the maximum total potential shrinkage at 212 °F has the value of 0.001 in/in.

3.4. Prestressing Steel

Most of the descriptions of property categories given in for concrete apply to prestressing steel as well.

3.4.1. Mechanical Properties

3.4.1.1. Stress-strain relationship

For a given range, the steel modulus can be obtained from Eq. (3.4) after substituting for the appropriate variable. The steel stress is then given by

$$\sigma_i(T,\epsilon) = \sigma_m(T_k) + E_{mn}\Delta\epsilon_{mi} \tag{3.14}$$

Fig. 3.7. gives the graphical representations of stress-strain law as used in this study.

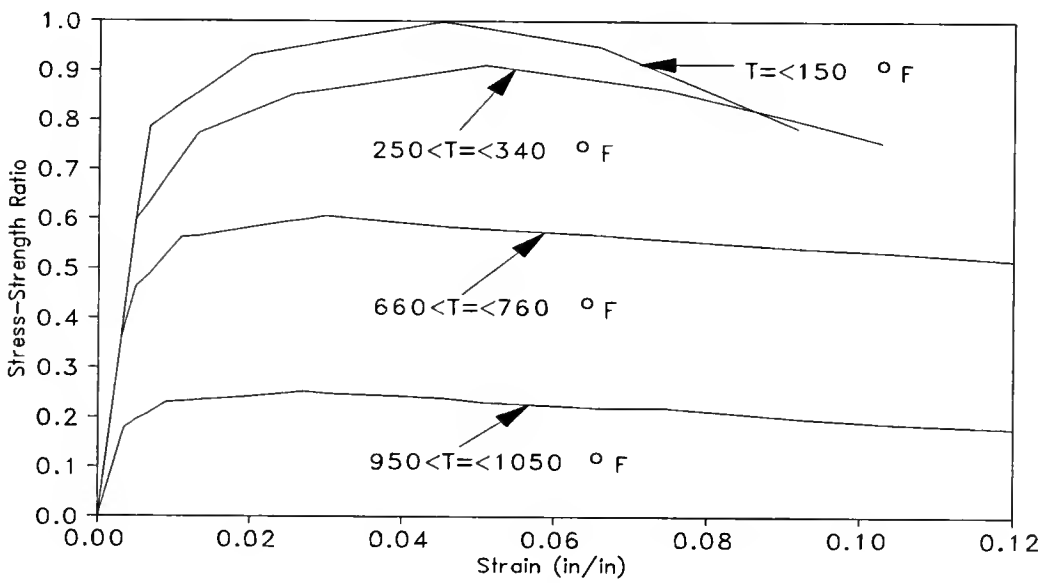

Fig. 3.7. Stress-strain curves for PS at various temperature levels (Source: Ref. [45])

3.4.1.2. Tensile strength

The tensile strength of prestressing steel decreases with the increase of temperature. According to the tests done by Abrams [6], the size of the strands and the rate of heating have no significant influence on the temperature-strength behaviors. Following the definitions given in Fig. 3.1, the tensile strength ratio is determined by

$$\begin{aligned} \Delta TSR(T_{mn}) &= TSR(T_n) - TSR(T_m) \\ \Delta T_{mi} &= T_i - T_m \\ S_{mn} &= \frac{\Delta TSR(T_{mn})}{\Delta T_{mn}} \\ TSR(T_i) &= TSR(T_m) + S_{mn}\Delta T_{mi} \end{aligned} \tag{3.15}$$

The tensile strength is obtained from

$$FPU(T_i) = TSR(T_i)\, FPU(T_0) \tag{3.16}$$

The graphical representation of the temperature-strength relationship for prestressing steel is given in Fig. 3.8.

3.4.2. Deformation Properties

3.4.2.1. Thermal strain

Coefficient of expansion of prestress steel increases with the increase of temperature. It is expressed in following form:

$$\alpha(T) = (6.667 + 0.001235T)\,(10^{-6}) \tag{3.17}$$

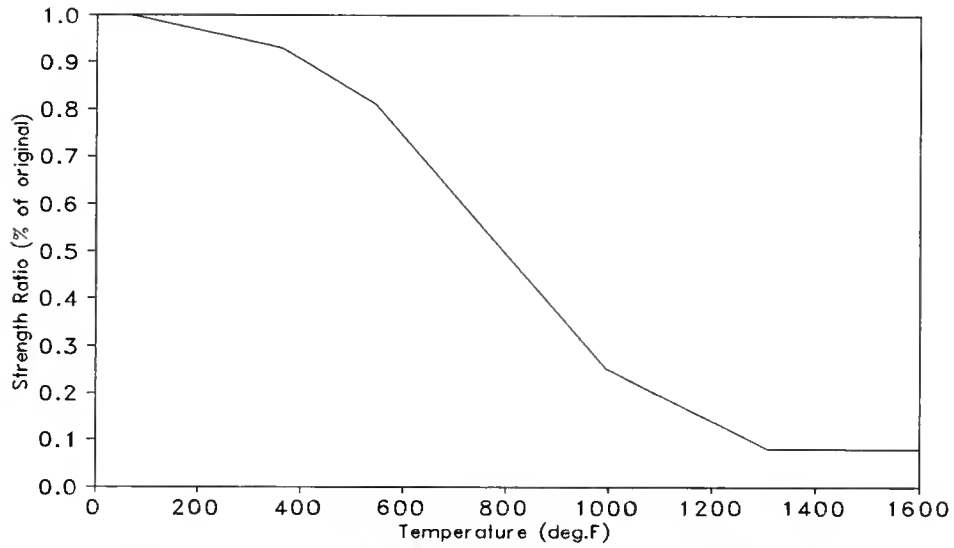

Fig. 3.8. Variation of prestress steel strength with temperature (Source: Ref. [5])

Variation of coefficient of thermal expansion of prestress steel with temperature is shown in Fig.3.9.

Within a time step the constant value of coefficient of thermal expansion used in computations is given by

$$\alpha_s = \frac{\alpha_n + \alpha_{n+1}}{2} \tag{3.18}$$

The corresponding thermal strain is expressed as

$$\epsilon_{th}(T_i) = \epsilon_n + \alpha_s \Delta T_{ni} \tag{3.19}$$

3.4.2.2. Relaxation/creep strain

The relaxation property of prestressing steel can be defined as the decrease in stress with time under constant strain. However, most of the reported tests have measured

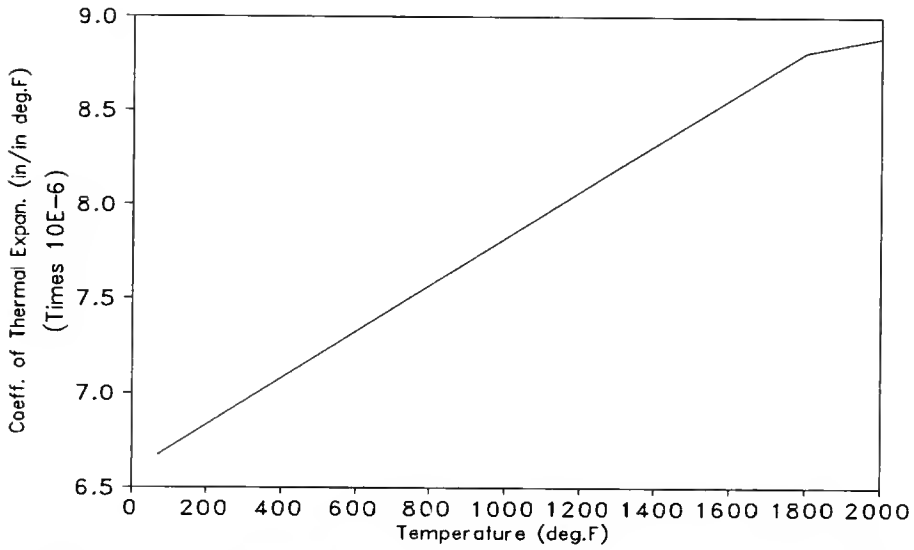

Fig. 3.9. Expansion coefficient of prestress steel as function of temperature (Source: Ref. [45])

it in terms of rate of loss of stress at given stress, that is, creep.

At high stresses and temperatures creep rate become substantial. According to tests by Yakovlev et al. [53], a prestressing of about 128,000 lb/in ^{2} in a wire was completely lost when heated to 572 °F in 40 minutes at a rate equal to that used during fire resistance tests of a prestressed concrete element.

According to the information given by Harmathy [54], the creep characteristics for prestress steel are described as follows:

$$\frac{\Delta H}{R} = 54000$$

$$Z = 8.21(10^{13})\, e^{0.0001\sigma} \qquad (3.20)$$

$$\epsilon_{cr} = Ze^{-\frac{\Delta H}{RT}}$$

where

ΔH/R is given in temperature units (R)

Z = Zener-Hollomon parameter (h^{-1})

T = absolute temperature of prestressing steel (R)

σ = stress in prestressing steel (lb/in^2)

εcr = creep rate (in/in.h).

Creep rates for some selected stress levels are presented in Fig. 3.10.

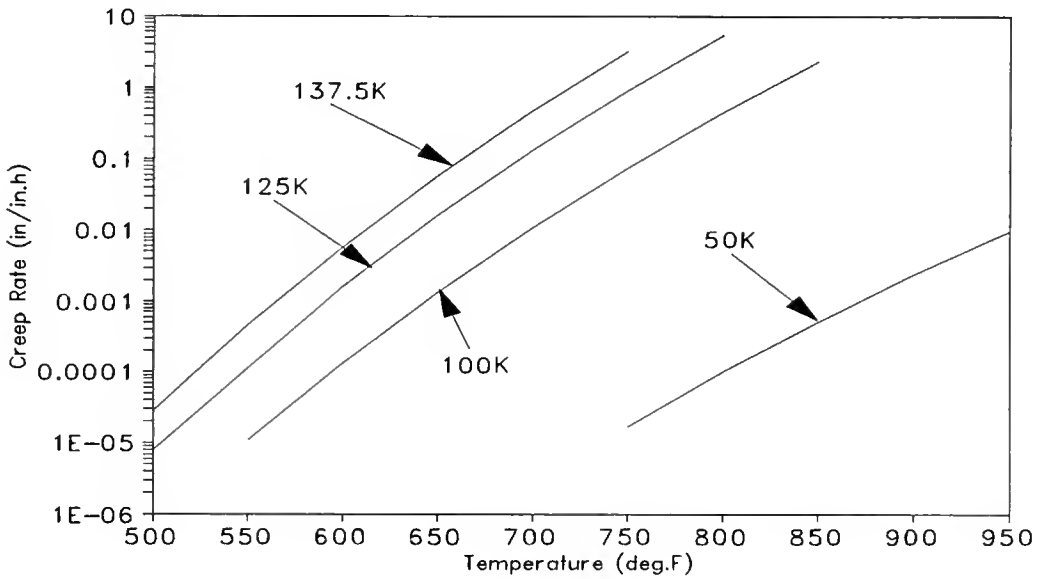

Fig. 3.10. Creep rate for prestress steel as function of temperature and stress (Source: Eq. (3.20))

3.5. Remarks

The models presented in this chapter have been formulated by approximating the test result curves by piecewise linear segments. Similar technique was used by Franklin [55] to model stress-strain relationship of concrete in his study of reinforced concrete frames. This approach was used in this study because of lack of mathematical models for most of the material properties considered. However, generalized empirical models have been used whenever possible.

CHAPTER 4
MODELING OF PRESTRESSED CONCRETE FRAME MEMBER

4.1. Introduction

This chapter discusses the modeling of prestressed concrete members. The formulation is based on direct stiffness method of structural analysis using two dimensional beam elements. Using the idealization of Fig. 1.4 the stiffness of an element is determined by integrating the temperature-dependent subelement properties.

4.2. Basic Finite Element Equations for a 2D Beam Element

Figure 4.1 presents a finite planar beam element with six nodal displacements, r_1 to r_6. These displacement components can be expressed in a generic form as

$$\boldsymbol{u} = \{u, v\}^T \tag{4.1}$$

where u represents displacement components associated with axial action in the x-axis and v represents both translation in y-axis and rotation due to flexural action about the z-axis. These components are shown in Fig. 4.2. Relationship between the generic displacement u and the nodal displacements [56] is given by

$$u = Nr \tag{4.2}$$

where **N** represents the displacement shape function, and **r** the nodal displacements as shown in Fig. 4.1.

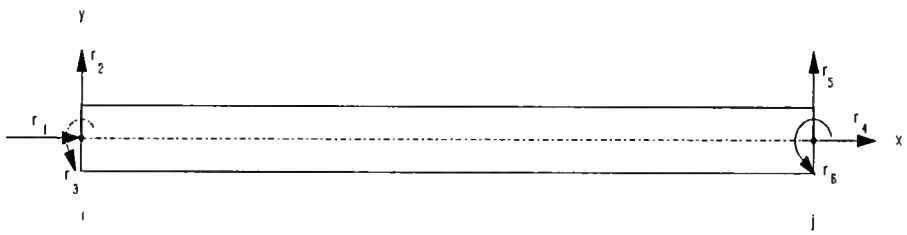

Fig.4.1. Displacement components of a 2D beam element

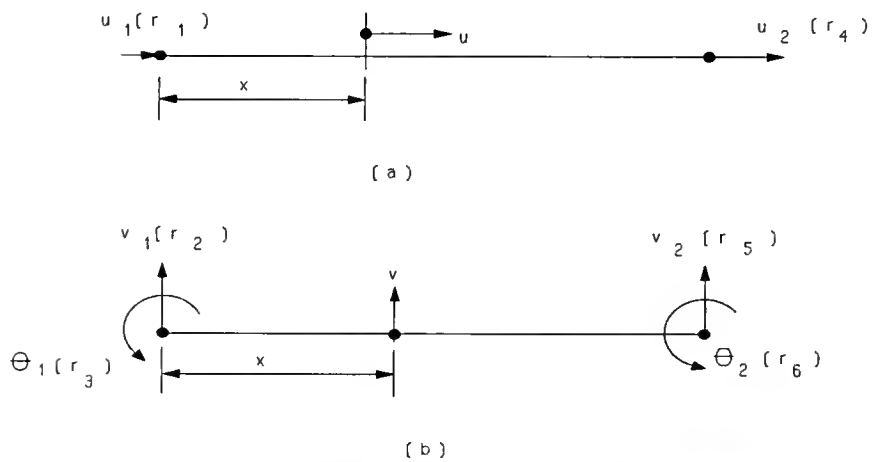

Fig. 4.2. Axial and flexural elements

Strain-displacement relationship is expressed as

$$\epsilon = du \tag{4.3}$$

where

ϵ = strain vector

d = linear differential operator

By Substituting Eq. (4.2) in Eq. (4.3), the strain equation becomes

$$\epsilon = dNr \tag{4.4}$$

resulting to the definition of strain-displacement matrix B

$$B = dN \tag{4.5}$$

The corresponding stress is given by

$$\begin{aligned} \sigma &= E\epsilon \\ &= EBr \end{aligned} \tag{4.6}$$

where

E = stress-strain matrix

EB = stress-displacement matrix

The relationship between the nodal displacements and the external load is expressed by

$$Kr = R \tag{4.7}$$

where K is the element stiffness matrix and R represents the load vector. The stiffness matrix is formulated as

$$K = \int_v B^T EB \, dv \tag{4.8}$$

The corresponding load vector **F**, due to strain energy of internal stresses in the element is computed from

$$\boldsymbol{F} = \int_v \boldsymbol{B}^T \boldsymbol{E} \epsilon \, dv \tag{4.9}$$

4.3. Evaluation of Displacement Functions for a Beam Element

Based on the actions associated with the nodal displacements shown in Fig. 4.1, the beam element is decomposed into: axial and flexural elements. The generic displacement equation for the axial element is expressed as

$$\boldsymbol{u} = u \tag{4.10}$$

where

$$\boldsymbol{r} = \{r_1, \; r_4\}T = \{u_1, \; u_2\}T \tag{4.11}$$

Corresponding displacement function is given by

$$u = c_1 + c_2 x \tag{4.12}$$

where c_1 and c_2 are constants corresponding to the nodal displacements. Expression for the shape function is

$$\boldsymbol{N} = \left[1 - \frac{x}{L} \;\; \frac{x}{L}\right] \tag{4.13}$$

Strain-displacement matrix **B** evaluates to

$$\boldsymbol{B} = \frac{1}{L}[-1 \;\; 1] \tag{4.14}$$

For the flexural element, displacement relation is given by

$$\boldsymbol{u} = v \tag{4.15}$$

The components are represented by

$$\boldsymbol{r} = \{r_2,\ r_3,\ r_5,\ r_6\}T = \{v_1,\ \theta_1,\ v_2,\ \theta_2\}T \tag{4.16}$$

where

$$\theta_1 = \frac{dv_1}{dx}$$
$$\theta_2 = \frac{dv_2}{dx} \tag{4.17}$$

Based on plain section theorem, translation in x direction of any point on the cross-section of the element is determined from

$$u = -y\frac{dv}{dx} \tag{4.18}$$

Substituting Eqs.(4.18) into (4.3), flexural strain becomes

$$\epsilon_x = \frac{du}{dx} = -y\frac{d^2v}{dx^2} = -y\phi \tag{4.19}$$

where ϕ represents the curvature. Differential operator takes the following form:

$$\boldsymbol{d} = -y\frac{d^2}{dx^2} \tag{4.20}$$

The displacement function is expressed as

$$v = c_1 + c_2 x + c_3 x^2 + c_4 x^3 \tag{4.21}$$

Shape functions are then given by

$$N^T = \frac{1}{L^3}\begin{bmatrix} 2x^3 - 3x^2L + L^3 \\ x^3L - 2x^2L^2 + xL^3 \\ -2x^3 + 3x^2L \\ x^3L - x^2L^2 \end{bmatrix} \tag{4.22}$$

By substituting Eqs.(4.20) and (4.22) in Eq.(4.5), the strain-displacement matrix B becomes

$$B^T = -\frac{y}{L^3}\begin{bmatrix} 12x - 6L \\ 6xL - 4L^2 \\ -12x + 6L \\ 6xL - 2L^2 \end{bmatrix} \tag{4.23}$$

4.4. Idealization of a Prestressed Concrete Member

A prestressed concrete member is modeled into a series of beam elements and tendon segments as shown in the Fig.4.3(a). A steel segment is assumed to be straight, has a constant tension force and spans the beam element. The interaction between the prestress steel and concrete is assumed to occur at the ends only.

The profile and the location of a steel segment in a beam element is defined by two end eccentricities and a

reference plane as shown in Fig. 4.3(b). It is determined by the expression given in Eq.(4.24).

$$y_p = \frac{1}{2}(e_i + e_j) \tag{4.24}$$

The reference plane is used to estimate steel segment temperature, incremental strains and contribution to the element stiffness.

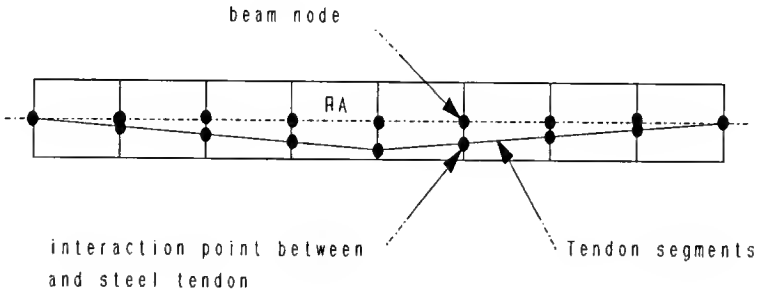

a) Finite Element Model of Beam Specimen and Steel Tendon

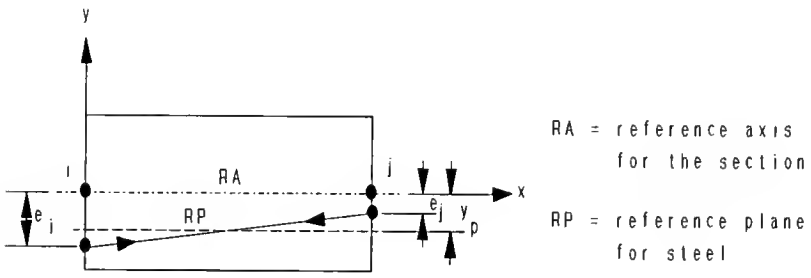

b) A Beam element with straight tendon segment
and a constant prestress force

Fig. 4.3. FE idealization of a PC member

4.5. Evaluation of Element Stiffness Matrix

The strain displacement matrices of Eqs. (4.14) and (4.23) are modified to accommodate all six displacement components shown in Fig. 4.1. The matrices become

$$\boldsymbol{B}_a = \frac{1}{L}[-1\ 0\ 0\ 1\ 0\ 0] \tag{4.25}$$

for the axial and

$$-y\boldsymbol{B}_b^T = -\frac{y}{L^3}\begin{bmatrix} 0 \\ 12x - 6L \\ 6xL - 4L^2 \\ 0 \\ -12x + 6L \\ 6xL - 2L^2 \end{bmatrix} \tag{4.26}$$

for the flexural element. Eq.(4.8) is then rewritten as

$$\boldsymbol{K} = \int_v [(\boldsymbol{B}_a - y\boldsymbol{B}_b)^T \boldsymbol{E}(\boldsymbol{B}_a - y\boldsymbol{B}_b)]\, dv \tag{4.27}$$

or as the following summation:

$$\boldsymbol{K} = \boldsymbol{K}_{aa} + \boldsymbol{K}_{ab} + \boldsymbol{K}_{ba} + \boldsymbol{K}_{bb} \tag{4.28}$$

where the components are expressed as follows:

$$\begin{aligned} \boldsymbol{K}_{aa} &= \int_v \boldsymbol{B}_a^T \boldsymbol{E} \boldsymbol{B}_a dv \\ \boldsymbol{K}_{ab} &= \int_v -y\boldsymbol{B}_a^T \boldsymbol{E} \boldsymbol{B}_b dv \\ \boldsymbol{K}_{ba} &= \int_v -y\boldsymbol{B}_b^T \boldsymbol{E} \boldsymbol{B}_a dv \\ \boldsymbol{K}_{bb} &= \int_v y^2 \boldsymbol{B}_b^T \boldsymbol{E} \boldsymbol{B}_b dv \end{aligned} \tag{4.29}$$

For convenience of integration, each part of Eq.(4.29) is decomposed in two integral terms as follows:

$$\begin{aligned} \boldsymbol{K}_{aa} &= \int_v \boldsymbol{B}_a^T \boldsymbol{E} \boldsymbol{B}_a dv = \int_A \boldsymbol{E} dA \cdot \int_L \boldsymbol{B}_a^T \boldsymbol{B}_a dx \\ \boldsymbol{K}_{ab} &= \int_v -y \boldsymbol{B}_a^T \boldsymbol{E} \boldsymbol{B}_b dv = -\int_A \boldsymbol{E} y dA \cdot \int_L \boldsymbol{B}_a^T \boldsymbol{B}_b dx \\ \boldsymbol{K}_{bb} &= \int_v y^2 \boldsymbol{B}_b^T \boldsymbol{E} \boldsymbol{B}_b dv = \int_A \boldsymbol{E} y^2 dA \cdot \int_L \boldsymbol{B}_b^T \boldsymbol{B}_b dx \\ \boldsymbol{K}_{ba} &= \boldsymbol{K}_{ab}^T \end{aligned} \qquad (4.30)$$

The variables in Eq. (4.30) have following properties: Matrix B_a is constant as shown in Eq. (4.25). Eq. (4.26) shows that matrix B_b is a variable of x only. These matrices will be integrated analytically. The stress-strain matrix E is temperature dependent and a function of both x and y. In this study each subelement, from the idealization of the beam element in thermal analysis, is assumed to have a uniform temperature. Thus for a given temperature E is constant for each subelement. The variable A is the section area of each subelement and is assumed constant along the element length L. Variable y gives the location of a subelement or the projected plane of the prestressing steel segment with respect to the reference axis of the element.

Based on the assumptions described above the stiffness matrix is evaluated term by term. The contribution of the prestressing steel to the element stiffness matrix is obtained by considering the steel segment as a subelement located at its projected reference plane defined in

Fig. 4.3. and given by Eq.(4.24). The first terms of Eq. (4.30) are integrated numerically as follows:

$$EA = \int_A E\,dA = \sum_{i=1}^{n_c} E_{ci}A_{ci} + \sum_{i=1}^{n_{ps}} E_{psi}A_{psi}$$

$$EQ = -\int_A Ey\,dA = -\sum_{i=1}^{n_c} E_{ci}y_{ci}A_{ci} - \sum_{i=1}^{n_{ps}} E_{psi}y_{psi}A_{psi} \qquad (4.31)$$

$$EI = \int_A Ey^2\,dA = \sum_{i=1}^{n_c} E_{ci}(I_{oi}+y_{ci}^2A_{ci}) + \sum_{i=1}^{n_{ps}} E_{psi}y_{psi}^2A_{psi}$$

where

n_c, n_{ps} = number of concrete subelements and steel segments respectively within an element,

A_{ps} = cross-section area of prestressing steel,

I_{oi} = second moment of area of a subelement about its centroid axis.

Integration of the second terms results in

$$\int_L \boldsymbol{B}_a^T\boldsymbol{B}_a\,dx = \frac{1}{L}\begin{bmatrix} 1 & 0 & 0 & -1 & 0 & 0 \\ & 0 & 0 & 0 & 0 & 0 \\ & & 0 & 0 & 0 & 0 \\ & SYM & & 1 & 0 & 0 \\ & & & & 0 & 0 \\ & & & & & 0 \end{bmatrix} \qquad (4.32)$$

$$\int_L \boldsymbol{B}_a^T\boldsymbol{B}_b\,dx = \frac{1}{L}\begin{bmatrix} 0 & 0 & 1 & 0 & 0 & -1 \\ 0 & 0 & 0 & 0 & 0 & 0 \\ 0 & 0 & 0 & 0 & 0 & 0 \\ 0 & 0 & -1 & 0 & 0 & 1 \\ 0 & 0 & 0 & 0 & 0 & 0 \\ 0 & 0 & 0 & 0 & 0 & 0 \end{bmatrix} \qquad (4.33)$$

$$\int_L \boldsymbol{B}_b^T \boldsymbol{B}_b \, dx = \frac{1}{L^3} \begin{bmatrix} 0 & 0 & 0 & 0 & 0 & 0 \\ & 12 & 6L & 0 & -12 & 6L \\ & & 4L^2 & 0 & -6L & 2L^2 \\ & & & 0 & 0 & 0 \\ & & SYM & & 12 & -6L \\ & & & & & 4L^2 \end{bmatrix} \tag{4.34}$$

The composite element stiffness matrix is obtained by substituting Eqs. (4.32), (4.33) and (4.34) back into Eq. (4.28). The resulting matrix is given by Eq. (4.35).

$$\boldsymbol{K} = \begin{bmatrix} \frac{EA}{L} & 0 & \frac{EQ}{L} & -\frac{EA}{L} & 0 & -\frac{EQ}{L} \\ 0 & \frac{12EI}{L^3} & \frac{6EI}{L^2} & 0 & \frac{-12EI}{L^3} & \frac{6EI}{L^2} \\ \frac{EQ}{L} & \frac{6EI}{L^2} & \frac{4EI}{L} & \frac{-EQ}{L} & \frac{-6EI}{L^2} & \frac{2EI}{L} \\ \frac{-EA}{L} & 0 & \frac{-EQ}{L} & \frac{EA}{L} & 0 & \frac{EQ}{L} \\ 0 & \frac{-12EI}{L^3} & \frac{-6EI}{L^2} & 0 & \frac{12EI}{L^3} & \frac{-6EI}{L^2} \\ \frac{-EQ}{L} & \frac{6EI}{L^2} & \frac{2EI}{L} & \frac{EQ}{L} & \frac{-6EI}{L^2} & \frac{4EI}{L} \end{bmatrix} \tag{4.35}$$

4.6. Incremental Strains in Concrete and Prestressing Steel

4.6.1. Concrete Deformations

Fig. 4.4 (a) shows the incremental displacements of the end nodes of a beam element after two successive operations. These displacements are with respect to the reference axis (RA). The centroid axis (CA) changes its location continuously due to changes in section properties. The incremental displacements are transformed to relate to the

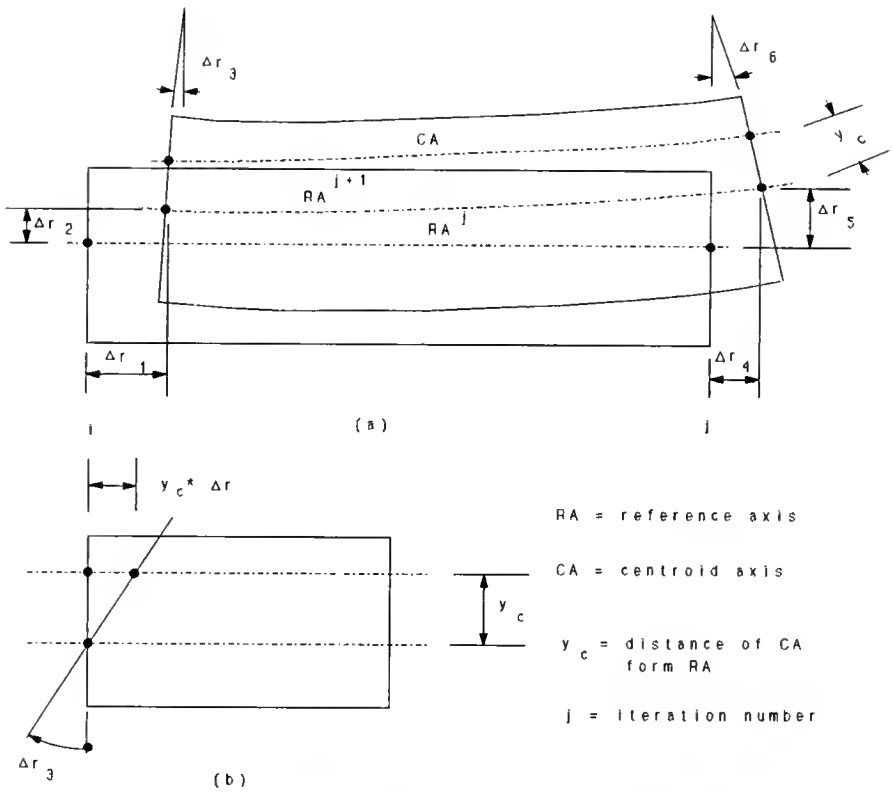

Fig. 4.4. Incremental nodal displacements

current location of the CA before computing the strains. The transformation is shown in Fig. 4.4 (b) and achieved by following expression:

$$\Delta r_1^{CA} = \Delta r_1^{RA} - y_c \Delta r_3$$
$$\Delta r_4^{CA} = \Delta r_4^{RA} - y_c \Delta r_6 \qquad (4.36)$$

Using the transformed values the effective incremental displacements translations and rotation are given by Eqs.(4.37) and (4.38), respectively.

$$\Delta x = \Delta r_4 - \Delta r_1$$
$$\Delta y = \Delta r_5 - \Delta r_2 \tag{4.37}$$

$$\Delta\theta = \Delta r_6 - \Delta r_3 \tag{4.38}$$

Curvature of the element local axis is expressed as

$$\Delta\phi = \frac{\Delta\theta}{L_o} \tag{4.39}$$

Incremental axial strain components are computed by

$$\Delta\epsilon_a = \frac{\Delta x}{L_o} \tag{4.40}$$

for axial action and

$$\Delta\epsilon_b = -y\Delta\phi \tag{4.41}$$

for bending action. L_o is the original element length and y is the distance from beam element centroid axis to the centroid of the subelement in considerations. The total incremental strain is obtained from summation of Eqs. (4.40) and (4.41), and expressed as

$$\Delta\epsilon = \Delta\epsilon_a + \Delta\epsilon_b \tag{4.42}$$

Cumulative incremental strain of a subelement for time step i and iteration j is given by Eq. (4.43).

$$\epsilon_i^j = \epsilon_i^{j-1} + \Delta\epsilon_i^J \tag{4.43}$$

4.6.2. Prestressing Steel Strains

Steel strain is first computed for the projected plane and then transformed to the correct profile. The procedure uses the following models:

$$\Delta\epsilon_b = -y_p \Delta\phi$$
$$\Delta\epsilon_{a\text{-}a} = \Delta\epsilon_a + \Delta\epsilon_b \qquad (4.44)$$
$$\Delta\epsilon = \Delta\epsilon_{A\text{-}A} = \frac{\Delta\epsilon_{a\text{-}a}}{\cos\alpha}$$

The cumulative strain for a steel segment is similarly computed from Eq. (4.43).

4.7. Load Vector due to Prestress Force

Element nodal forces resulting from prestress action are shown in Fig. 4.5. Following the definitions given in the figure the length of the steel segment and its orientation with reference to the x-axis of the element are computed as follows:

$$\Delta X = XJ - XI$$
$$\Delta Y = e_j - e_i$$
$$L_o = \sqrt{\Delta X^2 + \Delta Y^2} \qquad (4.45)$$
$$\cos\alpha = \frac{\Delta X}{L_o}$$
$$\sin\alpha = \frac{\Delta Y}{L_o}$$

where XI and XJ are the updated x-coordinates of element nodes i and j, respectively, and L_o is the original element length.

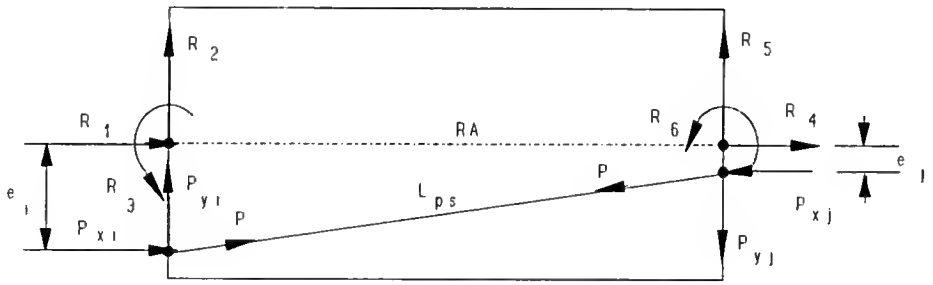

R_i (i = 1, . . . , 6) = element forces due to prestress action

P = tension in the tendon segment

P_x , P_y = components of P acting on concrete at interaction points

Fig.4.5. Idealization of Prestress Action into Beam Element Nodal Forces

Components of the prestress force along local axes are

$$P_x = P\cos\alpha$$
$$P_y = P\sin\alpha \qquad (4.45)$$

Translation of the components to element nodes i and j result in the following end moment expressions:

$$R_3 = M_i = -P_x e_i$$
$$R_6 = -M_j = P_x e_j \tag{4.47}$$

The element load vector due to prestress action is given by

$$\boldsymbol{R}_p = \{P_x \quad P_y \quad -P_x e_i \quad -P_x \quad -P_y \quad P_x e_j\}^T \tag{4.48}$$

4.8. Remarks

The formulation of the beam equations in this chapter is based on the standard displacement stiffness method. The evaluation of the stiffness matrix is performed term by term across the section element. This approach is applied in order to incorporate the variations of stiffness properties across the section due to the state of temperature distribution and stress-strain relationship within different parts of the section.

CHAPTER 5
SOLUTION METHOD FOR STRUCTURAL RESPONSE

5.1. Introduction

This chapter presents the technique for solving structural responses of prestressed concrete members subjected to high temperatures. The basic equilibrium equations to be solved are given as follows:

(a) At the beginning of a solution cycle

$$\begin{aligned} &(a) \quad \boldsymbol{K}\boldsymbol{r} = \boldsymbol{R} \\ &(b) \quad \boldsymbol{K}\Delta\boldsymbol{r} = \Delta\boldsymbol{R} \end{aligned} \tag{5.1}$$

where the stiffness function K and the applied load function R or ΔR are known. The task is to solve for the displacement function r or Δr.

(b) At the end of a solution cycle

$$\begin{aligned} &(a) \quad \boldsymbol{K}\boldsymbol{r} = \boldsymbol{F} \\ &(b) \quad \boldsymbol{K}\Delta\boldsymbol{r} = \Delta\boldsymbol{F} \end{aligned} \tag{5.2}$$

In this case the stiffness function K is an update based on the displacement function r or Δr computed in Eq. (5.1). The internal load function F is the unknown to be determined.

Techniques for evaluating the stiffness function K have been discussed in Chapter 4. The evaluation of the load

functions R and F requires the continuous determination of the following parameters in all solution cycles:

(a) Induction forces and

(b) effective prestress action

These parameters are discussed below.

5.2. Induction Forces

Induction forces are defined here as those forces which are caused by stress induced in the system as a result of the effects of temperature on properties of concrete and prestressing steel. The induction force vector ΔG is given by

$$\Delta G = \frac{\Delta\sigma}{L}\begin{Bmatrix} -A \\ 0 \\ yA \\ A \\ 0 \\ -yA \end{Bmatrix} \tag{5.3}$$

$$\Delta\sigma = \Delta\sigma^T + \Delta\sigma^D + \Delta\sigma^S$$

where $\Delta\sigma$ is the vector of the induced stress. The main contributing factors to the induced stress function are

(a) thermal and shrinkage strain of concrete ($\Delta\sigma^T$),

(b) strength degradation ($\Delta\sigma^D$) and

(c) shift in stress-strain relation ($\Delta\sigma^S$).

5.2.1. Thermal and Shrinkage Strain

Stresses induced to the system due thermal and shrinkage strains are the equivalent mechanical stresses required to effect equal strains if the system was free to undergo the deformation. Thermal strains of concrete are computed using Eq. (3.10) and shrinkage strains by Eq. (3.11). For each section subelement the induced thermal and shrinkage stresses at time step i are given by

$$\Delta\sigma_i^T = E_i \Delta\epsilon_i^T \tag{5.4}$$

where

$\Delta\sigma_i$ = induced stresses

$\Delta\epsilon_i$ = thermal and shrinkage strain

E_i = valid modulus

Since the temperature of a subelement does not change within a time step stresses due to thermal and shrinkage strains remain constant in all operations within a time step. They are computed at the beginning of the time step only.

5.2.2. Strength Degradation

Based on the material property-temperature relationship both concrete and prestressing steel degrade as temperature increases. Degradation is defined here as the deterioration in strength and stiffness properties. A concrete subelement is considered degraded when

(a) crushed: $\sigma_i \geq f'_c(T_i)$ determined by Eq. (3.7)

(b) cracked: $\sigma_i \geq f_t(T_i)$ determined by Eq. (3.8)

(c) $E_c \leq 0$ as determined by Eq. (3.4).

Criteria for prestress steel degradation are

(a) tension failure: $f_{ps} \geq f_{pu}(T_i)$ determined by Eq. (3.16)

(b) $E_s \leq 0$ as determined by Eq. (3.4).

Concrete subelements and steel segments flagged as degraded are excluded in the computation of section properties. The stress which was previously carried by a degraded concrete subelement is redistributed into the system. The above parameters controlling the material degradation are both temperature and strain dependent. Since total strain may change within a time step, these induced stresses are computed for each iteration. The stresses induced into the system due to degradation are expressed as

$$\Delta\sigma_{i+1}^{D,j+1} = \Delta\sigma_{i+1}^{j} \tag{5.5}$$

where i is the time step and j is the iteration number. Superscript D is an indicator for degradation induced function. For prestressing steel, the degraded steel segments do not contribute to the prestress action of the containing beam element.

5.2.3. Shift in stress

At the beginning of a time step the active stress-strain curve may change due to new temperature range. The resulting effect is that a concrete subelement will support less stress though the strain remains the same. This phenomenon is illustrated in Fig. 5.1. The stress induced in the system due to this concrete behavior is given by

$$\Delta\sigma^{S}_{i+1} = \sigma^{j}_{i} - \sigma^{0}_{i+1} \qquad (5.6)$$

where S indicates source as stress shift, and j is the last iteration of the previous time step.

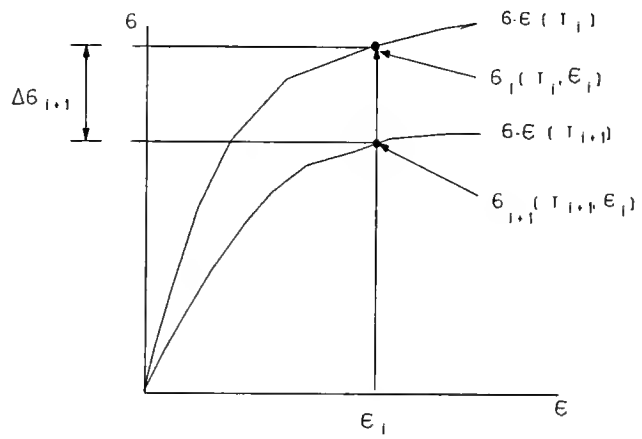

Fig. 5.1. Shift of stress-strain curve

5.3. Effective Prestress Action

Prestress action in a beam element is dependent on the effective tension in the contained steel segments. The tension in a steel segment is a function of total steel strain for a particular temperature range. Since strain changes with each iteration, steel tension has to be updated continuously within each time step.

The theoretical steel tension is subject to reduction due to partial loss of stress. The function considered in this study as the main sources of loss of prestress are stress relaxation, thermal and shrinkage strains of concrete and thermal strain of steel. The strains caused by these parameters are assumed to remain constant within a time step hence are determined at beginning of each time step. Though steel modulus and stress may change within a time step, for simplicity the partial loss of stress is held constant within a time step.

For a time step i the loss of stress is expressed as

$$\Delta\sigma_i = E^0_{ps,i}(\Delta\epsilon_{ps\theta,i} + \Delta\epsilon_{c\theta,i} + \Delta\epsilon_{sh,i} + \Delta\epsilon_{cr,i})$$
$$\sigma_i = \sigma_{i-1} + \Delta\sigma_i \qquad (5.7)$$

where

$\epsilon_{ps\theta}$ = thermal strain of steel, from Eq. (3.19)

$\epsilon_{c\theta}$ = thermal strain of concrete, from Eq. (3.10)

ϵ_{sh} = shrinkage strain, from Eq. (3.11)

ϵ_{cr} = creep strain of steel, from Eq. (3.20)

E_{ps} = modulus of steel at the beginning of time step, from Eq. (3.4)

The effective prestress force for time step i and iteration j is computed by following expressions:

$$f^j_{ps,i} = f^j_{ps,i} - \sigma_i$$
$$P^j_i = f^j_{ps,i} A_{ps} \tag{5.8}$$

where

A_{ps} = section area of prestress steel,

σ = cumulative stress loss, from Eq. (5.7)

5.4. Evaluation of Action Load Vector

The action load vector is defined as the effective loading of the system. It is derived from externally superimposed node and element loads, equivalent element node loads due to prestress action and induction forces discussed in Section 5.2. The transformation of the imposed element load into equivalent node loads is shown in Fig. 5.2.

Equivalent nodal load vector is then expressed as

$$\boldsymbol{R}^T_b = \{R1,\ R2,\ R3,\ R4,\ R5,\ R6\}$$
$$= \frac{b_y L}{12}\{0,\ 6,\ L,\ 0,\ 6,\ -L\} \tag{5.9}$$

where b_y is the uniform superimposed load acting in the positive y-direction. The action load vector is the summation of results of Eqs. (4.48), (5.1), (5.9) and external node loads. Thus for the time step i

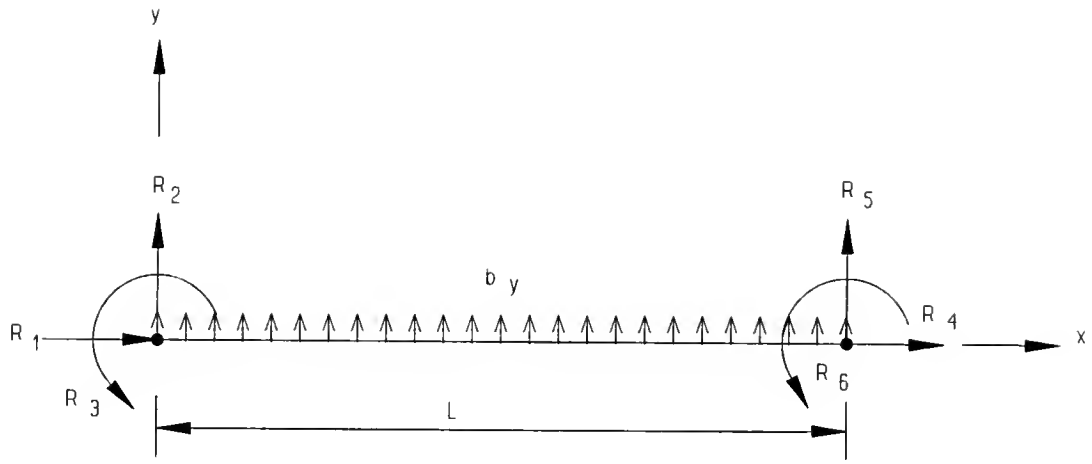

Fig. 5.2. Equivalent nodal forces

and iteration j the action load vector R is given by

$$R^{j}_{a,i+1} = R_n + R^{j}_{p,i+1} + R^{j}_{g,i+1} \tag{5.10}$$

where vector R_g is induction load vector given by Eq.(5.1) and R_p is the equivalent prestress load vector given by Eq.(4.48) which have been adjusted by Eq.(5.8). R_n is constant and includes elements of Eq.(5.9) and external point loads. Vector R_a is computed for each iteration due to the changing vectors R_g and R_p.

5.5. Solution of Displacement Response

The equilibrium equations to be solved for structural displacement responses are Eqs. (5.1) and (5.2). Action load vector R is computed by Eq. (5.10). Fig. 1.2. shows

that the internal load function F attains a different curve for each time step as the system attains a new deformed equilibrium state r. This characteristic is caused by changes in prestress load function P and stiffness function S as depicted in Fig. 1.3. The shifting behavior of the function F curve presents complications in the accurate determination of the new value of F at the beginning of each time step.

To avoid the problems of tracing a new curve of the function F in each time step, a method of unbalanced load adjustment is utilized. The strategy in this approach is to determine an equivalent incremental load function which will cause increment in the structure deformation from the equilibrium deformation attained in the previous time step. The computation techniques for the first time step are therefore different from the other time steps. The solution process in the first time step is shown in Fig. 5.3.

The initial operations involved in solving Eqs. (5.1) and (5.2) in the first cycle of the first time step are

$$\begin{aligned} &(a) \quad r_1^0 = 0 \\ &(b) \quad K_1^0 = f(r_1^0) \\ &(c) \quad R_1^0 = f(L, P(r_1^0)) \\ &(d) \quad K_1^0 \Delta r_1^1 = R_1^0 \end{aligned} \tag{5.11}$$

where letter f indicates functional dependence. Operations in subsequent iterations are expressed as follows:

$$
\begin{aligned}
&(a) \quad r_1^j = r_1^{j-1} + \Delta r_1^j \\
&(b) \quad K_1^j = f(r_1^j) \\
&(c) \quad \Delta F_1^j = K_1^j \Delta r_1^j \\
&(d) \quad R_1^j = f(L, P(r_1^j)) \\
&(e) \quad U_1^j = R_1^j - F_1^j \\
&(f) \quad K_1^j \Delta r_1^j = U_1^j
\end{aligned}
\tag{5.12}
$$

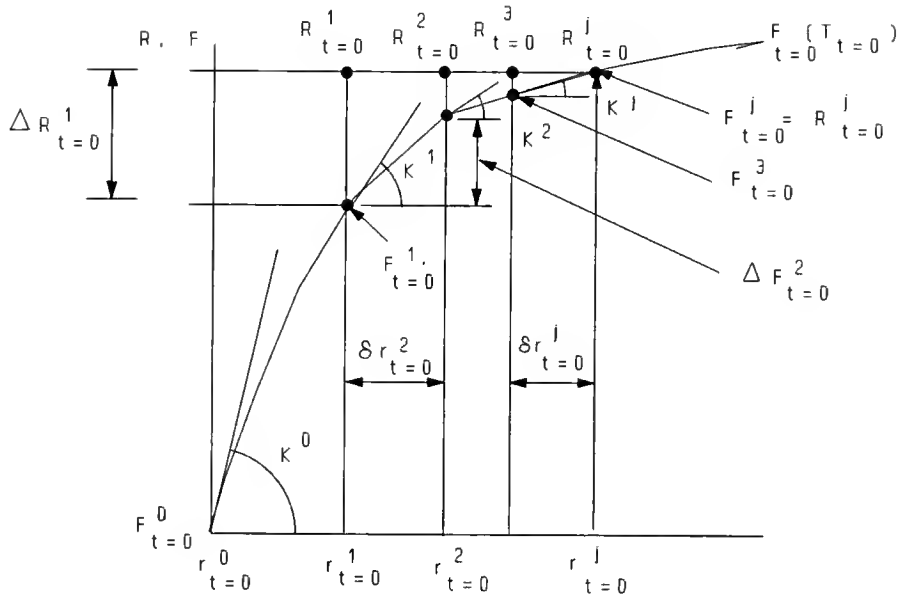

Fig. 5.3. Solution of equilibrium equations: 1st time step

where U is the unbalanced load vector to be determined.

The solution process for other time steps involves determination of incremental action load, and the incremental internal load vector. The process is presented graphically in Fig. 5.4.

The incremental loads to be computed at the beginning of each time step are

(a) induction forces due to thermal and shrinkage strain, material degradation and shift in stress-strain relation law and

(b) changes in the prestress action.

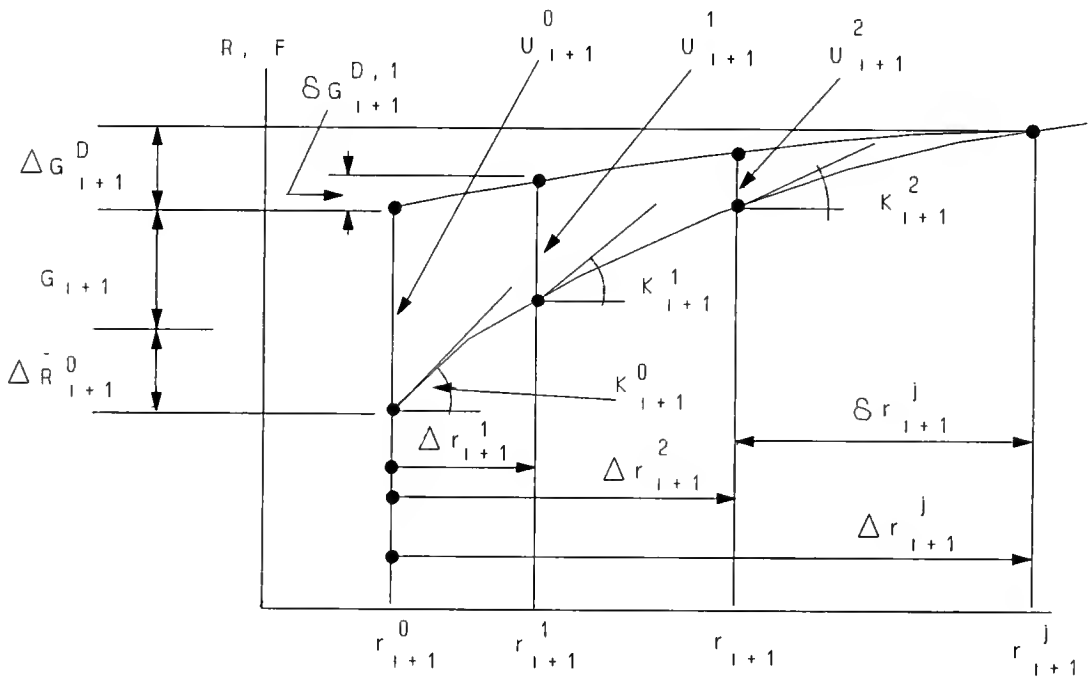

Fig. 5.4. Solution process at subsequent time steps

The operations required in this stage to compute the incremental loads are given by the following expressions:

$$
\begin{aligned}
&(a) \quad r^0_{i+1} = r^j_i \\
&(b) \quad K^0_{i+1} = f(r^0_{i+1}) \\
&(c) \quad \Delta\sigma^S_{i+1} = \sigma_i(T_i, \epsilon_i) - \sigma_{i+1}(T_{i+1}, \epsilon_i) \\
&(d) \quad G_{i+1} = f\left(\Delta\sigma^S_{i+1}, \Delta\sigma^T_{i+1}, \Delta\sigma^{D,0}_{i+1}\right) \qquad (5.13) \\
&(e) \quad \Delta\overline{R}^0_{i+1} = \overline{R}^0_{i+1}(L, P^0_{i+1}) - \overline{R}^j_i(L, P^j_i) \\
&(f) \quad \Delta R^0_{i+1} = \Delta\overline{R}^0_{i+1} + G_{i+1} + U^j_i \\
&(g) \quad K^0_{i+1}\Delta r^1_{i+1} = \Delta R^0_{i+1}
\end{aligned}
$$

where

U = unbalanced load function carried forward from the previous time step,

S = indicates induced stress due to shift in stress,

T = indicate induced stress due to thermal effects (shrinkage and expansion)

D = indicate induced stress due to material degradation (crushing or cracking)

Parameters to be computed in the subsequent iteration include

(a) current deformation of the system,

(b) update of stiffness matrix,

(b) induction force due to material degradation,

(c) update of prestress action and

(d) incremental internal load function.

Mathematically, these operations are described in Eq. (5.14). The total incremental displacement within a time step is given by Eq. (5.15). For both equations j

$$
\begin{aligned}
&(a) \quad r_{i+1}^{j} = r_{i+1}^{j-1} + \delta r_{i+1}^{j} \\
&(b) \quad K_{i+1}^{j} = f(r_{i+1}^{j}) \\
&(c) \quad \delta F_{i+1}^{j} = K_{i+1}^{j} \delta r_{i+1}^{j} \\
&(d) \quad \Delta F_{i+1}^{j} = \Delta F_{i+1}^{j-1} + \delta F_{i+1}^{j} \\
&(e) \quad \overline{R}_{i+1}^{j} = f(L, P_{i+1}^{j}) \\
&(f) \quad \delta \overline{R}_{i+1}^{j} = \overline{R}_{i+1}^{j} - \overline{R}_{i+1}^{j-1} \\
&(g) \quad \delta G_{i+1}^{D,j} = f\left(\sigma_{c,i+1}^{j}(r_{i+1}^{j}),\ f'^{,j}_{c,i+1}(T_{i+1})\right) \\
&(h) \quad \Delta R_{i+1}^{j} = \Delta R_{i+1}^{j-1} + \delta \overline{R}_{i+1}^{j} + \delta G_{i+1}^{j} \\
&(i) \quad U_{i+1}^{j} = \Delta R_{i+1}^{j} - \Delta F_{i+1}^{j} \\
&(j) \quad K_{i+1}^{j} \delta r_{i+1}^{j+1} = U_{i+1}^{j}
\end{aligned}
\tag{5.14}
$$

$$
\Delta \boldsymbol{r}_{i+1}^{j} = \sum_{1}^{j} \delta \boldsymbol{r}_{i+1}^{j} \tag{5.15}
$$

represents the number of iterations and $\delta \mathbf{r}_{i+1}$ is the displacement increment for each iteration. Total structure displacement response vector at the end of iteration j for the time step i+1 is determined by

$$
\boldsymbol{r}_{i+1}^{j} = \boldsymbol{r}_{i+1}^{0} + \Delta \boldsymbol{r}_{i+1}^{j} \tag{5.16}
$$

At the end of each iteration the system is tested for load convergence. The acceptable load tolerance level ϵ_R is determined by the following expression:

$$
\left\| \frac{U_{i+1}^{j}}{\frac{1}{2}\left(\Delta R_{i+1}^{j} + \Delta F_{i+1}^{j}\right)} \right\| \leq \epsilon_R \tag{5.17}
$$

5.7. Local and Global Values

The computations above involve transformation of matrices and vectors from local element to global structural coordinates, and vice versa. The transformation matrix **a** is expressed as

$$\boldsymbol{a} = \begin{bmatrix} c & s & 0 & & & \\ -s & c & 0 & & 0 & \\ 0 & 0 & 1 & & & \\ & & & c & s & 0 \\ & 0 & & -s & c & 0 \\ & & & 0 & 0 & 1 \end{bmatrix} \tag{5.18}$$

where

$c = \cos\ \theta$

$s = \sin\ \theta$

θ = angle between global and local x-axes

Thus the element stiffness matrix $\mathbf{K}_e$, given by Eq.(4.35), is transformed to structure matrix $\mathbf{K}_s$ by

$$\boldsymbol{K}_s = \boldsymbol{a}^T \boldsymbol{K}_e \boldsymbol{a} \tag{5.19}$$

The element load vector ($\mathbf{R}_e$) due to superimposed uniform load given by Eq. (5.9), and the equivalent prestress nodal action given by Eq. (4.48), is transformed to global load vector $\mathbf{R}_s$ by the following expression:

$$\boldsymbol{R}_s = \boldsymbol{a}^T \boldsymbol{R}_e \tag{5.20}$$

The global nodal displacements given by Eq. (5.16) are transformed to element nodal displacements by

$$\boldsymbol{r}_e = \boldsymbol{a}\boldsymbol{r}_s \tag{5.21}$$

5.8. Computation of Moment Capacity Response

The basic moment capacity equation for flexural members is given by Eq. (1.1). The moment equation is rewritten as

$$R = \frac{1}{r_c(0.85 f'_c b)}$$

$$r_s = \left(1 - \frac{0.5\rho f_{pu\theta}}{f'_c}\right) \tag{5.22}$$

$$M_{u\theta} = \sum_{i=1}^{n}\left[r_s F^i_{pu\theta}\left(d^i - 0.5 R r_s F^i_{pu\theta}\right)\right]$$

where

r_c = temperature coefficient of compressive strength of concrete,

r_s = coefficient for steel stress at ultimate load

n = number of steel segments contained in a beam element

Within the limits of the heat transmission end point criteria the average loss of compressive strength of concrete in the compression zone is 2% [6]. Therefore the coefficient r_c equals 0.98. At fire temperatures the coefficient r_s is taken as equal to 0.98 [57].

CHAPTER 6
COMPUTER IMPLEMENTATION

6.1. Introduction

The numerical procedures presented in Chapters 2 to 5 have been incorporated in the computer program PRECET (PREstressed Concrete subjected to Elevated Temperatures). This chapter describes the structure of the program. The instructions for preparation of input data file are given in Appendix A.

6.2. Main Program PRECET

The program PRECET consists of all the routines for reading and initial processing of input data. As the primary executor PRECET transfers initial controls to data modules and then to executors for temperature analysis, TEDIAN and for response analysis, STREAN. The hierarchical structure of the program PRECET is presented in Fig. 6.1.

6.3. Program TEDIAN

TEDIAN, TEmperature DIstribution ANalysis, is the executor for temperature distribution. It incorporates procedures discussed in Chapter 2.

In each time step TEDIAN is called first to determine temperature distribution across the beam cross-section. Temperature values for the subelement are saved for use in computing temperature-dependent material properties. The flow chart of the program TEDIAN is shown in Fig. 6.2.

6.4. Program STREAN

The program STREAN, STructure REsponse ANalysis is the main executor of response analysis. It incorporates procedures described in Chapters 4 and 5.

STREAN is activated at each time step after temperature analysis. It calls the material property routines to compute relevant properties of each subelement based on its temperature.

The flow chart of the execution logic of program STREAN is presented graphically in Fig. 6.3.

6.5. Program MAPRAN

MAPRAN, MAterial PRoperty ANalysis, consists of several independent modules each of which computes a specific property. The formulation of the routines is based on the material properties and procedures presented in Chapter 3.

Thermal property routines are called from TEDIAN while deformation and mechanical property modules are called from program STREAN.

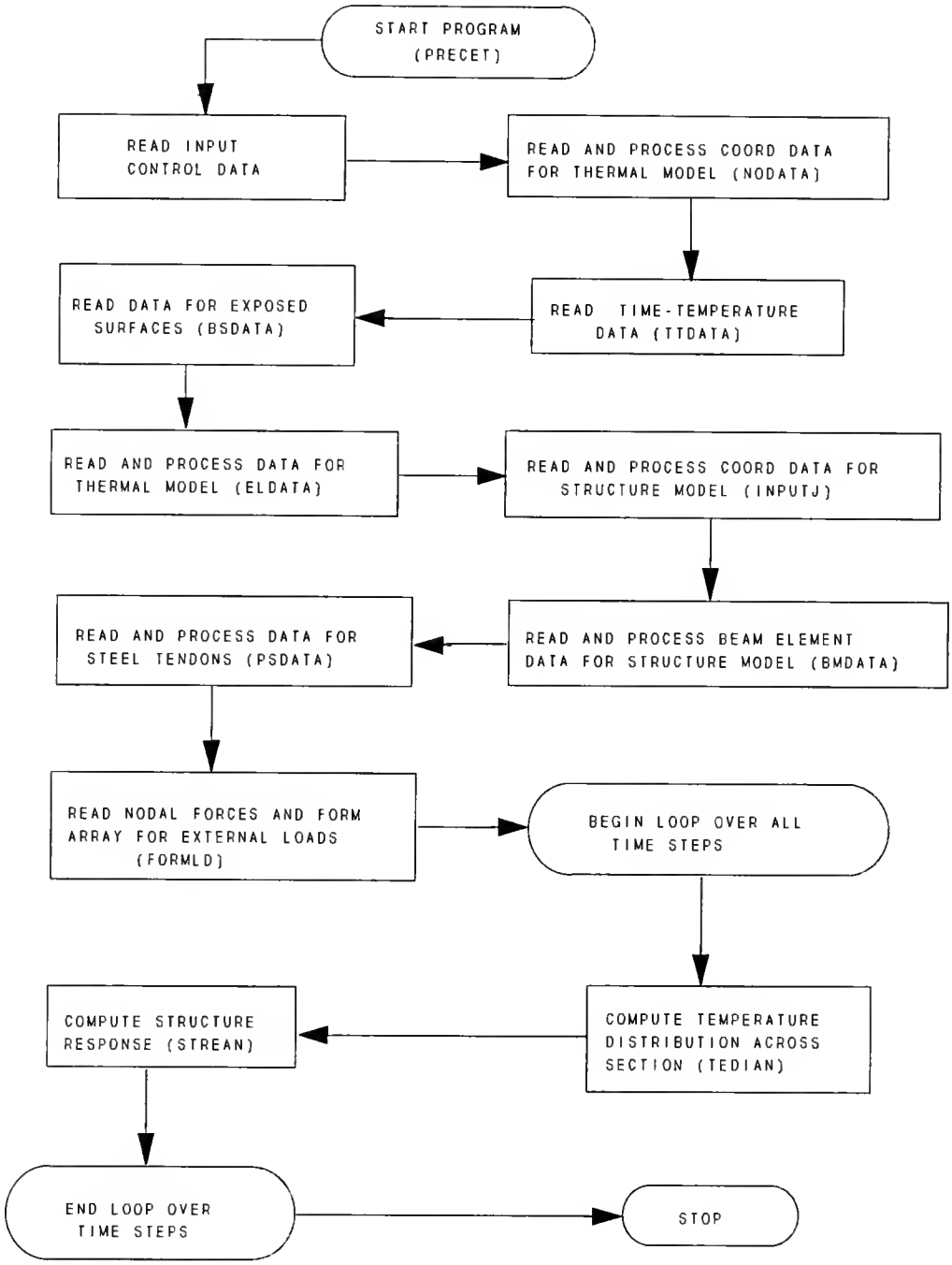

Fig. 6.1. Flow Chart of Program PRECET

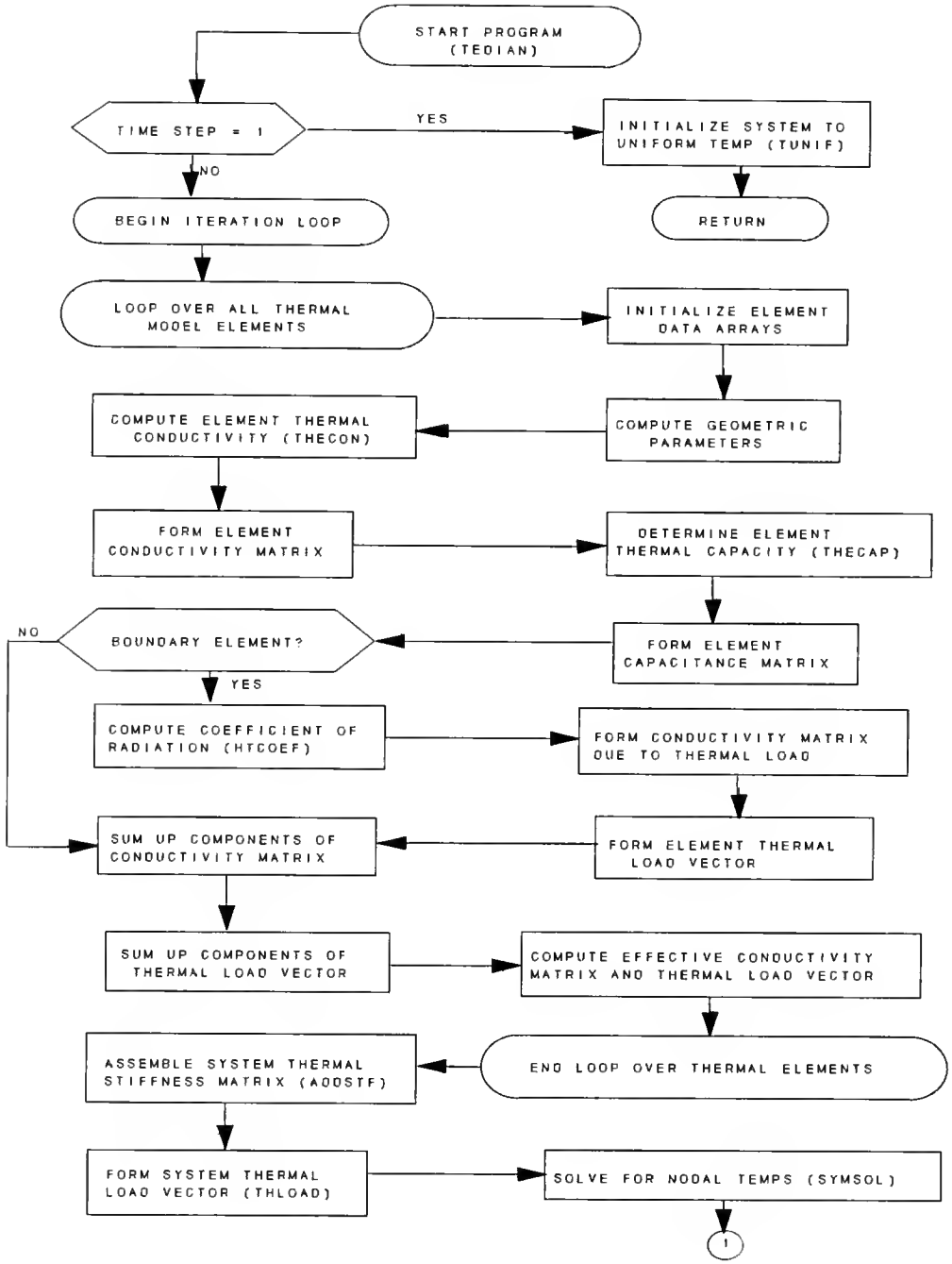

Fig. 6.2. Flow Chart for Temperature Distribution Analysis Program (TEDIAN)

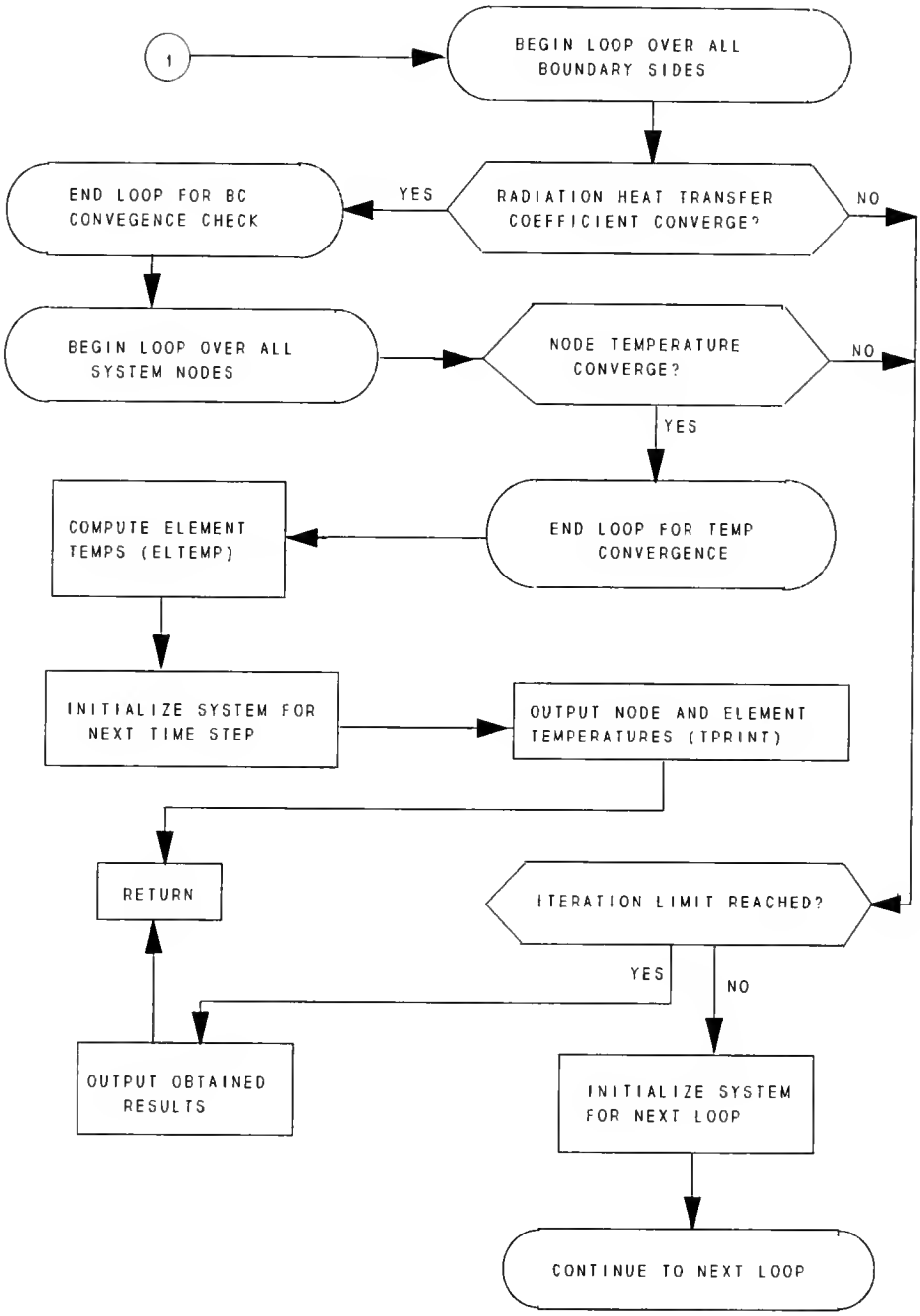

Fig. 6.2. Flow Chart for Temperature Distribution Analysis Program (TEDIAN) (cont'd).

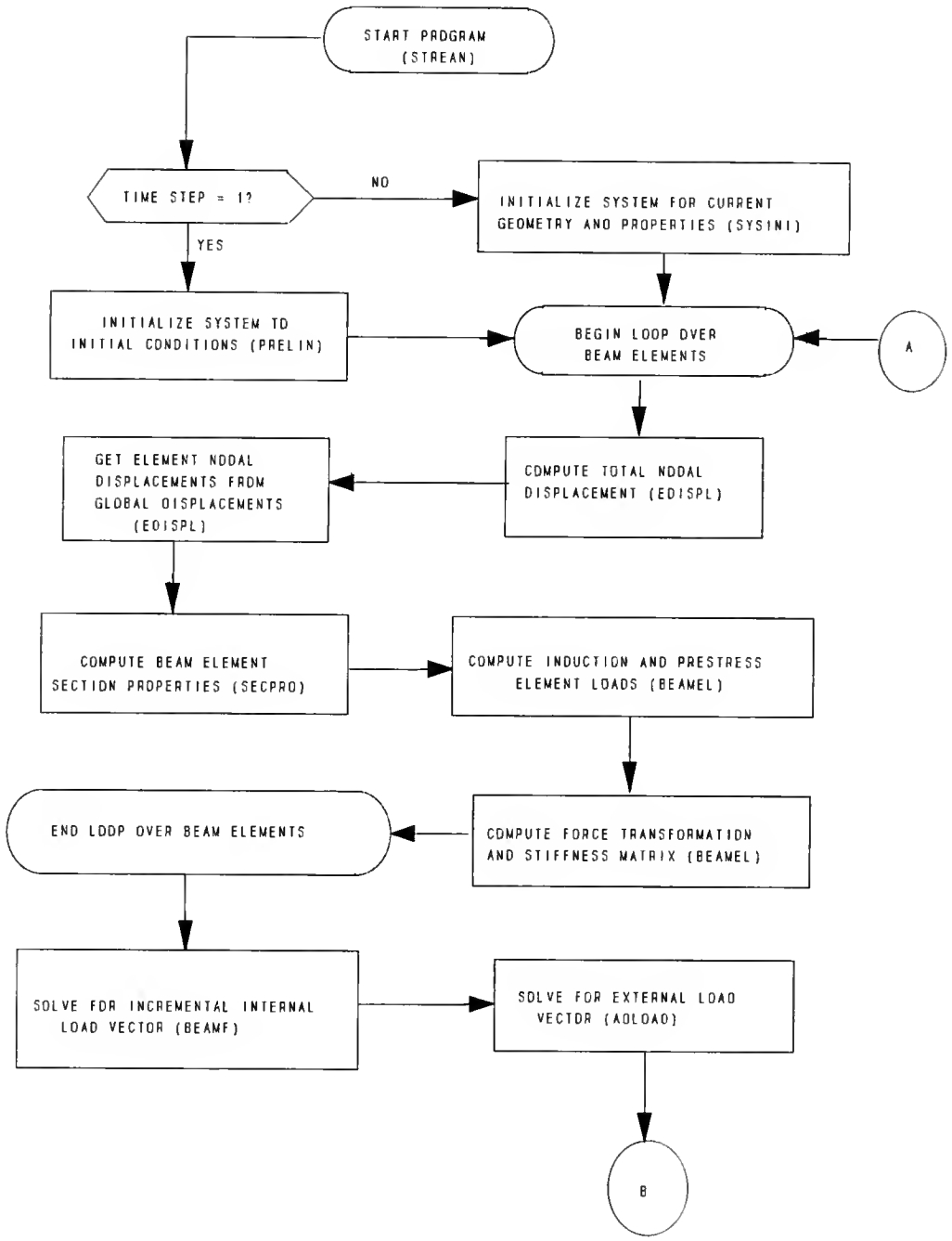

Fig. 6.3. Flow Chart for Structure Response Program (STREAN)

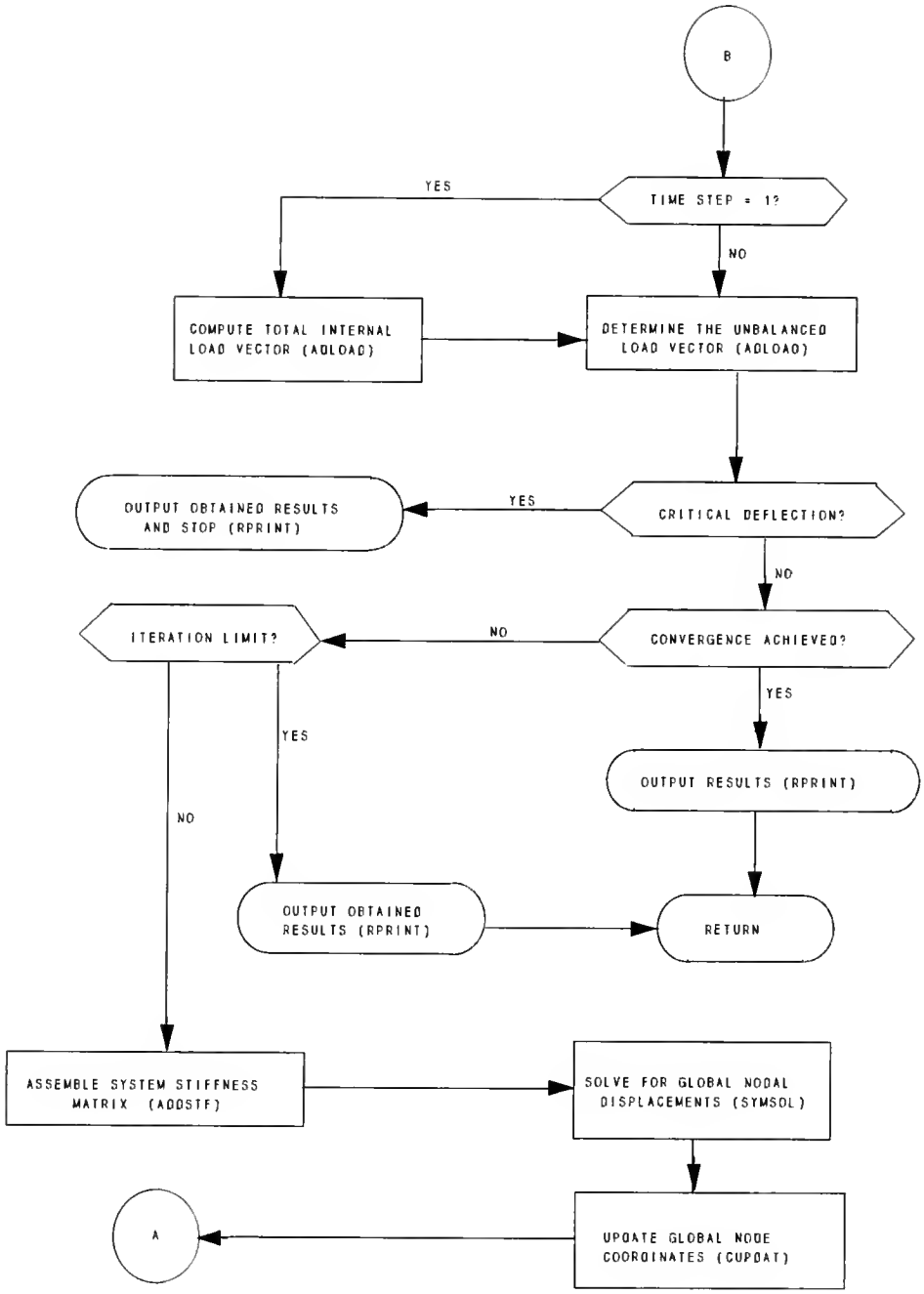

Fig. 6.3. Flow Chart for Structure Response Program (STREAN) (cont'd).

CHAPTER 7
NUMERICAL ANALYSIS

7.1. Introduction

This chapter presents the results of the application of program PRECET in predicting the structural response of prestressed concrete members subjected to elevated temperatures. The structural configurations analyzed have been subjected to standard fire tests. The results of the numerical model are compared with those obtained from the fire tests.

Two sets of problems analyzed are prestressed concrete beams and prestressed concrete slabs. Results presented include temperature distribution, mid-span deflection and moment capacity ratio for beams, mid-span deflection and moment capacity ratio for slabs.

7.2. Analysis of Prestressed Concrete Beams

7.2.1. Description of Test Specimen

The beam configurations used in the analysis are based on the fire tests conducted on eighteen prestressed concrete beams at the Portland Cement Association's Beam Furnace [2]. All the beams had identical cross-section and of the same

span of 20 ft. Types of concrete used were normal weight and lightweight aggregates. Three cover thicknesses of 1, 2, and 3 in. were investigated for each concrete type.

The specimens were divided in six groups each of three identical beams. The first three groups were of beams made of normal weight, silicious aggregate concrete and the rest were made of lightweight expanded shale concrete. The three groups in each concrete type were categorized in terms of the concrete covers described above.

7.2.2. Beam Testing

Fig. 7.1 (a) shows a schematic of the test setup for the beam fire test. During the test steel temperatures at selected locations in concrete were measured at five sections, A, B, C, D and E along the beam length. The beams were loaded with a design service load distributed along the beam length at five locations as shown in Fig. 7.1 (a).

Reported test results for each group have been averaged from results of the three beams in each group. In addition temperatures averages were determined from readings along the beam length. Temperature readings from the extreme locations, A and E, were lower than at sections B, C and D. For this reason only temperature values from sections B, C and D were used in computing the averages.

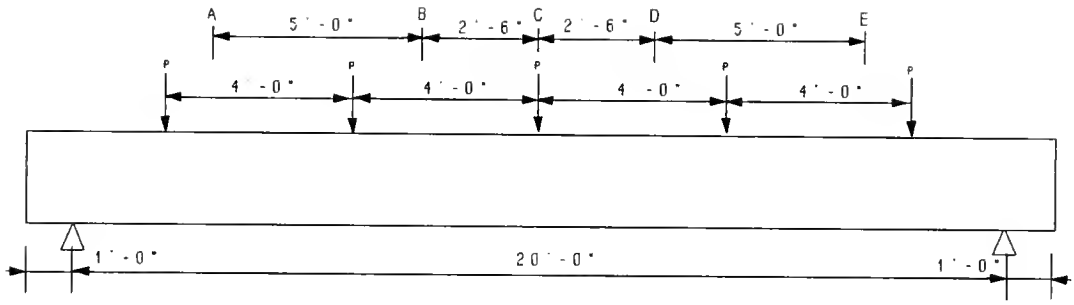

A, B, C, D, E are thermocouple locations

a) PC Beam Specimen

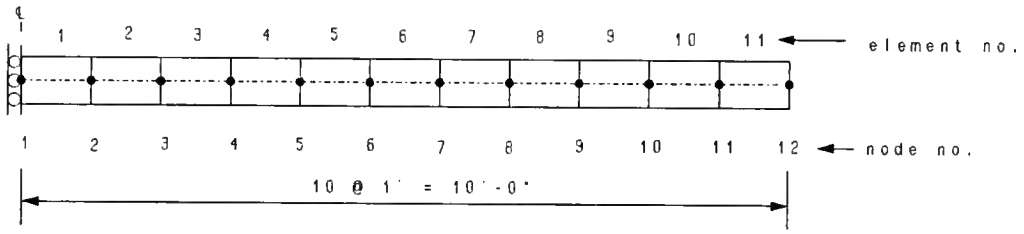

b) Finite Element Beam Element Model

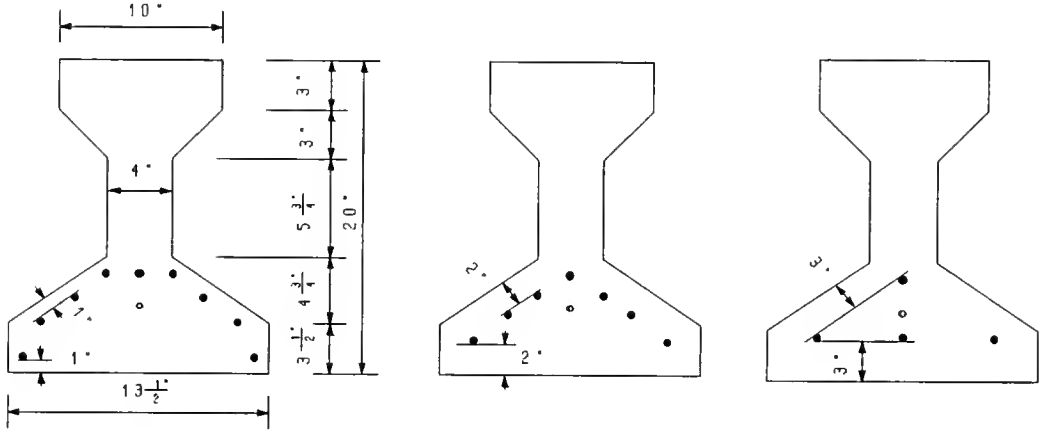

1" Cover 2" Cover 3" Cover

● 1/8" dia. prestressing steel strand

○ 0.195" dia. prestressing steel wire

c) Beam Sections Showing PS Paterns

Fig. 7.1. Design details of PC beam specimens

7.2.3. Design Details

The details of section design and prestress steel arrangements for the three beam categories are shown in Fig. 7.1 (c). Design specifications for materials and loadings are described below.

7.2.3.1. Materials

Prestressing steel specifications were

(a) Ultimate Strength, f_{pu} = 250,000 psi.

(b) Initial Prestress, $f_{si} = 0.7f_{pu}$ = 175,000 psi.

(c) Size of Prestress Steel Strand, ϕ_s = 3/8 in.

(d) Size of Prestress Steel Wire, ϕ_w = 0.195 in.

(e) Initial Force on each Strand = 14,000 lb.

(f) Initial Force on each Wire = 5,250 lb.

(g) Estimated Loss of initial Prestress = 18%.

Concrete data specifications were

(a) Compressive Strength, f'_c = 5000 psi, at 28 days.

(b) Minimum Concrete Strength, f'_{ci} = 4000 psi, at the time of transfer of steel stress to concrete.

(c) Unit Weight of Concrete is 145 pcf for normal weight and 97 pcf (2/3 of normal) for lightweight.

7.2.3.2. Superimposed loads

The superimposed load at each loading point for normal weight beams and each cover category are

(a) Beam # NWBEAM1: P = 28,000 lb.

(b) Beam # NWBEAM2: P = 21,650 lb.

(c) Beam # NWBEAM3: P = 12,500 lb.

Loads on lightweight beams are

(a) Beam # LWBEAM1: P = 28,000 lb.

(b) Beam # LWBEAM2: P = 21,650 lb.

(c) Beam # LWBEAM3: P = 12,500 lb.

7.2.3.3. Other design parameters

The minimum age of concrete during fire tests was one year. During that period all the beams were exposed to an environment of 35% RH at 73 °F. All beams were subjected to fire test while supporting their design service loads over a span of 20 ft. The limit of mid span deflection was selected at 15 in. This was estimated to occur only a few minutes before actual structural failure.

7.2.4. Numerical Model

Both normal and lightweight beam specimens were analyzed for temperature distribution, displacement response and moment capacity. The model for thermal analysis consisted of a mesh of 116 nodal points and 176 triangular elements over the half width of the cross section. Structure analysis problem was modeled using a system of 11

beam elements and 12 nodes over the half beam span. The finite element idealization of the structure model is shown in Fig. 7.1 (b).

7.2.5. Numerical and Test Result

Numerical results for temperature distribution and midspan deflections of all specimen groups have been plotted together with test results for comparison. No test results were available for moment capacity ratio therefore only results from numerical analysis are plotted.

7.2.5.1. Temperature distribution results

Results for temperature distribution for certain tendon locations are plotted in Figs. 7.2 to 7.4 for normal weight concrete beams and Figs. 7.5 to 7.7 for lightweight concrete beams. Numerical results show relatively good agreement with the test results for most of the exposure periods.

Fig. 7.8 shows average temperature distribution of the beam sides which are exposed to fire. Temperature values for lightweight concrete tend to be slightly higher than those for normal weight concrete. This may be due to the relative poor temperature distribution properties of lightweight concrete.

Fig. 7.9 presents the average coefficients of radiation heat transfer for both normal weight and lightweight concretes. The computations of the coefficients are based

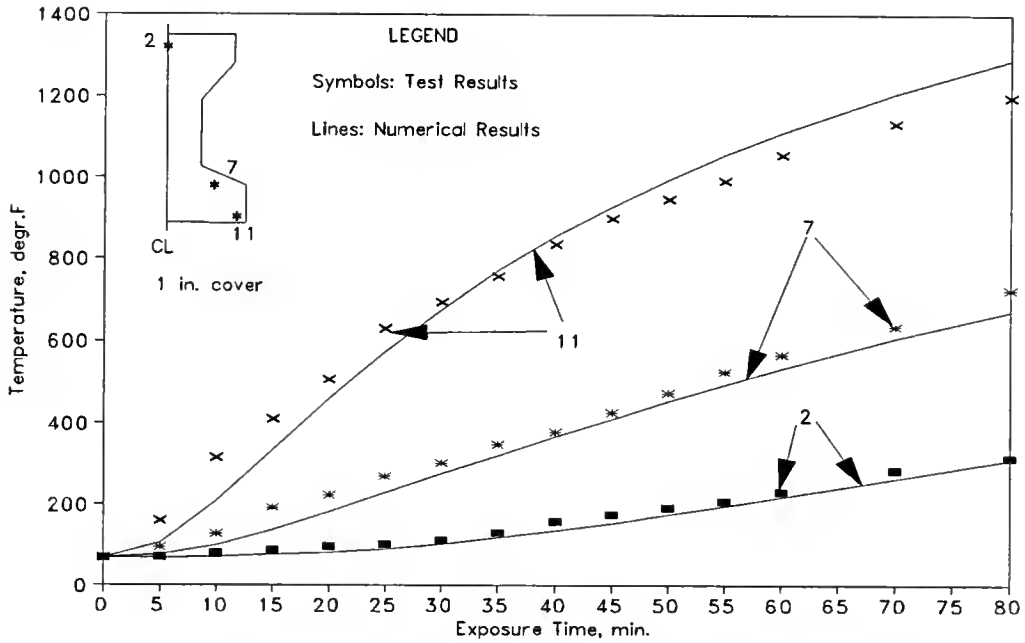

Fig. 7.2. Temperature distribution, normal weight beam, 1 in. concrete cover

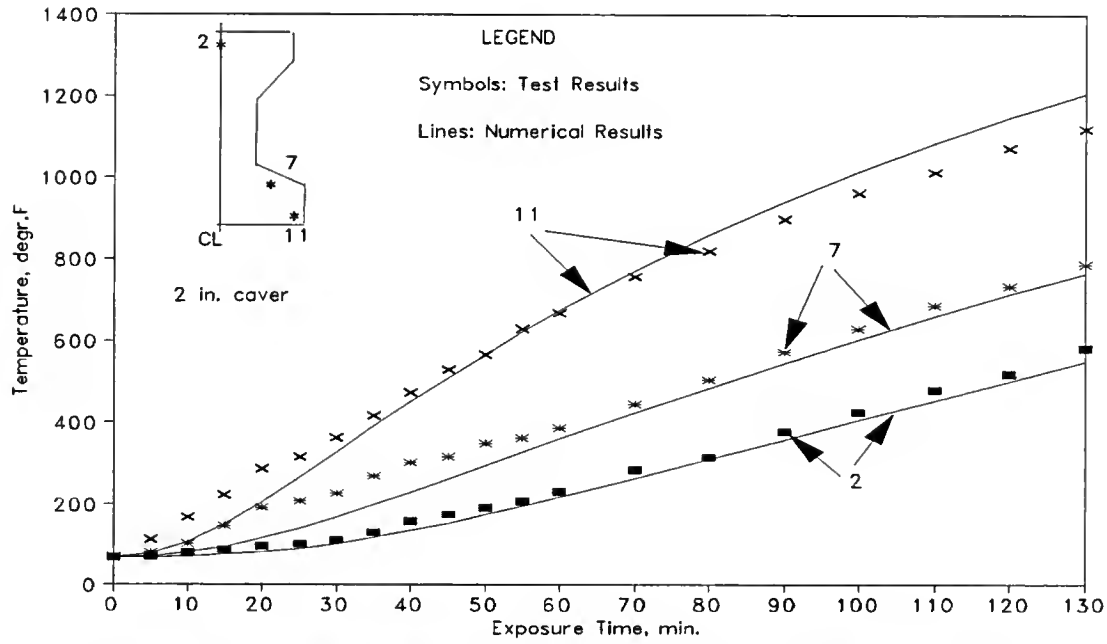

Fig. 7.3. Temparature distribution, normal weight beam, 2 in. concrete cover

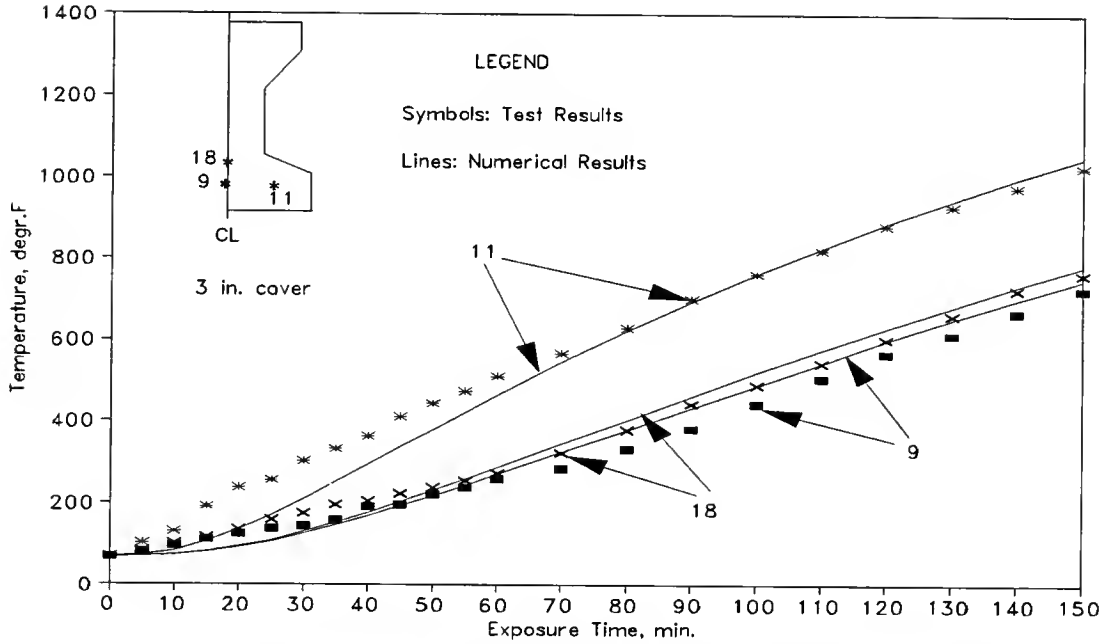

Fig. 7.4. Temperature distribution, normal weight beam, 3 in. concrete cover

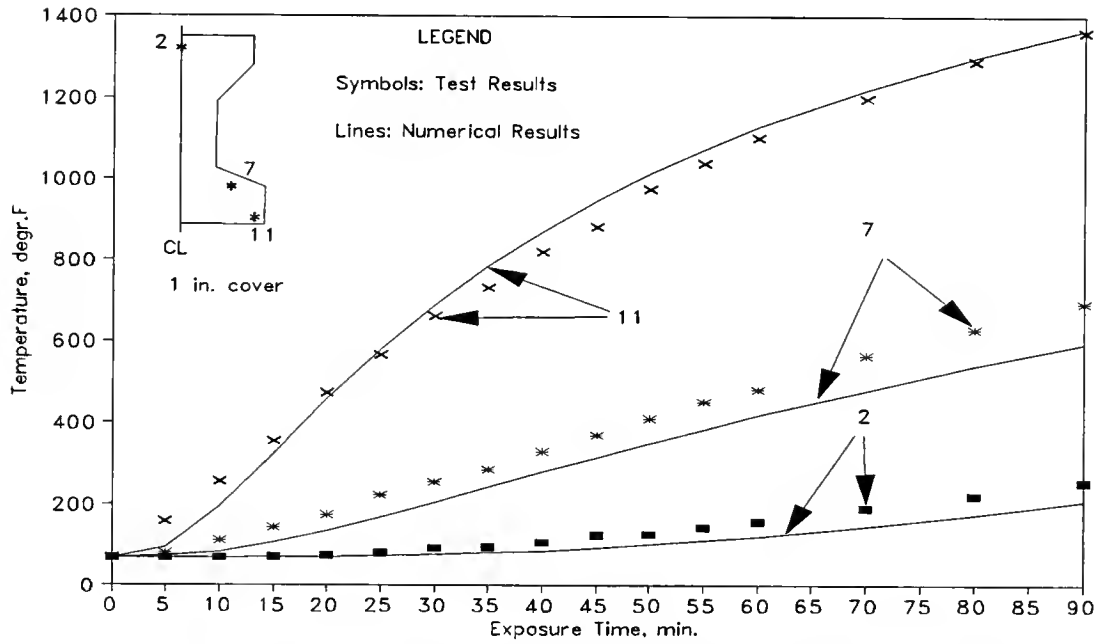

Fig. 7.5. Temperature distribution, lightweight beam, 1 in. concrete cover

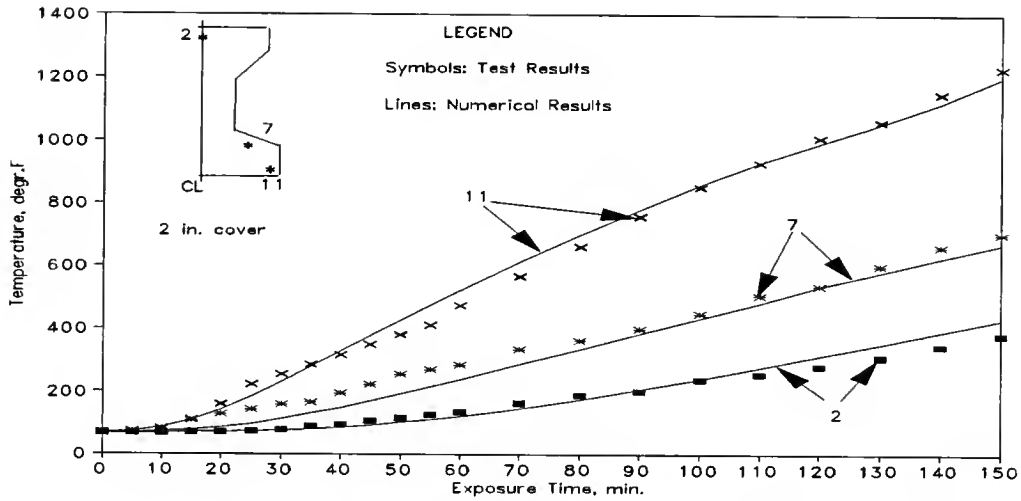

Fig. 7.6. Temperature distributions, lightweight beam, 2 in. concrete cover

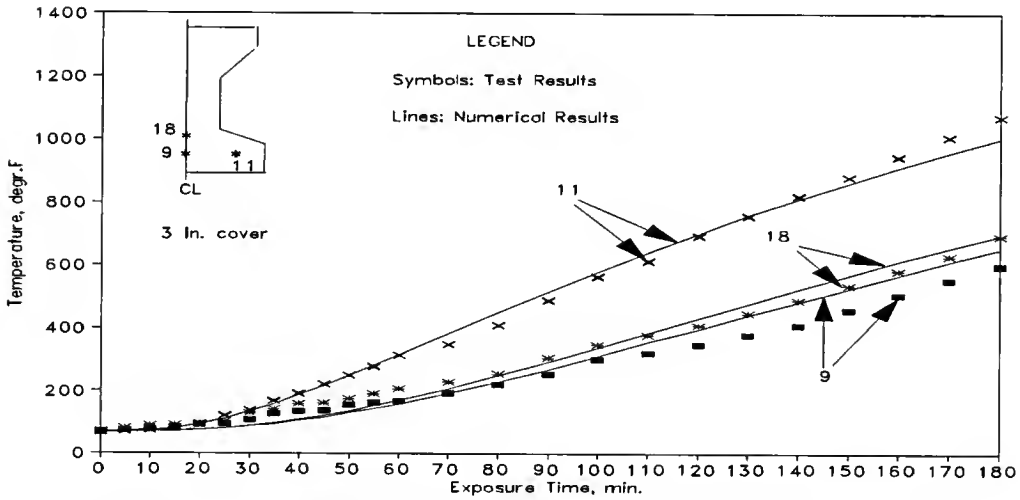

Fig. 7.7. Temperature distribution, lightweight concrete beam, 3 in. cover

on Eq. (2.5). Data presented in Figs. 7.8 and 7.9 can be useful for thermal analysis in general programs like ANSYS [58] which require such data as input.

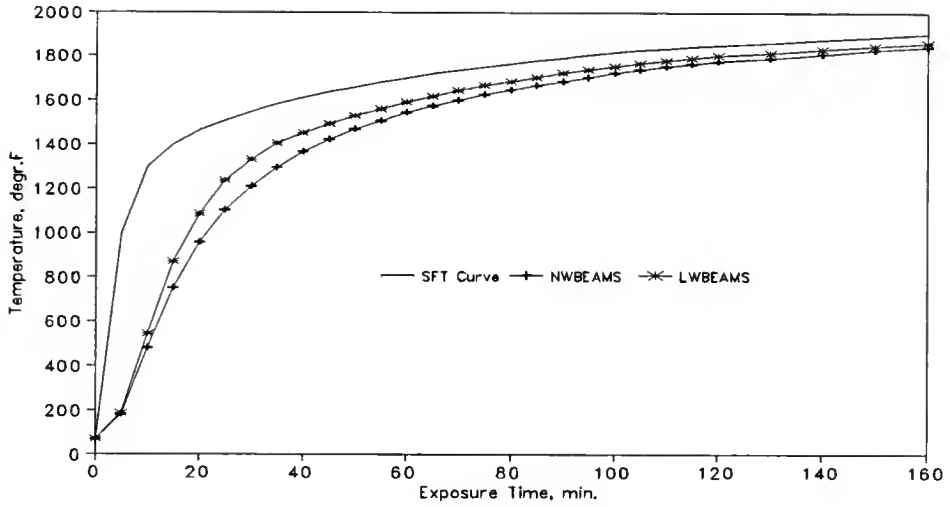

Fig. 7.8. Average of temperatures of beam sides exposed to fire

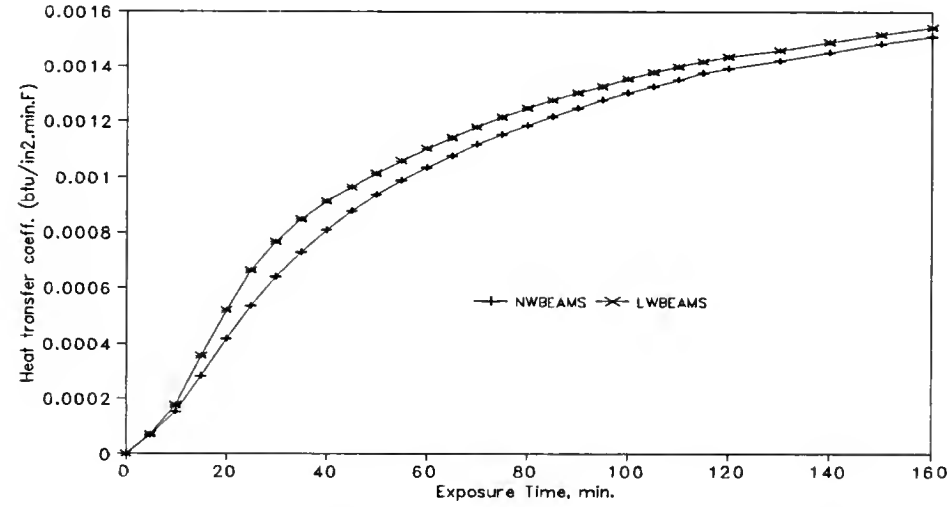

Fig. 7.9. Average of radiation heat transfer coefficients for beam sides exposed to fire

7.2.5.2. Mid span deflection of PC beams

Mid span deflection responses are plotted in Figs. 7.10 to 7.12 for normal weight concrete and in Figs. 7.13 to 7.15 for lightweight concrete. The figures show that the numerical model is stiffer than the test model for most of the exposure times. The reason for this may be partly

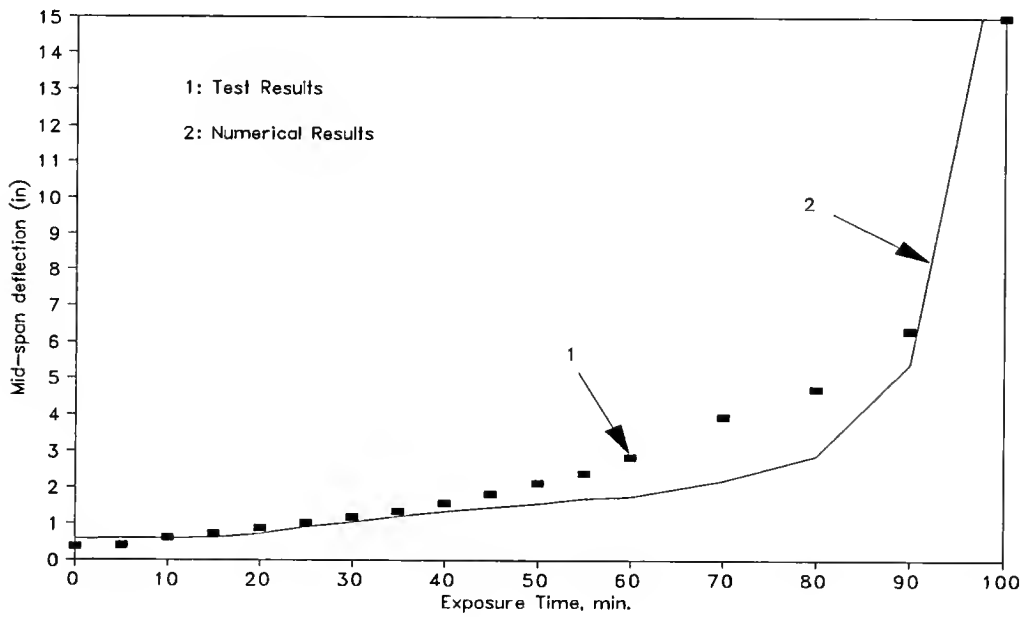

Fig. 7.10. Midspan deflection, normal weight concrete beam, 1 in. cover

attributed to the assumptions made on bond. In this study a perfect bond between concrete and prestress steel is assumed for all the temperature ranges. This assumption results in full transfer of prestress action from steel to concrete.

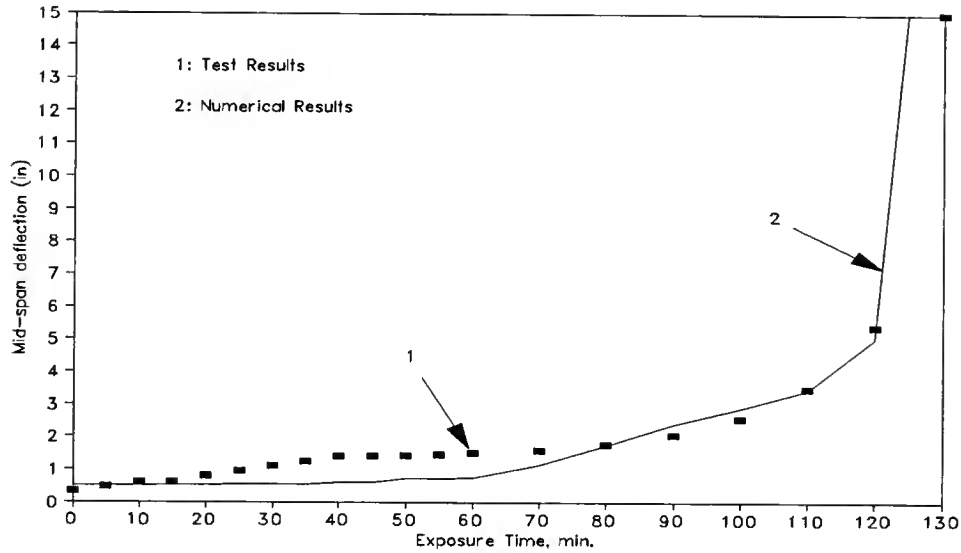

Fig. 7.11. Mid span deflection, normal weight concrete beam, 2 in. cover

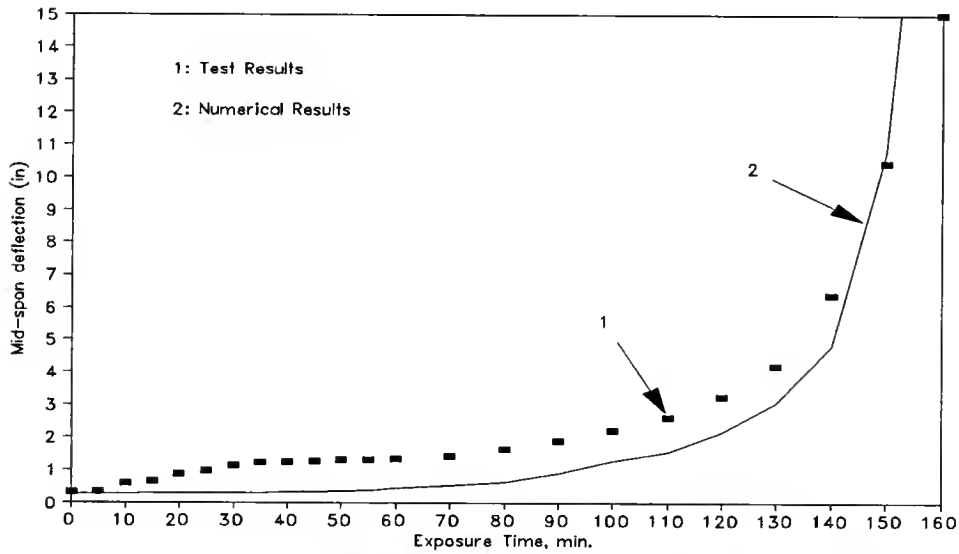

Fig. 7.12. Mid span deflection, normal weight concrete beam, 3 in. cover

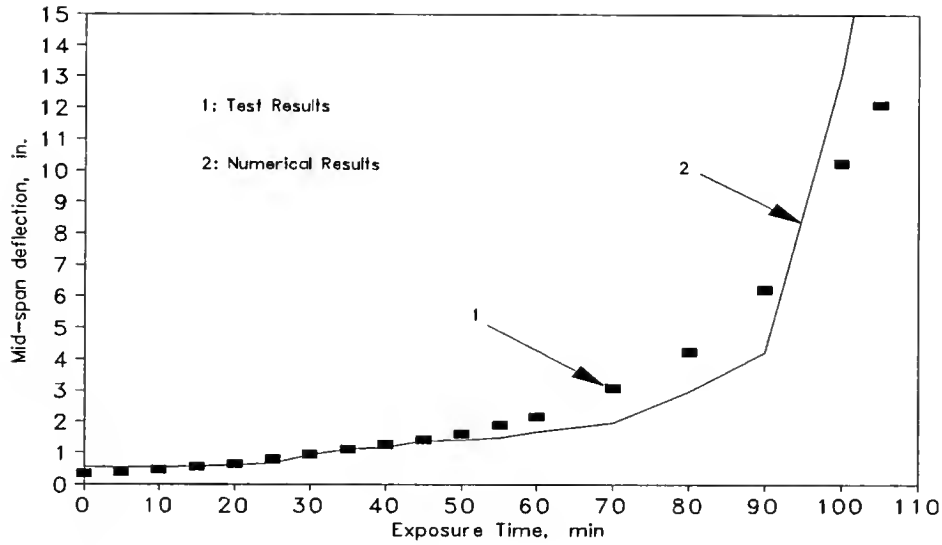

Fig. 7.13. Mid span deflection, lightweight concrete beam, 1 in. cover

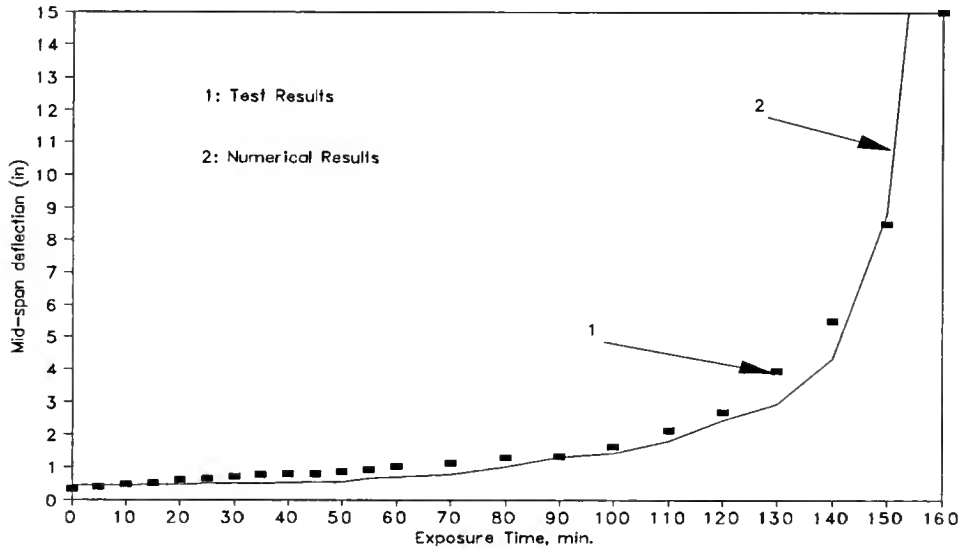

Fig. 7.14. Mid span deflection, lightweight concrete beam, 2 in. cover

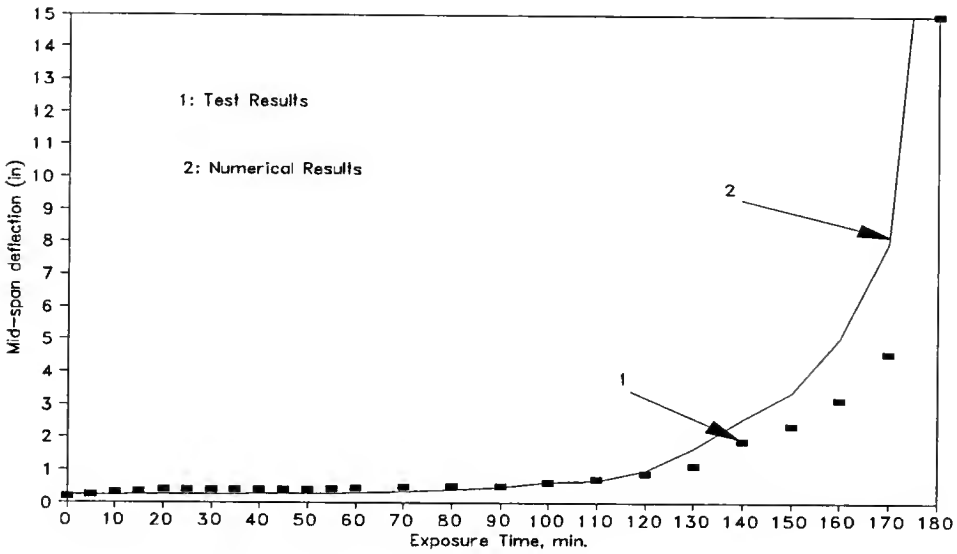

Fig. 7.15. Mid span deflection, lightweight concrete beam, 3 in. cover

concrete. However, according to tests by Fagundo [19] high temperatures cause bond slip between concrete and prestress steel. Thus in the real structure efficiency of transfer of prestress action decreases at high temperature. This may be manifested by higher deflection results for the test model.

On the other hand, numerical results tend to be higher than test results at higher temperatures close to the end point. The reason for this may be due to the fact that at higher temperatures significant portions of the section have degraded. The algorithm of this study treats all the recently degraded elements as having zero stiffness and carrying no stress. In reality these degraded elements retain some diminishing stiffness and stresses. This discrepancy results in a higher load vector and lower

stiffness values for the numerical model which is then manifested by higher deflections for the numerical model.

7.2.5.3. Moment capacity ratio

Moment capacity ratio is defined here as the ratio of the service load moment to the residual temperature-dependent moment capacity of a member considered. The history of the moment capacity ratio for normal weight concrete beams is presented in Fig. 7.16, and in Fig. 7.17 for lightweight concrete beams.

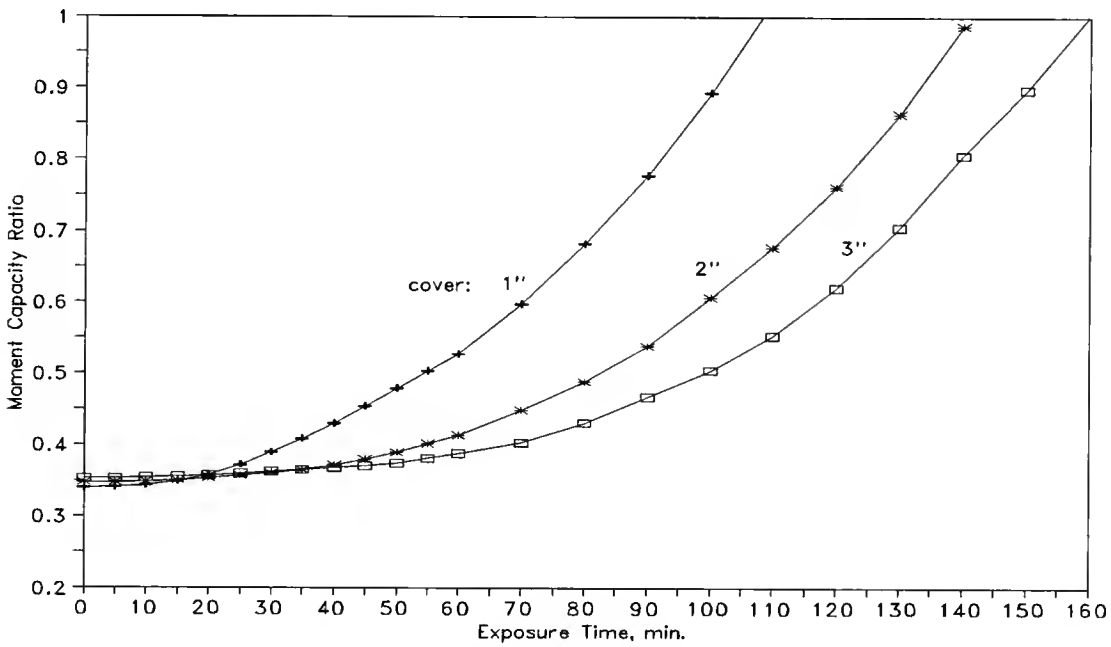

Fig. 7.16. Moment capacity ratios for normal weight concrete beams

The end point values from the numerical models of this study are compared with values computed by the method described by Eq. (1.1) and reported in Ref. [6]. The

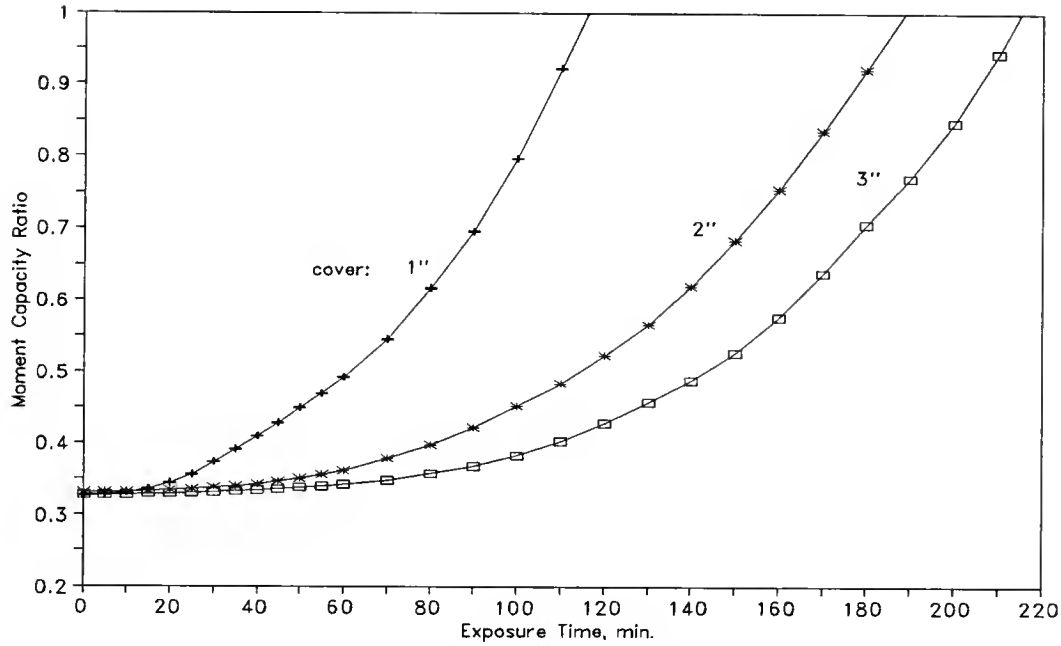

Fig. 7.17. Moment capacity ratios for lightweight concrete beams

Table 7.1. Moment Capacities for PC Beams

1	2	3	4	5
Beam Type	Concrete Type	Concrete Cover,in.	Moment Capacity,in.ksi	
			Eq.(1.1)	Eq.(5.22)
NWBEAM1	NW	1	976	1099
NWBEAM2	NW	2	778	792
NWBEAM3	NW	3	492	494
LWBEAM1	LW	1	941	1026
LWBEAM2	LW	2	744	811
LWBEAM3	LW	3	458	489

variables used in Eq. (1.1) are derived from measured steel temperatures at the end of test time. The results for both numerical procedures are shown in Table 7.1. The good agreement of the results shows that the developed numerical method can predict well the fire endurance of beams.

7.3. Prestressed Concrete Slabs

Fire endurance tests on simply supported prestressed concrete slabs have reported by Gustaferro [21]. The fire tests were conducted on eleven pretensioned concrete slab specimens. Six of the specimens were made of normal weight concrete, and the rest were made of lightweight concrete. Due to the qualitative similarity of results only comparison results of normal weight concrete slabs are presented in this section.

7.3.1. Description of Test Specimen

All the slabs used in this series of tests were 6.5 in. thick. Three thicknesses of concrete cover were used, that is, 1, 2, and 3 in. Three of the normal weight concrete slabs were pretensioned with five 7/16-in. diameter seven-wire strands. The cross section details for these slabs is shown in Fig. 7.18 (b). The other three were pretensioned with fifteen 1/4-in. diameter seven-wire strands. Fig. 7.19 (b) shows the cross section details of steel arrangement for this group.

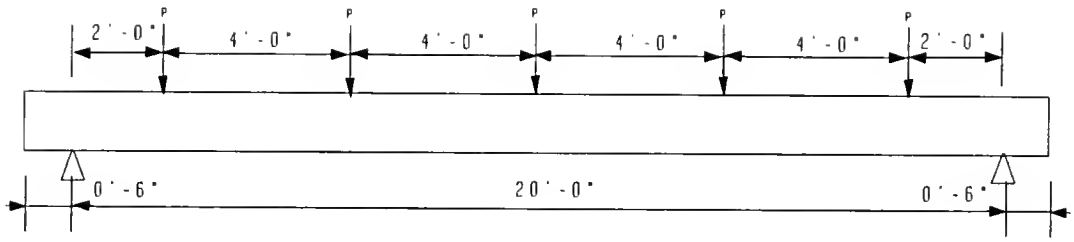

(a) Loading arrangements

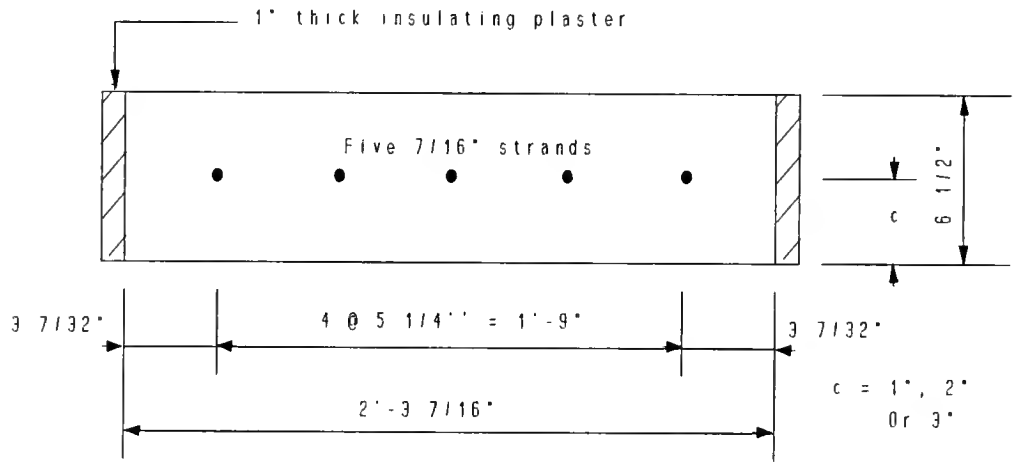

(b) Slab cross section

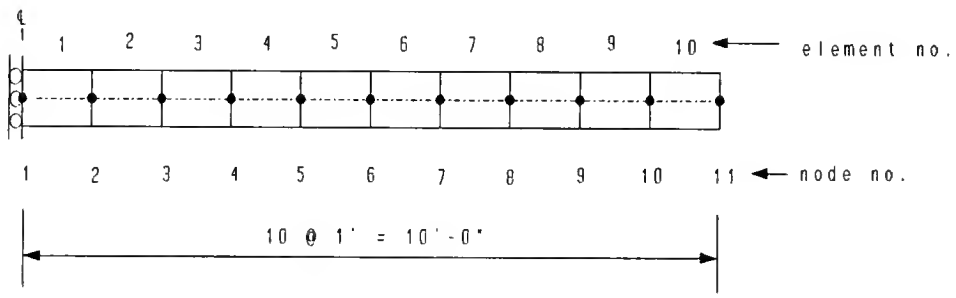

c) Finite Element Beam Element Model

Fig. 7.18. Design details for slab specimens, 5- 7/16" steel, 20 ft. span

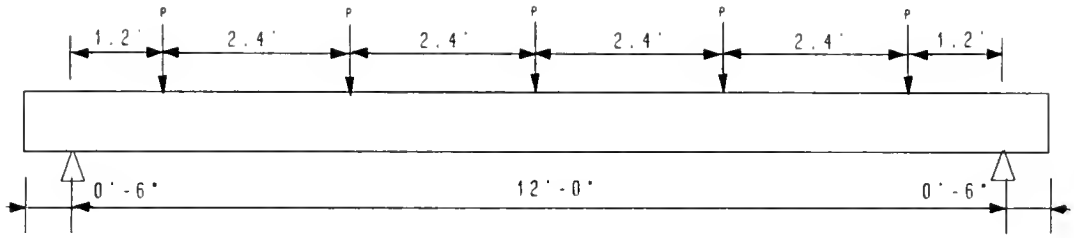

(a) Loading arrangements

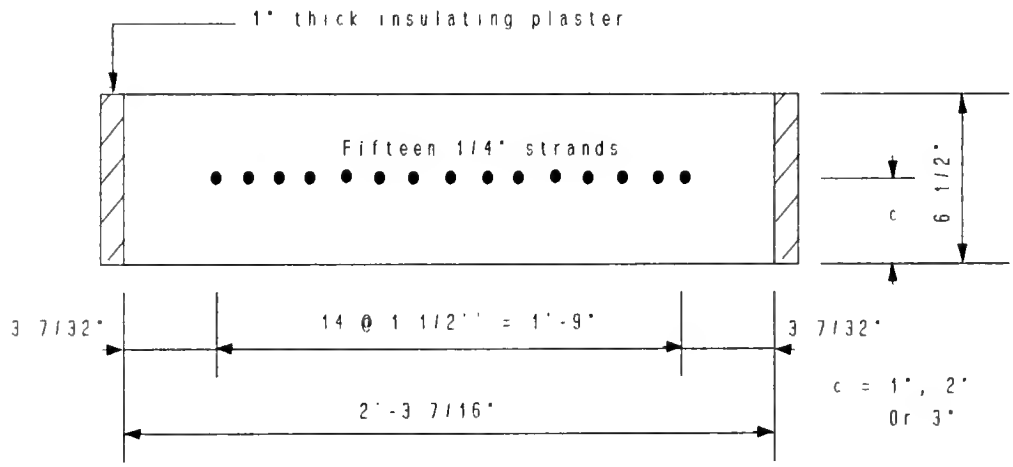

(b) Slab cross section

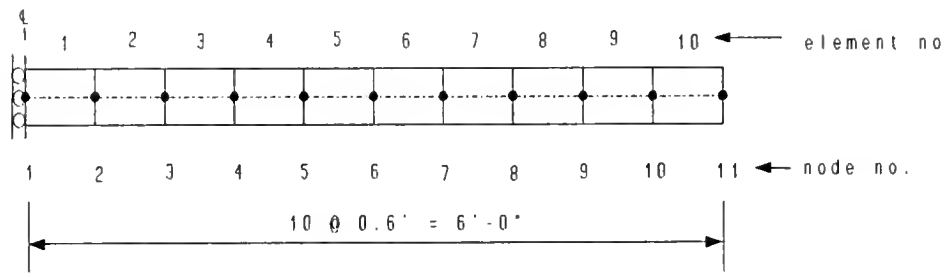

c) Finite Element Beam Element Model

Fig. 7.19. Design details for slab specimen, 15- 1/4" steel, 12 ft. span

7.3.2. Material Specifications

The measured ultimate tensile strength for the 1/4-in. strands was 275,000 psi and 262,000 psi for the 7/16-in. strands. All the strands were initially pretensioned to a nominal 175,000 psi. Partial loss of prestress is assumed to be 18%. Details of concrete strengths and loadings are presented in Table 7.2.

Table 7.2. Specimen strength and loading details. (Source: Ref. [21])

Slab Type	Concrete Cover, in.	Concrete Strength (psi)	Number and Size of Strands	Applied Load, P (lb)
NWSLAB1	1	5400	5-7/16 in.	1297
NWSLAB2	2	5010	5-7/16 in.	977
NWSLAB3	3	6300	5-7/16 in.	643
NWSLAB7	1	5180	15-1/4 in.	2569
NWSLAB8	2	7740	15-1/4 in.	2035
NWSLAB9	3	5430	15-1/4 in.	1365

7.3.3. Testing Procedures

All specimens were simply supported on rocker-rollers, and fire tested while supporting their designed service loads. The loading was applied through five equally-spaced hydraulic rams, as shown in Figs. 7.18 (a) and 7.19 (a). Specimens pretensioned with 7/16-in. strands were tested on a 20-ft. span. The other specimens were tested on 12-ft.

span. The relative humidity of the specimens at the beginning of the fire test was 70%. Tests were conducted until the structural end point was imminent.

The fire exposures were conducted in accordance with ASTM E-119. Temperature of steel strands was measured by attaching thermocouples to several of the strands near midspan and at a distance of 5-ft. from midspan.

7.3.4. Finite Element Model

The finite element model for thermal analysis consisted of 224 triangular elements, and 135 node points over one half of the slab width. For structure response analysis the half span length of the specimens was modeled int 10 beam elements. The idealization is shown in Fig. 7.18 (c) for the 20-ft. span and in Fig. 7.19 (c) for the 12-ft. span.

7.3.5. Comparison of Numerical and Test Results

7.3.5.2. Temperature distribution

Fig. 7.20 shows the average temperature of the face of the slab exposed to fire as function of time. Also presented is the average and the maximum temperature histories of the unexposed surface. The curve for the coefficient of radiation heat transfer for normal weight concrete slabs is presented in Fig. 7.21. Comparison of numerical and test results for temperature distribution across slab section are not presented because the

corresponding test results were not available. As for the beams the exposed surface temperatures given in Fig. 7.20 and the radiation heat transfer coefficients given in Fig. 7.21 can be used in general thermal analysis programs as input data for computing temperature distribution in slabs subjected to fire tests.

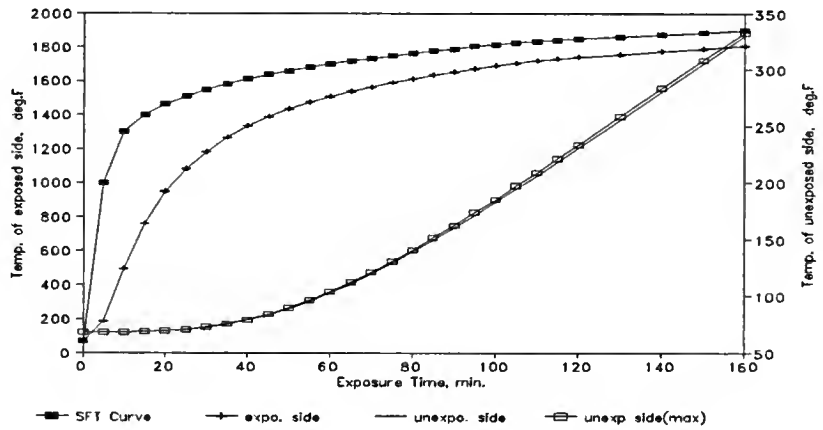

Fig. 7.20. Exposed and unexposed surface temperatures, normal weight concrete slabs

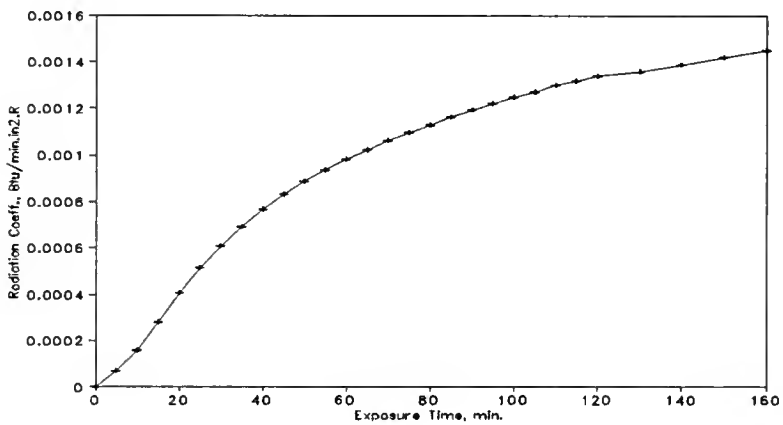

Fig. 7.21. Coefficient of radiation heat transfer for normal weight slab exposed surfaces

The curve for unexposed surface temperature and the maximum temperature curve determine the heat transmission end point for slabs.

7.3.5.2. Mid-span deflection of slabs

The comparison of test and numerical results of mid span deflections for normal weight concrete slabs is illustrated in Figs. 7.22, 7.23 and 7.24 for 20-ft span, and in Figs. 7.25, 7.26 and 7.27 for the 12-ft span. The

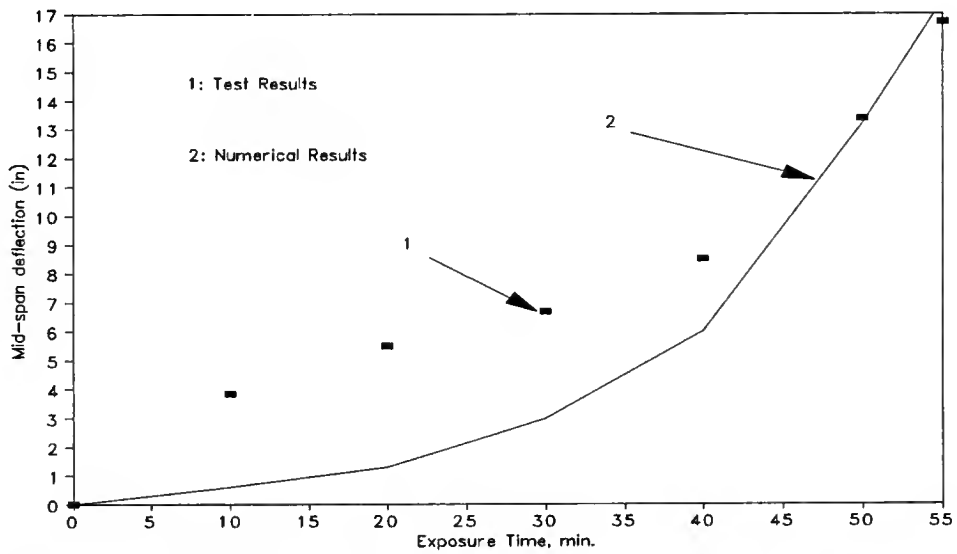

Fig. 7.22. Mid span deflection, normal weight slab, 5- 7/16" steel, 1 in. cover, 20 ft. span

results in these figures shows only the increase of deflection due to effects of the increase in temperature. The initial deflection due to loading and prestress action has been deducted from the computed deflection results.

As was the case with the beams numerical results are relatively lower than the corresponding test results for

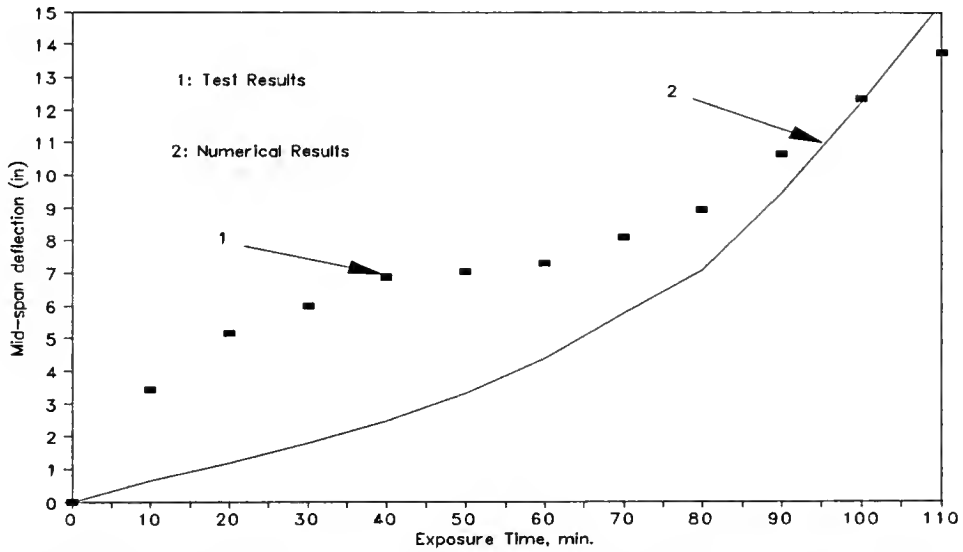

Fig. 7.23. Mid span deflection for normal weight slab, 5- 7/16" steel, 2 in. cover, 20 ft. span

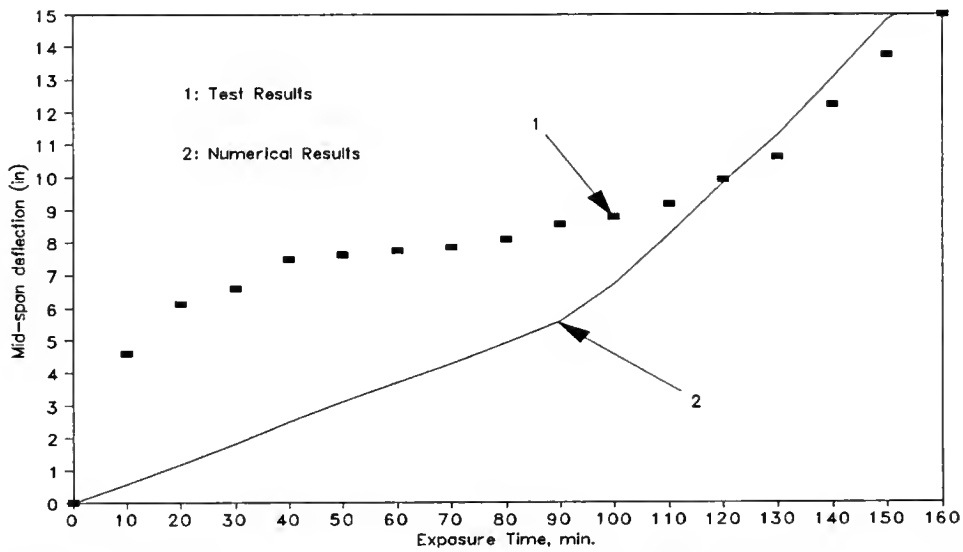

Fig. 7.24. Mid span deflection, normal weight slab, 5- 7/16" steel, 3 in. cover, 20 ft. span

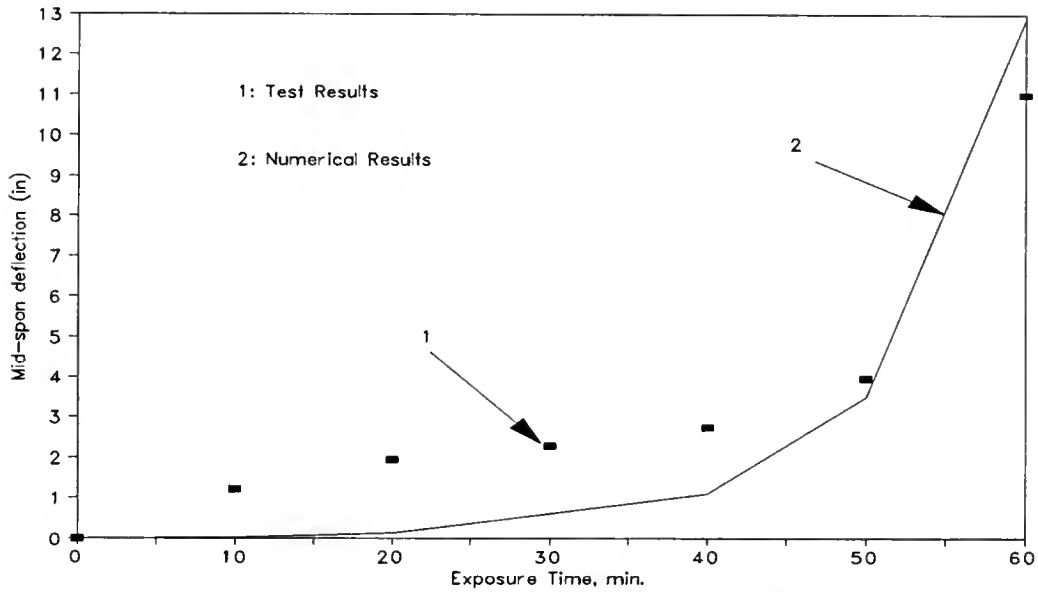

Fig. 7.25. Mid span deflection, normal weight slab, 15- 1/4" steel, 1 in. cover, 12 ft. span

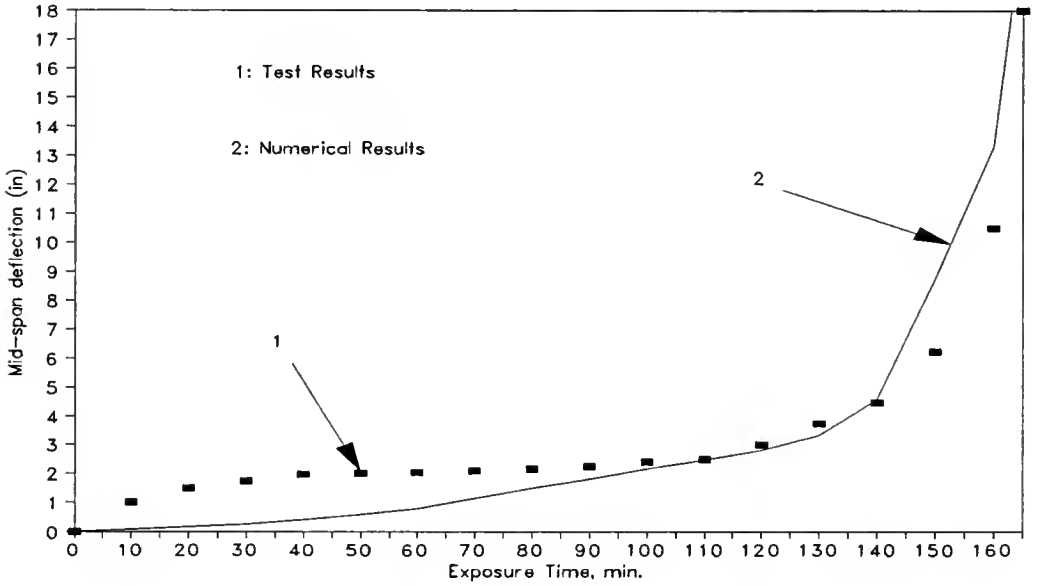

Fig. 7.26. Mid span deflection, normal weight slab, 15- 1/4" steel, 2 in.cover, 12 ft. span

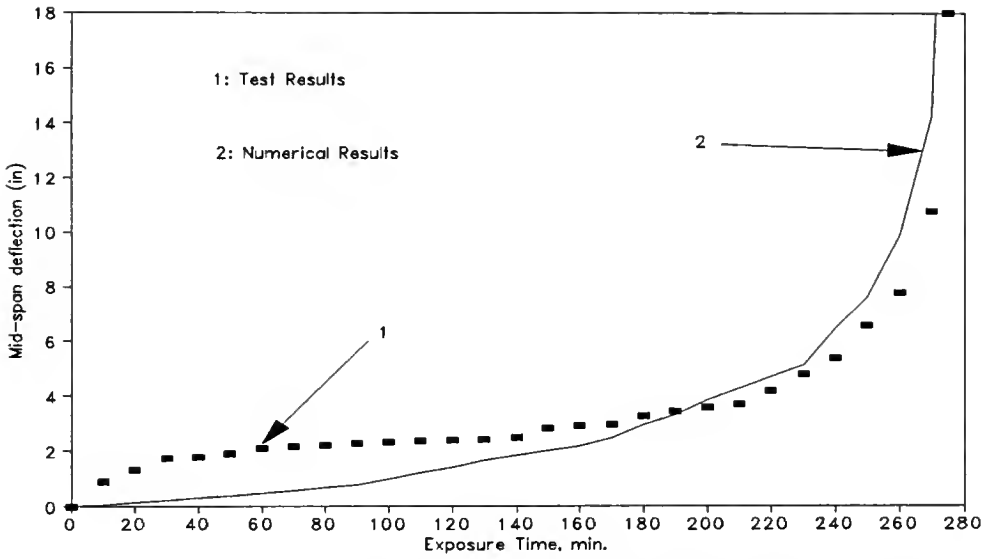

Fig. 7.27. Mid span deflection, normal weight slab, 15- 1/4" steel, 3 in. cover, 12 ft. span

most of the lower temperatures. It can also be noticed that the discrepancy between numerical and test results is greater for slabs than for beams. However, the arguments on the results presented for beams are also valid for slabs.

7.3.5.3. Moment capacities ratios for slabs

The variations of moment capacity ratios as related to exposure time are presented in Fig. 7.28 for the 20-ft. span slabs and in Fig. 7.29 for the 12-ft. span slabs. The end point moment capacities generated from the method of this study and those of the method of Eq. (1.1) are compared in Table 7.3. The closeness of results verifies the validity of the numerical model used in this study.

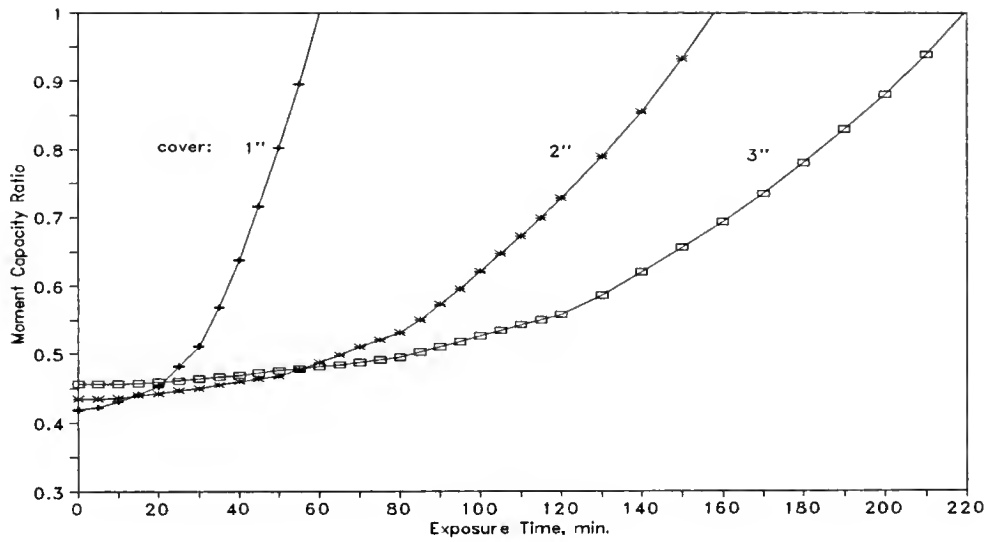

Fig. 7.28. Moment capacity ratios for normal weight concrete slabs of 20 ft. span

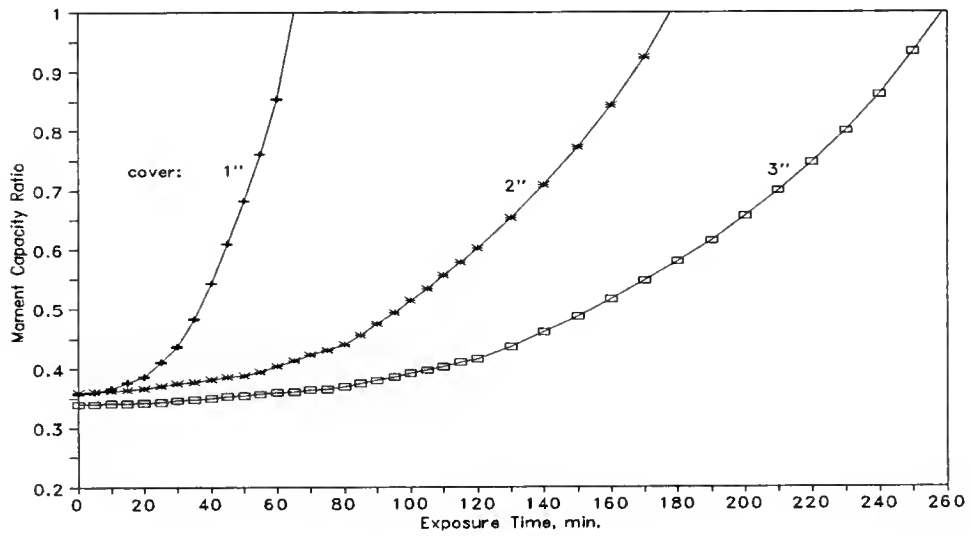

Fig. 7.29. Moment capacity ratios for normal weight slabs of 12 ft. span

Table 7.3 End point moment capacities of PC slabs

1	2	3	4	5
Slab Type	Span ft.	Concrete Cover,in.	Moment Capacity,in.ksi	
			Eq.(1.1)	Eq.(5.22)
NWSLAB1	20	1	336	352
NWSLAB2	20	2	315	336
NWSLAB3	20	3	214	227
NWSLAB7	12	1	283	329
NWSLAB8	12	2	230	250
NWSLAB9	12	3	178	166

7.4. Evaluation of Influences of Material Properties

Data in Chapter 3 demonstrates the effect of higher temperatures on properties of concrete and prestressing steel. These effects on material properties have different influences on the temperature distribution and structural response observed above. This section presents the evaluations of influences of certain material properties on the computed deflections, moment capacities and temperature distributions.

Numerical results based on the temperature dependent properties of concrete and steel are considered the base for evaluating the influences of the effects of temperature on material properties. The technique used in determining the influence of a particular parameter is to treat the parameter as independent of temperature during the analysis.

7.4.1. Effect of Thermal Properties on Temperature Distribution

Thermal conductivity, thermal capacity and their combinations are alternatively considered constant in the analysis of temperature distribution. The resulting sets of temperature distributions are plotted in Fig. 7.30 for normal weight concrete and in Fig. 7.31 for lightweight concrete. The curves denote the temperature of tendon location marked by number 11 as shown in both figures.

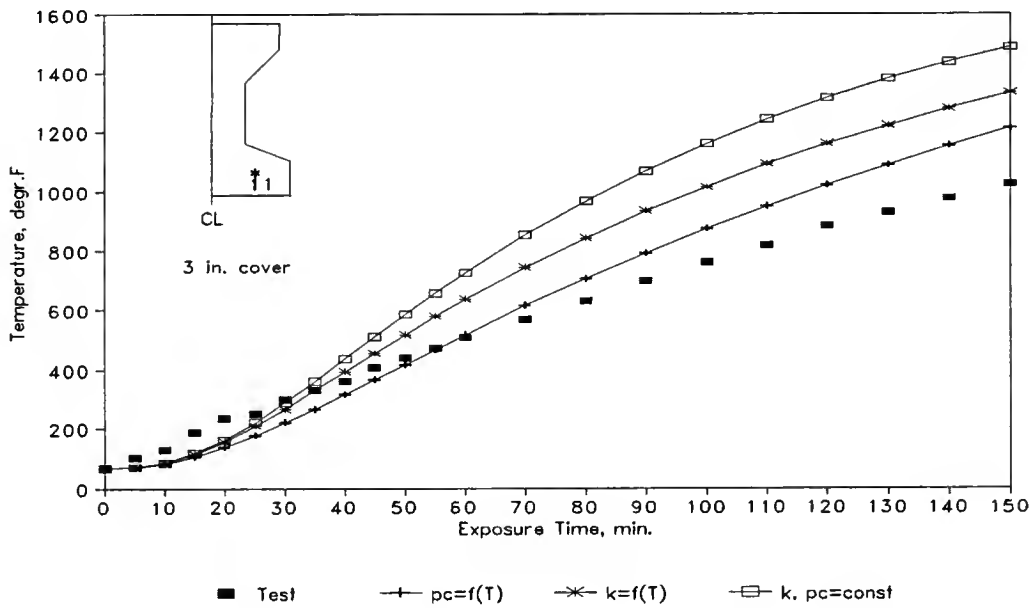

Fig. 7.30. Influences of thermal properties in temperature distribution of normal weight beams

For normal weight concrete the maximum temperature value is increased by 42% when both conductivity and thermal

capacity are assumed constant. When only thermal conductivity is temperature dependent the maximum based temperature is increased by 27%, while the increase is 16% when only thermal capacity is temperature dependent. This analysis show that temperature distribution in normal weight concrete is more sensitive to thermal capacity than thermal conductivity.

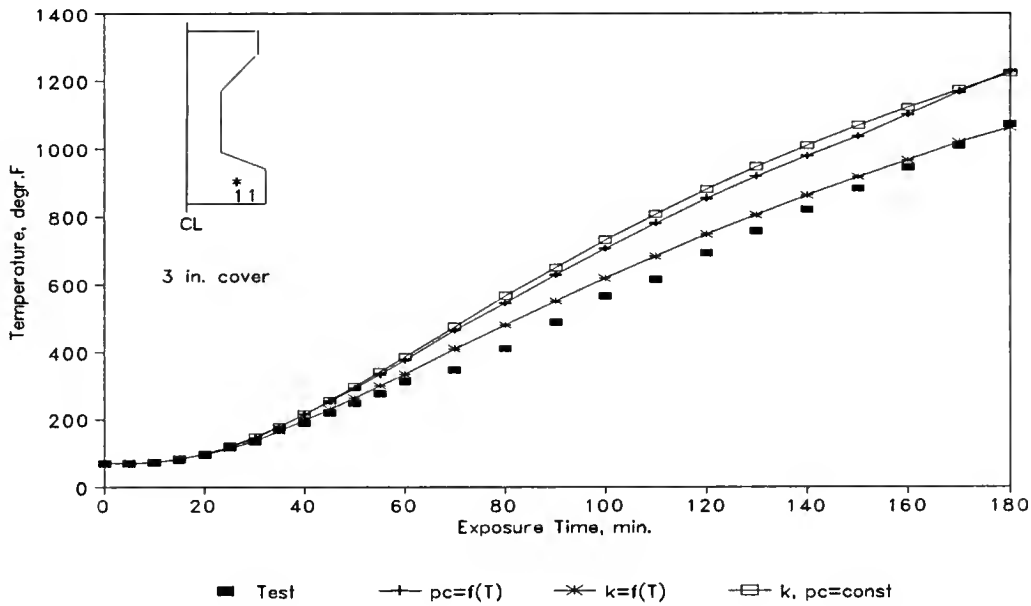

Fig. 7.31. Influences of thermal properties on temperature distribution for lightweight concrete beams

Thermal analysis for lightweight concrete with constant thermal properties results in 24% increase in the maximum base temperature. When only thermal capacity changes with temperature the base temperature is increased by 20%, and by

6% when only thermal conductivity is temperature dependent. The data indicate that temperature distribution for lightweight concrete is highly sensitive to the thermal properties of the concrete.

7.4.2. Effect of other Material Properties on Deflection

In this analysis the thermal properties of concrete are temperature dependent. Other properties are grouped and given identification symbols as follows: modulus properties (Ec, Es), strength properties (fc, fpu), deformation properties which include thermal and shrinkage strain (Def.) and relaxation properties of steel (Rel.). The parameters whose influences are to be evaluated are assumed to be independent of temperature. The results will reflect sensitivity of the basic deflection on the evaluated parameters. The model used for the analysis is the normal weight beam with 2 in. cover.

The deflection curves based on various modes of temperature-dependence material properties considerations are presented in Fig. 7.32. The plotted data show that the influence of temperature on individual property groups investigated is mostly significant only at higher temperatures near the structural end point.

Evaluation of results show the following. When relaxation property of steel is independent of temperature the time taken to reach the 15 in. deflection limit is

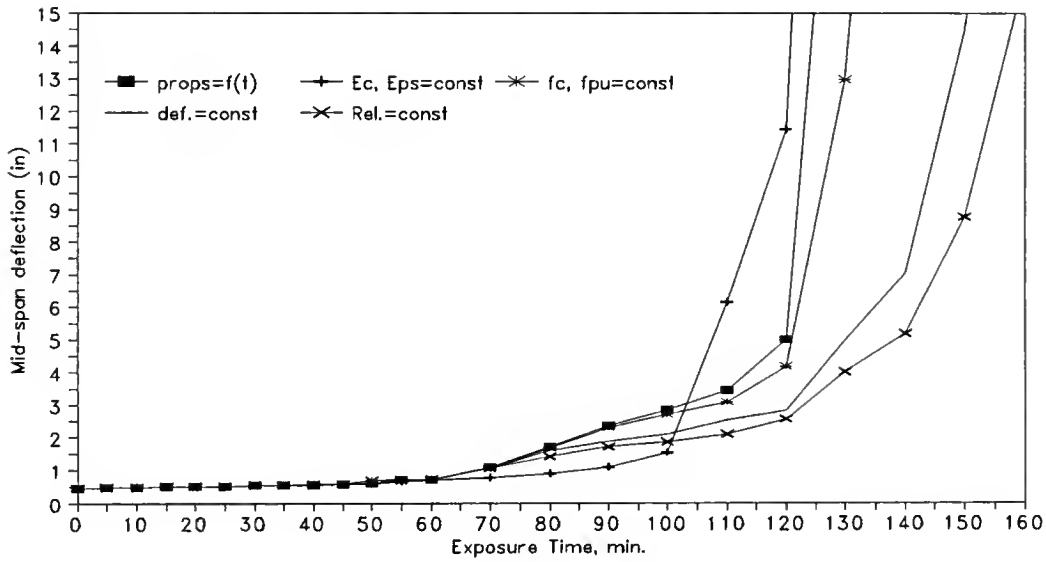

Fig. 7.32. Influence of non-thermal material properties on deflection for normal weight beams

increased by 26%. If the influence of temperature on deformation properties is neglected the end time is increased by 18% while the increase is only 4% for constant strength properties. When the modulus properties are assumed independent of temperature the resulting deflection is lower than that of other groups for lower temperatures. This is probably due to higher modulus values which increase structural stiffness. However in this case, instead of increasing, the time to reach end point deflection is reduced by 4%.

This analysis shows that the deflection behavior of prestressed concrete member exposed to fire is mostly

sensitive to the effects of temperature on the relaxation properties of the prestressing steel.

7.4.3. Effect of Thermal Properties on Structural Response

This section demonstrates how thermal properties of concrete affect deflections and moment capacities of prestressed concrete members subjected to fire. The analysis is carried out with improved thermal properties of concrete. In this analysis thermal properties are improved by reducing thermal conductivity values and by increasing thermal capacity values. Thus 5% improvement means the basic temperature dependent thermal conductivity values are reduced by 5% while thermal capacity values are increased by the same level. All other material properties are considered at their basic functional values.

Four levels of modifications have been arbitrarily chosen for consideration: 5%, 10%, 15% and 20%. Deflections resulting from these considerations are plotted and presented in Fig. 7.33. Corresponding moment capacity ratios are shown in Fig. 7.34.

The deflection results indicate that improving thermal properties by only 5% would increase the end point time by 5%, while a 10% improvement result to a 19% increase.

Results of moment capacity show that a 5% improvement of thermal properties increases fire endurance by 7%. An improvement of 10% increases the fire endurance by 16%.

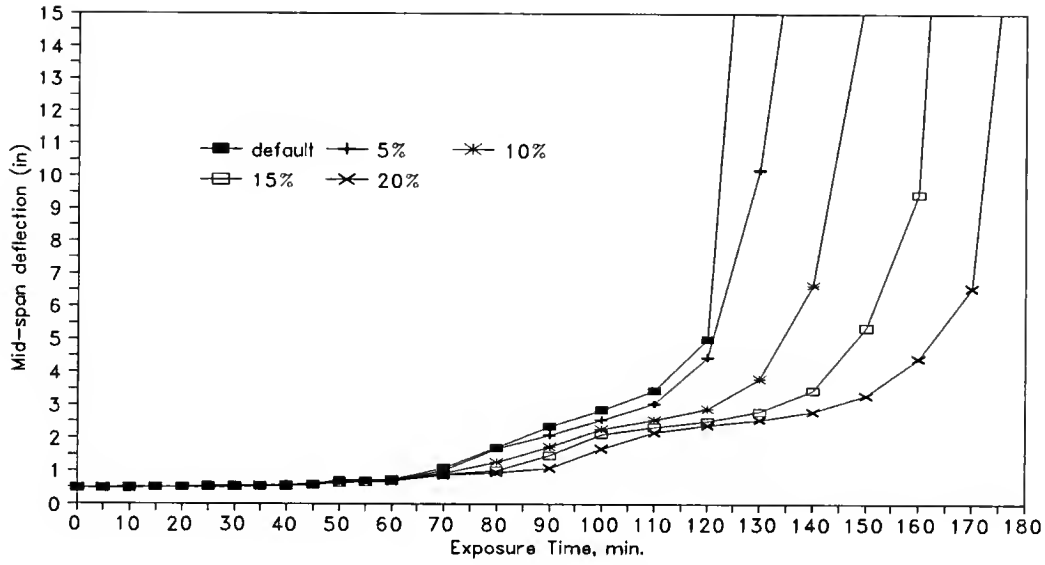

Fig. 7.33. Influences of thermal properties of concrete on deflections of normal weight concrete beams

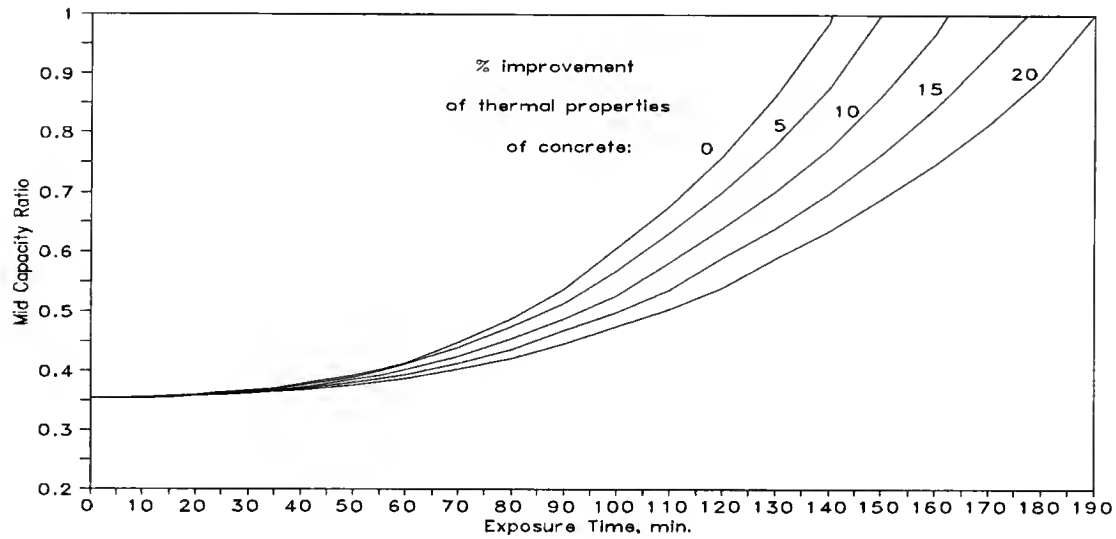

Fig. 7.34. Influences of thermal properties of concrete on moment capacities of normal weight concrete beams

7.5. Method of Estimating Fire Endurance of Beams

7.5.1. Effects of Exposure Conditions

Slabs are exposed to fire on the bottom surface only. Thus the temperature of steel in the slabs, and hence, the fire endurance of prestressed concrete slabs, can be predicted satisfactorily using the numerical procedures described in Sec. 1.6.3, pg. 19 of this document and in Ref. [3]. The accuracy of the procedure has been confirmed by the method of the current study as shown in Table 7.3.

Beams, however, are exposed to fire on three surfaces. This exposure condition makes it difficulty to estimate temperature of prestressing steels using the temperature curves [3]. Thus the numerical procedure described in [3] is not quite accurate for predicting fire endurance of prestressed concrete beams.

This section presents simple design charts for predicting fire endurance of prestressed concrete beams. The procedures of developing the charts by using the method of this study is also presented.

7.5.2. Specimen for Analysis

The beam specimen used in the analysis is shown in Fig. 7.35. The number and arrangement of the steel tendons and the values of the variables depth h, width b and tendon eccentricity e are based on the design recommendations given

in page 2.24 of Ref. [57]. The minimum spacing s between steel tendons is given in Sec. 7 of Ref. [32]. This approach is utilized in order to produce uniformity in tendon arrangement for all the cover thicknesses considered. Thus the variation of the initial moment capacity between beams of the same size will be due to the influence of cover thickness on the number of tendons that can be accommodated in the beams.

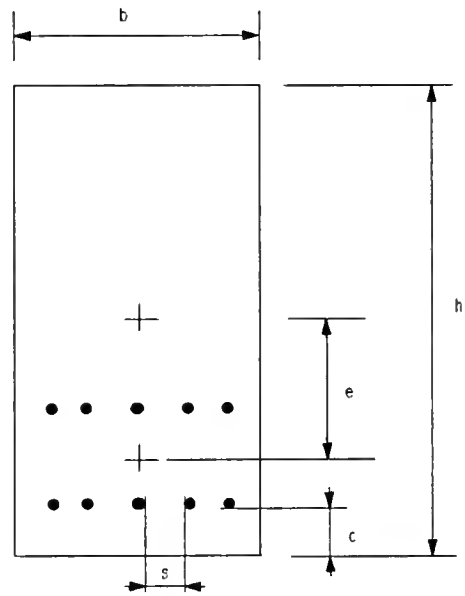

Fig. 7.35. A typical PC beam section

7.5.3. The Analysis Procedure and Results

The analysis involved three cover thickness groups of 1, 2, and 3 in. in normal and lightweight aggregate

concretes. The design variables considered in each cover group are beam size, tendon strength and moment intensity. The moment intensity is defined here as the ratio of service load moment M to the moment capacity M_n of the beam specimen at normal temperature. Beam sizes investigated were 12 and 16-in. width, and 24 and 32-in. height. The tensile strength of tendons were 250 and 270-ksi. The moment intensities ranged from 0.2 to 0.7.

By arranging steel tendons in layers and maintaining the same tendon eccentricity [57] and size it was possible to arrange in a beam the same number of tendons for both 1 and 2-in. covers thicknesses. However, the number of tendons were less for 3 in. cover thickness due to limitation of clearance between strands. This tendon arrangement is adopted only for convenience of analysis. It does not have a significant effect on the resulting curves since fire endurance is expressed as function of a dimensionless parameter, that is, moment intensity.

For each cover group the beam specimen involving the design variables described above are analyzed for fire endurance. The analysis is conducted as follows. Consider, for example, a 2 in. cover group. For this group a beam of size 12 by 24-in., tendon strength 250 ksi and moment intensity 0.3 is analyzed to determine the history of moment capacity ratio. Holding the variables of size and tendon strength constant the beam is analyzed for other

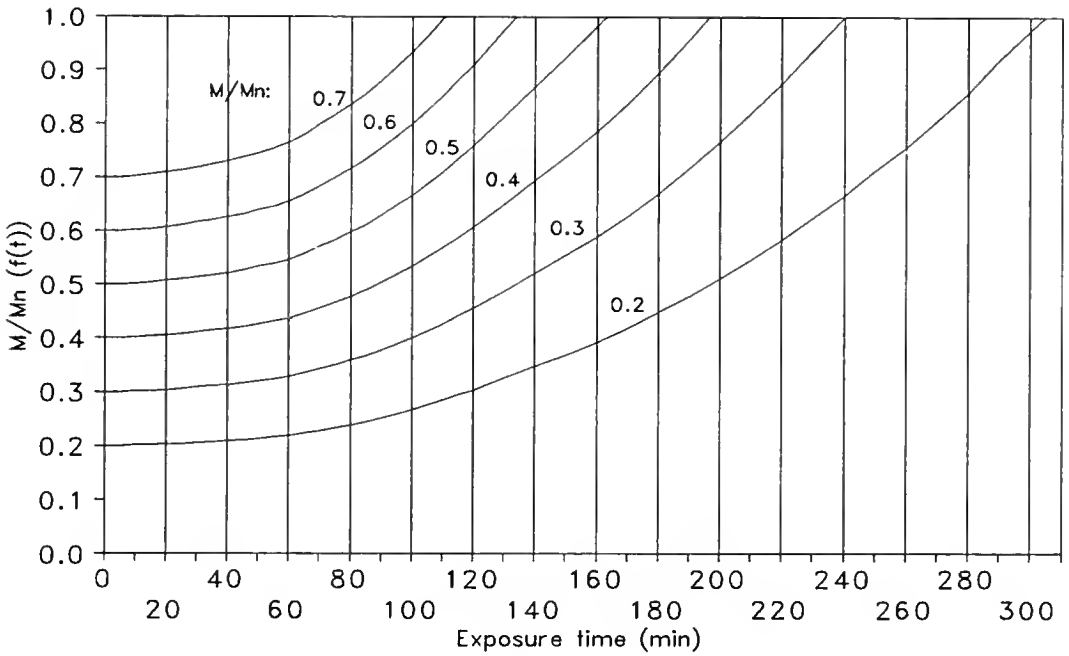

Fig. 7.36. Moment capacity ratio versus time for a normal weight concrete beam, 2 in. cover thickness

moment intensity values. The results of all the analyses for the whole range of moment intensity are then plotted together as shown in Fig. 7.36.

The fire endurance period for each moment intensity value investigated is then determined as the time when the service moment M equals the temperature-dependent moment capacity $M_{n\theta}$. These values of fire endurance versus moment intensity form a set of results of fire endurance for a 12 by 24-in beam prestressed with tendons of 250 ksi strength.

This process is repeated to produce other sets of results of fire endurance for all the combination of beam sizes and tendon strengths within the 2 in. cover group.

All the sets of results of fire endurance within the 2 in. cover group are plotted together. The reason for this approach is to determine the range of scatter of fire endurance data as influenced by beam size and tendon strength. This step is illustrated in Fig. 7.37. The

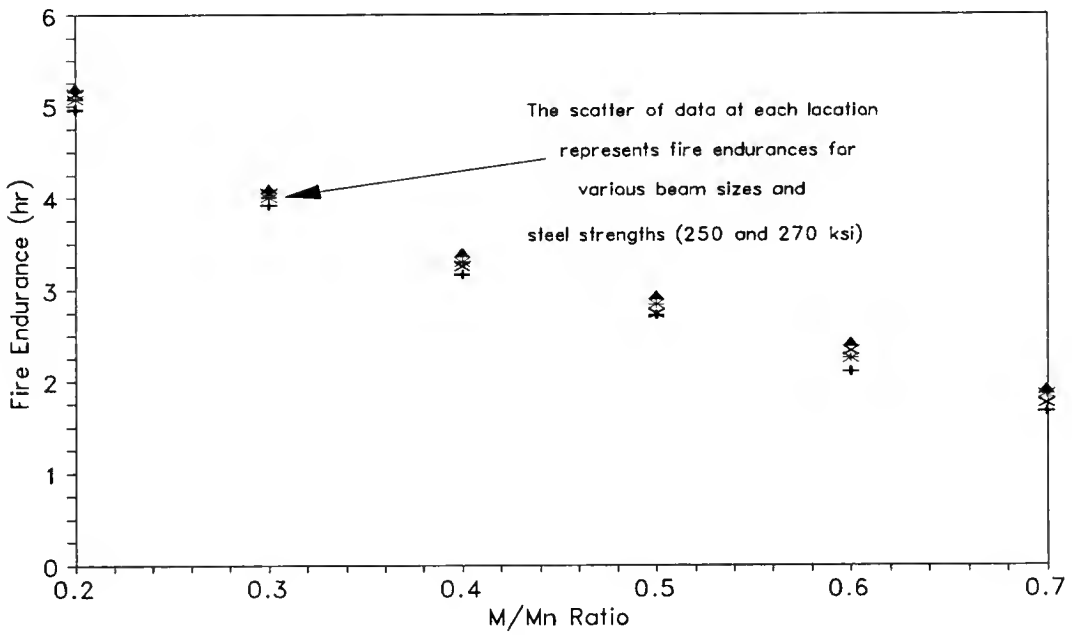

Fig. 7.37. Fire endurance of various beam sizes and steel strengths for a 2 in. cover thickness, normal weight concrete

whole analysis process is also performed for 1 and 3-in. cover groups and for both normal and lightweight concretes.

The set of fire endurance results plotted in Fig. 7.37 are very close together. This indicates that beam sizes and tendon strengths have no significant effect on the fire endurance of a prestressed concrete beam with 2 in. cover thickness. Similar behavior has also been observed for beams of 1 and 3-in. concrete covers. The final values of fire endurance of prestressed concrete beams are computed by averaging all the sets of fire endurance results within a cover group. The resulting values of fire endurance for all the cover groups considered are plotted together to form design charts.

The developed design charts for estimating fire endurance of prestressed concrete beams are shown in Fig. 7.38 for normal weight concretes and in Fig. 7.39 for lightweight concretes. The charts involves the variables concrete cover, moment intensity and fire endurance. When any two of these parameters are known, the third can be determined.

The application of the charts in determining fire endurance is demonstrated through the following example. It required to determine the fire endurance of a 12 by 24-in. prestressed concrete rectangular beam (12RB24) prestressed with 10-1/2-in. diameter tendons. The beam section and the design data are given in Fig. 7.40. The basic calculations needed are for the determination of the load intensity.

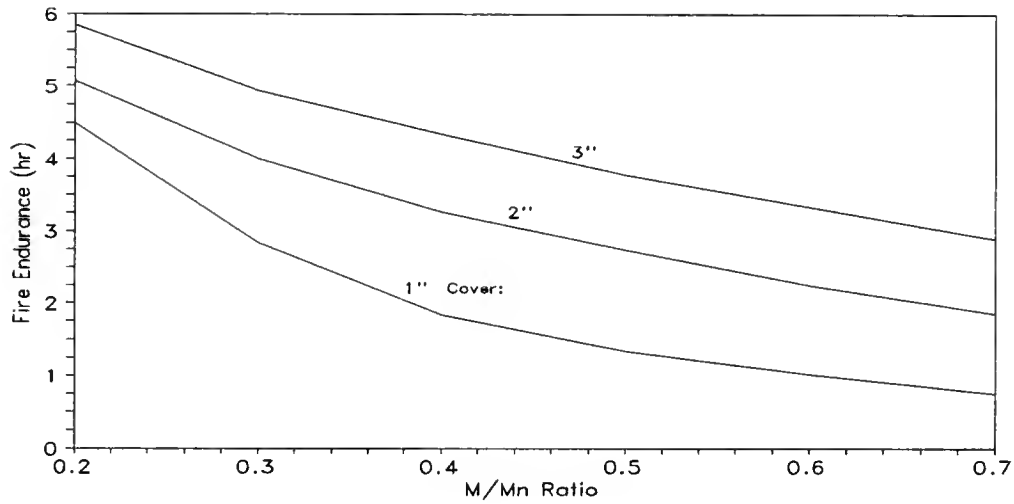

Fig. 7.38. Fire endurance as function of moment intensity, for normal weight PC beams

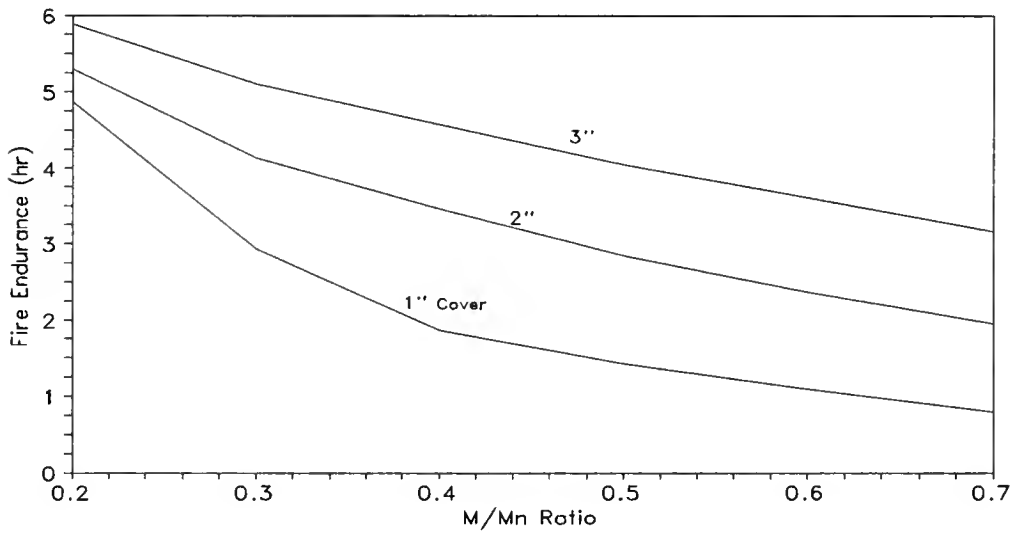

Fig. 7.39. Fire endurance as function of moment intensity, for lightweight PC beams

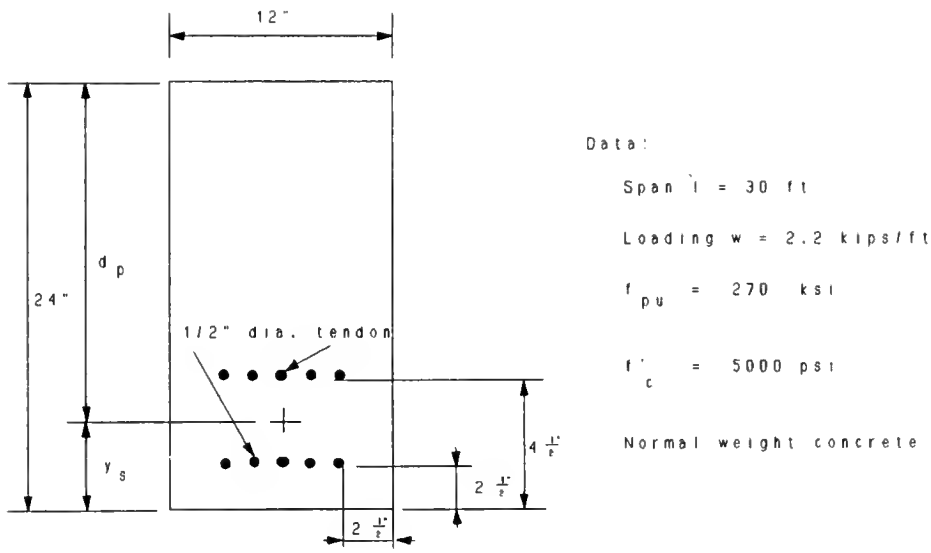

Fig. 7.40 Section details for a 12RB24 beam

The solution is as follows:

$$A_{ps} = 10(0.153) = 1.53 \text{ in}^2$$
$$y_s = [5(2.5)+5(4.5)]/10 = 3.5 \text{ in.}$$
$$d_p = 24-3.5 = 20.5 \text{ in.}$$

Using Eq. (1.1)

$$f_{ps} = 270[1-(0.5*1.53*270)/(12*20.5*5) = 224.7 \text{ ksi.}$$
$$a = (1.53*224.7)/(0.85*5*12) = 6.74$$

Nominal moment strength is given by

$$M_n = (1.53*224.7)*(20.5-6.74) = 4730 \text{ kips-in.}$$

Applied moment is

$$M = wl^2/8 = 2.2(30)^2/8 = 247.5 \text{ kips-ft.}$$
$$= 2970 \text{ kips-in.}$$

Load intensity is

$$M/M_n = 2970/4730 = 0.63$$

With M/M_n=0.63 and cover c=2.5 in. fire endurance of the given beam is determined from Fig. 7.38 as 2 hr and 45 min.

CHAPTER 8
SUMMARY AND CONCLUSIONS

8.1. Summary

A numerical procedure and computer program for a nonlinear analysis of the structural response of prestressed concrete members subjected to elevated temperatures has been presented. The parameters defining the structural response are deflection and moment capacity. The method applies the time-temperature relationship of the standard fire test (SFT) to simulate building fires. The numerical model is capable of determining temperature distributions across prestressed concrete member sections, and predicting deflections and moment capacity of such a member supporting its designed service loads, throughout the simulated fire exposure period.

The effects of elevated temperatures on the material properties of concrete and prestressing steel are included in the model. The material properties considered are: thermal conductivity and thermal capacity of concrete, stress-strain relationship for both concrete and prestressing steel, compressive and tensile strength of concrete, tensile strength of steel, thermal strain of concrete and steel, concrete shrinkage, and relaxation of

prestressing steel. The behavior of these properties as related to temperature has been derived from data published in the literature. This information is developed into mathematical relations to be used in the numerical model.

The formulation of the numerical model and the solution of the equilibrium equations is based on the displacement finite element method. The member cross section is idealized into a finite number of triangular elements for temperature distribution analysis. This idealization also is used to account for the variation of material properties within a section. The properties of individual elements are numerically integrated across the section in order to determine the section's stiffness properties. The member is modeled into discrete number of beam elements for the deflection and moment capacity analysis.

The exposure time-dependent analysis is performed by dividing the time scale into finite time step intervals. For each time step equilibrium equations are set and solved for temperature distributions and structural response. The solution of the equilibrium equations for deflections is iterative and includes determination of the incremental loads induced into the system due to changes in temperature dependent material properties. Incremental deflections for each iteration are cumulatively added along the time domain to determine total deflection for each time interval.

The computer program implementation of the developed numerical procedures is used to analyzes a series of prestressed concrete beams and slabs which have been fire tested according to SFT procedures. The temperature distribution and structural response results of the numerical model are compared graphically with those obtained from fire tests in order to investigate the validity and applicability of the numerical method. Analyses have also been performed to evaluate the degree of influences of categories of temperature-dependent properties of concrete and steel on the computed structural response.
The numerical model has also been used to develop charts for estimating fire endurance of prestressed concrete beams.

8.2. Conclusions

Based on the structural response analyses performed, and the comparison made between numerical and test results, the following conclusions are reached regarding the numerical procedures developed together with the corresponding computer implementations:

1. The numerical model is capable of predicting deflection response of prestressed concrete members subjected to elevated temperatures. In accordance with results of fire tests utilized in the evaluations, the model is more accurate for predicting deflections of beams than of slabs.

2. The developed numerical method is also capable of predicting the history of the moment capacity of a prestressed concrete member throughout the fire exposure period. The estimation of the structural end point based on moment capacity ratio agrees well with results from other previously developed numerical approaches.

3. The computer implementation of the numerical procedures developed in this study provides means of evaluating the sensitivity of the computed structural response to influences of temperature on material properties.

Evaluation of the results obtained from using the current numerical procedures to determine degrees of influences of combinations of temperature dependent material properties leads to the following conclusions:

1. For normal weight concretes, temperature distribution is more sensitive to the influence of temperature on thermal capacity than on thermal conductivity. However, temperature distribution in lightweight concretes is highly sensitive to the influence of temperature on thermal conductivity.

2. The influence of temperature on the relaxation properties of prestressing steel have the highest effect on deflection, followed by the combined effect temperature on shrinkage properties of concrete, and thermal expansion properties of concrete and prestress steel.

3. Slight improvements in thermal qualities of concrete can result in significant improvement in the performance of prestressed concrete members at high temperatures.

8.3. Recommendations

In accordance with the conclusions reached above and the results presented, the following recommendations are given:

1. For enhancing the performance of prestressed concrete members in fire environment much effort should be devoted in improving the thermal properties of concrete.

2. More studies to be conducted in the area of bond slip and its effects on the performance of prestressed concrete members subjected to high temperatures.

REFERENCES

1. ASTM E 119-88, Standards in Building Codes, 27th Edition, Vol. II, Philadelphia, 1990, pp. 963-983.

2. Carlson C.C., and Tatman P.J., "The New Beam Furnace at PCA and Some Experiences Gained from its Use", Research Department, PCA, Bulletin 142, Skokie.

3. Gustaferro A.H. and Martin L.D., Design for Fire Resistance of Precast Prestressed Concrete, Prestressed Concrete Institute, Second Edition, Skokie, 1989.

4. Gustaferro A.H., "Design of Prestressed Concrete for Fire Resistance", PCI Journal, Vol.18, No.6, Nov-Dec 1973, pp. 941-967.

5. ACI Committee 216, "Guide for Determining the Fire Endurance of Concrete Elements", Concrete International, Vol.3, No.2, Febr. 1981, pp. 13-47.

6. Abrams M.S. and Cruz C.R., "The Behavior at High Temperature of Steel Strand for Prestressed Concrete", PCA Research Journal, Vol.3, No.3, Sept. 1961, pp. 8-18.

7. Malhorta H.L., "The Effects of Temperature on the Compressive Strength of Concrete", Magazine of Concrete Research, Vol.8, No.22., March 1956, pp. 85-94.

8. Day M.F., "Effects of Elevated Temperature on High-Tensile Steel Wires for Prestressed Concrete", Institution of Civil Engineers, Vol.16, May 1960, pp. 55-70.

9. Abrams M.S., "Compressive Strength of Concrete at Temperatures up to 1600 °F", Symposium on Effect of Temperature on Concrete, ACI Publication SP25, Detroit, Michigan, 1971, pp. 17-32.

10. Podolny W., "Understanding the Steel in Prestressing", PCI Journal, Vol.12., No.5, October 1967, pp. 55-67.

11. Carlson C.C., "Fire Endurance Testing Procedures", Symposium of Fire Resistance of Concrete, ACI Special Publication SP-5, Detroit, Michigan, 1979, pp 3-24.

12. Cruz C.R., "Elastic Properties of Concrete at High Temperatures", PCA Research Journal, Vol.8, No.1, January 1966, pp. 37-45.

13. Harada T., "Research on Fire Proof of Concrete and Reinforced Concrete Construction", Tokyo Institute of Technology, Tokyo, Japan, 1961.

14. Morley P.D., "Effects of Elevated Temperature on Bond in Reinforced Concrete", Ph.D. dissertation, University of Edinburgh, 1982.

15. Morley P.D and Royles R., "Response of Bond in Reinforced Concrete to High Temperatures", Magazine of Concrete Research, Vol.35, No.123, June 1983.

16. Diederichs U and Schneider U., Bond Strength at High Temperature", Magazine of Concrete Research, Vol.33, No.115, June 1981, pp. 75-84.

17. Zia, P; and Mostafa, F., "Development Length of Prestressing Strands", Journal of PCI, Vol.22, No.4, September-October 1977, pp. 54-65.

18. Janney, J.R., "Nature of Bond in Pre-Tensioned Prestressed Concrete", Journal of ACI, Vol.25, No.9, May 1954, pp. 717-736.

19. Fagundo E.F., and Richardson D., "Bond Slip of Epoxy-Coated Strands (EC) at Elevated Temperature", Department of Civil Engineering, University of Florida, March 1991, Unpublished Report.

20. Gustaferro A.H., "Fire Resistance of Post-Tensioned Structures", PCI Journal, Vol.18, No.2, March-April 1973, pp. 39-63.

21. Gustaferro A.H., "Fire Endurance of Simply Supported Prestressed Concrete Slabs", PCI Journal, Vol.12, No.1, February 1967, pp. 37-52.

22. Gustaferro A.H. and Carlson C.C., "Interpretation of Results of Fire Tests on Prestressed Concrete Building Components", PCI Journal, Vol.7, No.5, October 1962, pp. 15-43.

23. Petterson O., "Structural Fire Behavior-Development Trends", in Fire Safety Science, by Grant C.E. and Pagni P.J. (eds), Hemisphere Publishing Corporation, Washington, 1986, pp. 229-247.

24. Emerson M., "The Calculation of the Distribution of Temperature in Bridges", TRRL Report LR 561, Transport and Road Research Laboratory, Crowthrone, Berkshire, 1973.

25. Priestley M.J.N., "Temperature Gradients in Bridges-Some Design Considerations,' New Zealand Engineering, Vol.27, Part 7, July 1972, pp. 228-233.

26. Lanigan A.G., The Temperature Response of Concrete Box Girder Bridged", Ph.D. Dissertation, University of Auckland, 1973.

27. Inding R.J., Brestler B. and Nizamuddin Z., "FIRES-T3, A Computer Program for the Fire Response of Structures-Thermal", Report No. UCB FRG77-15, University of California, Berkeley, October 1977.

28. Jeanes D.C., "Developing Design Concepts for Structural Fire Endurance using Computer Models", in Design of Structures Against Fire, by Anchor R.D., Malhorta H.L. and Purkiss J.A, (eds), Elsevier Applied Science Publishers, London, 1986, pp. 127-153.

29. Anderberg Y., Forsen N.E. and Aasen B., "Measured and Predicted Behavior of Steel Beams and Columns in Fire", in Fire Safety Science, by Grant C.E. and Pagni P.J. (eds), Hemisphere Publishing Corporation, Washington, 1986, pp. 259-269.

30. Bresler B. and Iding R.H., "Effects of Fire Exposure on Structural Response and Fireproofing Requirements of Structural Steel Assemblies", in Fire Safety Science, by Grant C.E. and Pagni P.J. (eds), Hemisphere Publishing Corporation, Washington, 1986, pp. 206-222.

31. Nakamura K., Shinoda K., Hirota M. and Kawage K., "Structural Behavior of Steel frame in Building Fire", in Fire Safety Science, by Grant C.E. and Pagni P.J. (eds), Hemisphere Publishing Corporation, Washington, 1986, pp. 271-280.

32. Building Code Requirement for Reinforced Concrete, ACI 318-89, Section 8.5.1, ACI, Detroit, 1989.

33. Gustaferro A.H., "Design Implementation-Concrete Structures", in Design of Structures Against Fire, by Anchor R.D., Malhorta H.L. and Purkiss J.A, (eds), Elsevier Applied Science Publishers, London, 1986, pp. 189-211.

34. Lie T.T. and Lin T.D., "Fire Performance of Reinforced Concrete Columns", in Fire Safety-Science and Engineering, by Harmathy T.Z., (ed), ASTM, Philadelphia, 1985, pp. 176-205.

35. Wilson E.L., and Nickell R.E., "Application of the Finite Element Method to Heat Conduction", Nuclear Engineering and Design, Vol.4, 1966, pp. 276-286.

36. Wilson E.L., and Farhoomand I., "Nonlinear Heat Transfer Analysis of Axisymmetric Solids", Report No. UC SESM 71-6, Structural Engineering Laboratory, University of California, Berkeley, 1971.

37. Zienkiewicz O.C., The Finite Element Method in Structural and Continuum Mechanics, McGraw Hill Book Company, London, 1967.

38. Segerlind L.J., Applied Finite Element Analysis, John Wiley, New York, 1976.

39. Malhorta H.L., Design of Fire Resisting Structures, Surrey University Press, London, 1982.

40. Design Manual on the European Recommendations for the Fire Safety of Steel Structures, ECCS Technical Committee 3, Brussels, pp. 41-63.

41. Desai C.S., Elementary Finite Element Method, Englewood Cliffs, NJ, Printice Hall, 1979.

42. Rao S.S., The Finite Element Method in Engineering, Pergamon Press, New York, 1988.

43. Kleiber M., and Czeslaw W., Nonlinear Mechanics of Structures, Kluwer Academic Publishers, Boston, 1991.

44. Zienkiewicz O.C., and Taylor R.L., The Finite Element Method, 4th Edition, Vol.1, McGraw Hill Book Company, London, 1989.

45. Abrams M.S., "Behavior of Iorganic Materials in Fire", in Design of Buildings for Fire Safety, Smith E.E. and Harmathy T.Z., (eds), ASTM, Philadelphia, 1978, pp. 14-78.

46. Schneider U., "Modeling of Concrete Behavior at High Temperatures", in Design of Structures Against Fire, Anchor R.D., Malhorta H.L., and Purkiss J.A., (eds), Elservier Applied Science Publishers, London, 1986, pp. 53-86.

47. Harmathy T.Z., "Thermal Properties of Concrete at Elevated Temperatures", Journal of Materials, Vol.5, No.1, 1970, pp. 47-74.

48. Zoldners N.G., "Thermal Properties of Concrete under Sustained Elevated Temperatures", Temperature and Concrete, ACI Special Publication, 1971, pp. 1-31.

49. Lie T.T., (ed), Structural Fire Protection, ASCE Committee on Fire Protection, ASCE, New York, N.Y., 1992, pp. 199-201.

50. Bardhan-Roy B.K., "Fire Resistance-Design and Detailing", in Handbook of Structural Concrete, by Kong F.K., Evans R.H., Cohen E. and Roll F., (eds), McGraw-Hill Book Company, New York, 1983, pp. 14.1-14.46.

51. Anderberg Y. and Thelandersson N., "Stress and Deformation Characteristics of Concrete at High temperatures", Division of Structural Mechanics and Concrete Construction, Bulletin 54, Lund Institute of Technology, Lund, 1976.

52. Bazant Z.P., Mathematical Model for Creep and Thermal Shrinkage of Concrete at High Temperature", Report No. 82-10/249m, The Technical Institute, Northwestern University, Evanston, 1982.

53. Yakovlev A.I., Bushev V.A., Pchelintsev V.A., and Fedorenko V.S., Fire Resistance of Buildings, National Leading Library for Science and Technology, Boston Spa, England, 1966.

54. Harmathy T.Z. and Stanzak W.W., "Elevated-Temperature Tensile and Creep Properties of some Structural and Prestressing Steels", American Society for Testing and Materials, Special Technical Publication 464, pp. 186-208.

55. Franklin H.A., "Nonlinear Analysis of Reinforced Concrete Frames Panels", Ph.D. dissertation, University of California, Berkeley, 1970.

56. William Weaver, Jr., and Pau R. Johnston, Finite Elements for Structural Analysis, Prentice-Hall, Inc., Englewood Cliffs, New Jersey, 1984.

57. PCI Design Hand Book, Precast and Prestressed Concrete, 3rd Edition, PCI, Chicago, 1985, p. 9-44.

58. ANSYS Program, Swanson Analysis System, Inc., Johnson Road, Houston, Texas, USA.

APPENDIX A
INSTRUCTIONS FOR THE PREPARATION OF THE INPUT DATA FILE FOR THE PRECET PROGRAM

INTRODUCTION

This document presents the information required to create an input file for the program PRECET. The document is arranged into sections, which form the data categories of the input file. The input data consists of information for both the thermal and the structure model.

Due to symmetry, only half of the cross-section is considered in the thermal model. The section is modeled using only triangular elements. Each element must have one side (base) parallel to the x-axis. Elements are numbered in counter-clock-wise direction in the i-j-k sequence.

The structure is modeled using two dimensional beam elements. The uniform distributed loads (element loads) are defined positive when their direction is towards the positive y-axis.

In entering model data, two back-slash symbols, '\\', have to be used to indicate continuation of data covering more than one line. Total number of characters no to exceed 160.

SECTION ONE: PROBLEM DEFINITIONS

Line #1: Problem Heading

PROBLEMHEADING

Line #2: Temperature dependence control data

NR1,NR2,NR3,NR4,NR5,NR6,NR7,NR8,NR9,NR10,NR11,NR12

where the entries have value either 1 or 0 in which

NRI = 0 means property not temperature dependence, for I = 1 to 10; thermal analysis only, for I = 11; and moment capacity analysis only, for I = 12.

= 1 means property is temperature dependence, for I = 1 to 10; thermal and moment capacity analysis, for I = 11;

and complete analysis, for I = 12.

The properties in considerations are

NR1 = thermal conductivity of concrete
NR2 = thermal capacity of concrete
NR3 = stress-strain relation for concrete
NR4 = stress-strain relation for prestressing steel
NR5 = strength of concrete (compressive and tensile)
NR6 = tensile strength of concrete
NR7 = thermal strain of concrete
NR8 = thermal strain of prestressing steel
NR9 = shrinkage strain
NR10 = relaxation of prestressing steel

SECTION TWO: ITERATION CONTROLS

Line #1: Convergence control header

CONVERGENCE

Line #2: Convergence criteria

NR1,NR2,RD3,RD4,RD5,RD6,RD7

where,

NR1 = maximum number of iterations in thermal analysis
NR2 = maximum number of iterations in response analysis
RD3 = allowed error in nodal temperatures
RD4 = allowed error in radiation coefficient
RD5 = allowed error in nodal forces
RD6 = allowed error in nodal displacement
RD7 = critical deflection

SECTION THREE: MATERIAL PROPERTIES

Line #1: Material control header

MATERIALS

Line #2: Property data

NR1,NR2,RD3,RD4,RD5,RD6

where,

NR1 = concrete type with entries either 1, 2, or 3, in which 1 is normal weight concrete (carbonate aggr.), 2 is normal weight concrete (silicon aggr.), and 3 is lightweight concrete
NR2 = number of different categories of steel tendons
RD3 = capacity reduction factor
RD4 = specified compressive strength of concrete (psi)
RD5 = emissivity
RD6 = convection heat transfer coefficient (btu/in2.min.F). If RD5, RD6 = 0, default values will be used.

SECTION FOUR: BEGINNING OF THERMAL MODEL DATA

Line #1: Thermal control separator

THERMAL

Line #2: Control data for thermal model

NR1,NR2,NR3,NR4,NR5,NR6,NR7,NR8

where,

NR1 = number of nodes for the thermal model
NR2 = number of time steps
NR3 = number of sides exposed to fire
NR4 = number of elements of the thermal model
NR5 = mode of conductivity data input
NR6 = mode of thermal capacity data input
NR7 = number of points defining conductivity data
NR8 = number of points defining capacity data
NRI = 0 default values used,
= 1 user input data, for I = 5 and 6.

SECTION FIVE: NODAL COORDINATES FOR THERMAL MODEL

Line #1: Node control header

NODES

Subsequent lines: nodal coordinates

NI X=XI Y=YI G=N1,N2,N3

where,

NI = node number
XI = x- coordinate for node NI
YI = y- coordinate for node NI
G = initiates the generation sequence
N1 = first node in the generation sequence
N2 = last node in the generation sequence
N3 = node increment number (default is 1)

NOTE: * coordinates of nodes N1 and N2 must have been defined
* G is omitted if no generation
* this section must end with a blank line

SECTION SIX: TIME-TEMPERATURE RELATIONSHIP

Line #1: Heading separator

TIMESTEPS

Subsequent lines (NR2 in Sect. Four): Time-temp data

NR1,RD2,RD3

where,

NR1 = time step number
RD2 = time (minutes)
RD3 = temperature (degr. F)

SECTION SEVEN: USER INPUT CONDUCTIVITY DATA (omit this section if NR5 = 0 in Section four

Line #1: Control header

CONDUCTIVITY

Subsequent lines (NR7 in Section Four)

RD1,RD2

where,

RD1 = temperature value
RD2 = conductivity value

SECTION EIGHT: USER INPUT CAPACITY DATA (omit this section if NR6 = 0 in Section four

Line #1: Control header

CAPACITY

Subsequent lines (NR8 in Section Four)

RD1,RD2

where,

RD1 = temperature value
RD2 = thermal capacity value

SECTION NINE: BOUNDARY (EXPOSED) SURFACES DEFINITION

Line #1: Surface control header

SURFACE

Subsequent lines (NR3 in Sect. Four): Exposed surface data

NR1,NR2,NR3

where,

NR1 = side number
NR2 = node I of side NR1
NR3 = node J of side NR1

SECTION TEN: ELEMENT INFORMATION

Line #1: Element header separator

ELEMENT

Subsequent lines (NR4 in Sect. Four): Element description data

NR1,NR2,NR3,NR4,NR5,NR6

where,

NR1 = element number
NR2 = node I of element NR1
NR3 = node J
NR4 = node K
NR5 = number of element sides exposed to fire
NR6 = number of the side parallel to x-axis, where
1 is for side bound by nodes I-J
2 is for side bound by nodes J-K
3 is for side bound by nodes K-I

NOTE: IF ONLY THERMAL ANALYSIS IS REQUIRED, (i.e. NR11=0 IN SECT. ONE), THE INPUT DATA FILE MAY ENDS HERE.

SECTION ELEVEN: BEGIN OF STRUCTURE MODEL DATA

Line #1: Control heading separator

STRUCTURE

Line #2: Control data

NR1,NR2,NR3

where,

NR1 = number of nodes for the structure model
NR2 = number of beam elements
NR3 = number of steel tendons

SECTION TWELVE: NODE INFORMATION

Line #1: Coordinate separator

COORDINATES

Subsequent lines: nodal coordinates data

NI X=XI Y=YI Z=ZI G=N1,N2,N3

where the terms are as defined in Section Five above

NOTE: * This section must end with a blank line

SECTION THIRTEEN: BOUNDARY CONDITIONS

Line #1: Boundary control header

BOUNDARY

Subsequent lines: Node boundary conditions

N1,N2,N3 DOF=FDX,FDY,FDZ,FRX,FRY,FRZ

where,

N1 = first node in the generation sequence
N2 = last node in the generation sequence
N3 = nodal increment number (default is 1)
FD's, FR's represent the boundary condition status for the three nodal translations and rotations respectively. Each entry takes the symbol either F or R, in which,
R = free translation/ rotation condition
F = fixed condition

NOTE: * If no node generation, N2 and N3 are omitted
* This section must end with a blank line

SECTION FOURTEEN: BEAM ELEMENT DATA

Line #1: Heading separator

BEAM

Subsequent lines (NR2 in Sect. Eleven): Element definition

NR1,NR2,NR3 W=BY I=HI,BI J=HJ,BJ

where,

NR1 = beam element number
NR2 = node I of beam NR1
NR3 = node J of beam NR1
BY = element load (uniformly distributed in lb/in) in the positive y-direction
HX = overall height of section at end X (in.)
BX = width of compression zone at end X (in.) of beam element NR1

SECTION FIFTEEN: INFORMATION FOR PRESTRESSING STEEL

Line #1: Steel control header

STEEL

Subsequent lines (NR3 in Sect. Nine): Steel property data

NR1 A=APS S=FPU P=PE

where,

NR1 = steel property type number
APS = area of steel tendon type NR1
FPU = ultimate tensile strength of steel
PE = effective prestressing force (after loses)

Subsequent lines (NR2*NR3 in Sect. Nine): Segment definition

NR1,NR2,NR3,RD4,RD5 M=MI

where,

NR1 = beam element number containing the steel segment

NR2 = steel segment number in element NR1
NR3 = subelement number defining steel temperature
RD4 = y-eccentricity of end I of the steel segment
RD5 = y-eccentricity of end J of segment NR2
MI = material property number of steel segment NR2

SECTION SIXTEEN: EXTERNAL CONCENTRATED LOADS

Line #1: Loads control header

LOADS

Subsequent lines: Nodal load data

N1,N2,N3 L=LC F=FX,FY,FZ,FXX,FYY,FZZ

where,

N1, N2, N3 bare the same definitions as in Sect. Eleven
LC = load case number
FX = nodal load in x-direction
FY = nodal load in y-direction
FZ = nodal load in z-direction
FXX = moment about x-axis
FYY = moment about y-axis
FZZ = moment about z-axis

NOTE: * If no concentrated loads, this section can be omitted
* This section must end with a blank line.

** END **

APPENDIX B
EXAMPLE OF INPUT DATA FILE

```
NWBEAM3
1,1,1,1,1,1,1,1,1,1,1,1

C:allowable errors

CONVERGENCE
20,20,0.05,0.005,0.01,0.01,20

C:material input data

MATERIALS
2,2,1.0,5000,0.5,5.09E-04

C:input data for thermal model

THERMAL MODEL CONTROL DATA
116,43,28,176,1,1,4,9

C:node coords for thermal model

NODES
1   X=0     Y=0
7   X=6                 G=1,7
8   X=6.75
9   X=0     Y=0.5
15  X=6                 G=9,15
16  X=6.75
17  X=0     Y=1.5
23  X=6                 G=17,23
24  X=6.75
25  X=0     Y=2.5
31  X=6                 G=25,31
32  X=6.75
33  X=0     Y=3.5
39  X=6                 G=33,39
40  X=6.75
41  X=0     Y=4.25
47  X=6                 G=41,47
48  X=0     Y=5.25
53  X=5                 G=48,53
54  X=0     Y=6.25
58  X=4                 G=54,58
```

```
59  X=0     Y=7.25
62  X=3                 G=59,62
63  X=0     Y=8.25
78          Y=13.25     G=63,78,3
64  X=1     Y=8.25
79          Y=13.25     G=64,79,3
65  X=2     Y=8.25
80          Y=13.25     G=65,80,3
81  X=0     Y=14
83  X=2                 G=81,83
84  X=0     Y=15
87  X=3                 G=84,87
88  X=0     Y=16
92  X=4                 G=88,92
93  X=0     Y=17
98  X=5                 G=93,98
99  X=0     Y=18
104 X=5                 G=99,104
105 X=0     Y=19
110 X=5                 G=105,110
111 X=0     Y=20
116 X=5                 G=111,116

C:time temperature data

TIMESTEP  TEMPERATURE DATA
1,0,68
2,5,1000
3,10,1300
4,15,1399
5,20,1462
6,25,1510
7,30,1550
8,35,1584
9,40,1613
10,45,1638
11,50,1661
12,55,1681
13,60,1700
14,65,1718
15,70,1735
16,75,1750
17,80,1765
18,85,1779
19,90,1792
20,95,1804
21,100,1815
22,105,1826
23,110,1835
24,115,1843
25,120,1850
26,130,1862
```

```
27,140,1875
28,150,1888
29,160,1900
30,170,1912
31,180,1925
32,190,1938
33,200,1950
34,210,1962
35,220,1975
36,230,1988
37,240,2000
38,250,2012
39,260,2025
40,270,2038
41,280,2050
42,290,2062
43,300,2075

C:user input thermal conductivity data

CONDUCTIVITY
68,0.001193
560,0.001057
1112,0.000904
1470,0.000804

C:user input theraml capacity data

CAPACITY
68,0.015534
390,0.023349
752,0.023304
770,0.024424
788,0.025546
815,0.027229
833,0.028351
932,0.034522
1112,0.023303

C:boundary surface data

SURFACE
1,1,2
2,2,3
3,3,4
4,4,5
5,5,6
6,6,7
7,7,8
8,8,16
9,16,24
10,24,32
```

```
11,32,40
12,40,47
13,47,53
14,53,58
15,58,62
16,62,65
17,65,68
18,68,71
19,71,74
20,74,77
21,77,80
22,80,83
23,83,87
24,87,92
25,92,98
26,98,104
27,104,110
28,110,116

C:element information

ELEMENTS
1,1,2,9,1,1
2,2,10,9,0,2
3,2,3,10,1,1
4,3,11,10,0,2
5,3,4,11,1,1
6,4,12,11,0,2
7,4,5,12,1,1
8,5,13,12,0,2
9,5,6,13,1,1
10,6,14,13,0,2
11,6,7,14,1,1
12,7,15,14,0,2
13,7,8,15,1,1
14,8,16,15,1,2
15,9,10,17,0,1
16,10,18,17,0,2
17,10,11,18,0,1
18,11,19,18,0,2
19,11,12,19,0,1
20,12,20,19,0,2
21,12,13,20,0,1
22,13,21,20,0,2
23,13,14,21,0,1
24,14,22,21,0,2
25,14,15,22,0,1
26,15,23,22,0,2
27,15,16,23,0,1
28,16,24,23,1,2
29,17,18,25,0,1
30,18,26,25,0,2
```

```
31,18,19,26,0,1
32,19,27,26,0,2
33,19,20,27,0,1
34,20,28,27,0,2
35,20,21,28,0,1
36,21,29,28,0,2
37,21,22,29,0,1
38,22,30,29,0,2
39,22,23,30,0,1
40,23,31,30,0,2
41,23,24,31,0,1
42,24,32,31,1,2
43,25,26,33,0,1
44,26,34,33,0,2
45,26,27,34,0,1
46,27,35,34,0,2
47,27,28,35,0,1
48,28,36,35,0,2
49,28,29,36,0,1
50,29,37,36,0,2
51,29,30,37,0,1
52,30,38,37,0,2
53,30,31,38,0,1
54,31,39,38,0,2
55,31,32,39,0,1
56,32,40,39,1,2
57,33,34,41,0,1
58,34,42,41,0,2
59,34,35,42,0,1
60,35,43,44,0,2
61,35,36,43,0,1
62,36,44,43,0,2
63,36,37,44,0,1
64,37,45,44,0,2
65,37,38,45,0,1
66,38,46,45,0,2
67,38,39,46,0,1
68,39,47,46,0,2
69,40,47,39,1,3
70,41,42,48,0,1
71,42,49,48,0,2
72,42,43,49,0,1
73,43,50,49,0,2
74,43,44,50,0,1
75,44,51,50,0,2
76,44,45,51,0,1
77,45,52,51,0,2
78,45,46,52,0,1
79,46,53,52,0,2
80,47,53,46,1,3
81,48,49,54,0,1
82,49,55,54,0,2
```

```
83,49,50,55,0,1
84,50,56,55,0,2
85,50,51,56,0,1
86,51,57,56,0,2
87,51,52,57,0,1
88,52,58,57,0,2
89,53,58,52,1,3
90,54,55,59,0,1
91,55,60,59,0,2
92,55,56,60,0,1
93,56,61,60,0,2
94,56,57,61,0,1
95,57,62,61,0,2
96,58,62,57,1,3
97,59,60,63,0,1
98,60,64,63,0,2
99,60,61,64,0,1
100,61,65,64,0,2
101,62,65,61,1,3
102,63,64,66,0,1
103,64,67,66,0,2
104,64,65,67,0,1
105,65,68,67,1,2
106,66,67,69,0,1
107,67,70,69,0,2
108,67,68,70,0,1
109,68,71,70,1,2
110,69,70,72,0,1
111,70,73,72,0,2
112,70,71,73,0,1
113,71,74,73,1,2
114,72,73,75,0,1
115,73,76,75,0,2
116,73,74,76,0,1
117,74,77,76,1,2
118,75,76,78,0,1
119,76,79,78,0,2
120,76,77,79,0,1
121,77,80,79,1,2
122,78,79,81,0,1
123,79,82,81,0,2
124,79,80,82,0,1
125,80,83,82,1,2
126,81,85,84,0,2
127,81,82,85,0,1
128,82,86,85,0,2
129,82,83,86,0,1
130,83,87,86,1,2
131,84,89,88,0,2
132,84,85,89,0,1
133,85,90,89,0,2
134,85,86,90,0,1
```

```
135,86,91,90,0,2
136,86,87,91,0,1
137,87,92,91,1,2
138,88,94,93,0,2
139,88,89,94,0,1
140,89,95,94,0,2
141,89,90,95,0,1
142,90,96,95,0,2
143,90,91,96,0,1
144,91,97,96,0,2
145,91,92,97,0,1
146,92,98,97,1,2
147,93,100,99,0,2
148,93,94,100,0,1
149,94,101,100,0,2
150,94,95,101,0,1
151,95,102,101,0,2
152,95,96,102,0,1
153,96,103,102,0,2
154,96,97,103,0,1
155,97,104,103,0,2
156,98,104,97,1,3
157,99,106,105,0,2
158,99,100,106,0,1
159,100,107,106,0,2
160,100,101,107,0,1
161,101,108,107,0,2
162,101,102,108,0,1
163,102,109,108,0,2
164,102,103,109,0,1
165,103,110,109,0,2
166,104,110,103,1,3
167,105,112,111,0,2
168,105,106,112,0,1
169,106,113,112,0,2
170,106,107,113,0,1
171,107,114,113,0,2
172,107,108,114,0,1
173,108,115,114,0,2
174,108,109,115,0,1
175,109,116,115,0,2
176,110,116,109,1,3

C:input data for structure model

STRUCTURE
12,11,5

C:node coords for structure model

COORDINATES
1    X=0 Y=0 Z=0
```

```
12  X=11*12          G=1,12

C:node boundary conditions

BOUNDARY
1       DOF=F,R,F,F,F,F
2,10    DOF=R,R,F,F,F,R
11      DOF=R,F,F,F,F,R
12      DOF=R,R,F,F,F,R

C:beam element information

BEAM
1,1,2       W=-14.926     I=20.0,10.0  J=20.0,10.0
2,2,3       W=-14.926     I=20.0,10.0  J=20.0,10.0
3,3,4       W=-14.926     I=20.0,10.0  J=20.0,10.0
4,4,5       W=-14.926     I=20.0,10.0  J=20.0,10.0
5,5,6       W=-14.926     I=20.0,10.0  J=20.0,10.0
6,6,7       W=-14.926     I=20.0,10.0  J=20.0,10.0
7,7,8       W=-14.926     I=20.0,10.0  J=20.0,10.0
8,8,9       W=-14.926     I=20.0,10.0  J=20.0,10.0
9,9,10      W=-14.926     I=20.0,10.0  J=20.0,10.0
10,10,11    W=-14.926     I=20.0,10.0  J=20.0,10.0
11,11,12    W=-14.926     I=20.0,10.0  J=20.0,10.0

C:prestressing steel information

STEEL
1 A=0.080  S=250000  P=11480
2 A=0.0302  S=250000  P=4305
1,1,50,3.27,3.27       M=1
1,2,81,5.74,5.74       M=1
1,3,50,3.27,3.27       M=1
1,4,44,3.27,3.27       M=1
1,5,70,4.55,4.55       M=2
2,1,50,3.27,3.27       M=1
2,2,81,5.74,5.74       M=1
2,3,50,3.27,3.27       M=1
2,4,44,3.27,3.27       M=1
2,5,70,4.55,4.55       M=2
3,1,50,3.27,3.27       M=1
3,2,81,5.74,5.74       M=1
3,3,50,3.27,3.27       M=1
3,4,44,3.27,3.27       M=1
3,5,70,4.55,4.55       M=2
4,1,50,3.27,3.27       M=1
4,2,81,5.74,5.74       M=1
4,3,50,3.27,3.27       M=1
4,4,44,3.27,3.27       M=1
4,5,70,4.55,4.55       M=2
5,1,50,3.27,3.27       M=1
5,2,81,5.74,5.74       M=1
```

```
5,3,50,3.27,3.27       M=1
5,4,44,3.27,3.27       M=1
5,5,70,4.55,4.55       M=2
6,1,50,3.27,3.27       M=1
6,2,81,5.74,5.74       M=1
6,3,50,3.27,3.27       M=1
6,4,44,3.27,3.27       M=1
6,5,70,4.55,4.55       M=2
7,1,50,3.27,3.27       M=1
7,2,81,5.74,5.74       M=1
7,3,50,3.27,3.27       M=1
7,4,44,3.27,3.27       M=1
7,5,70,4.55,4.55       M=2
8,1,50,3.27,3.27       M=1
8,2,81,5.74,5.74       M=1
8,3,50,3.27,3.27       M=1
8,4,44,3.27,3.27       M=1
8,5,70,4.55,4.55       M=2
9,1,50,3.27,3.27       M=1
9,2,81,5.74,5.74       M=1
9,3,50,3.27,3.27       M=1
9,4,44,3.27,3.27       M=1
9,5,70,4.55,4.55       M=2
10,1,50,3.27,3.27       M=1
10,2,81,5.74,5.74       M=1
10,3,50,3.27,3.27       M=1
10,4,44,3.27,3.27       M=1
10,5,70,4.55,4.55       M=2
11,1,50,3.27,3.27       M=1
11,2,81,5.74,5.74       M=1
11,3,50,3.27,3.27       M=1
11,4,44,3.27,3.27       M=1
11,5,70,4.55,4.55       M=2

C:external point loads

LOADS
1  L=1  F=0.0,-1250.0,0,0,0,0
5       F=0.0,-2500.0,0,0,0,0
9       F=0.0,-2500.0,0,0,0,0

C:end of input data file
```

BIOGRAPHICAL SKETCH

The author, Mr. William J. Mbwambo, was born in the Republic of Tanzania in November 1956. He received his Bachelor of Science degree in civil engineering from the University of Dar es Salaam, Tanzania, in 1984. In 1987 he graduated from the same university with master's degree in building technology. He joined the University of Florida in Fall 1988 to pursue doctorate studies in civil engineering. He expects to graduate in Spring 1995.

I certify that I have read this study and that in my opinion it conforms to acceptable standards of scholarly presentation and is fully adequate, in scope and quality, as a dissertation for the degree of Doctor of Philosophy.

Fernando E. Fagundo, Chair
Professor of Civil
Engineering

I certify that I have read this study and that in my opinion it conforms to acceptable standards of scholarly presentation and is fully adequate, in scope and quality, as a dissertation for the degree of Doctor of Philosophy.

Ronald A. Cook, Cochair
Associate Professor of
Civil Engineering

I certify that I have read this study and that in my opinion it conforms to acceptable standards of scholarly presentation and is fully adequate, in scope and quality, as a dissertation for the degree of Doctor of Philosophy.

Marc I. Hoit
Associate Professor of
Civil Engineering

I certify that I have read this study and that in my opinion it conforms to acceptable standards of scholarly presentation and is fully adequate, in scope and quality, as a dissertation for the degree of Doctor of Philosophy.

Mang Tia
Professor of Civil
Engineering

I certify that I have read this study and that in my opinion it conforms to acceptable standards of scholarly presentation and is fully adequate, in scope and quality, as a dissertation for the degree of Doctor of Philosophy.

Weilin P. Chang
Professor of Building Construction

This dissertation was submitted to the Graduate Faculty of the College of Engineering and to the Graduate School and was accepted as partial fulfillment of the requirements for the degree of Doctor of Philosophy.

May 1995

for Dean, College of Engineering

Dean, Graduate School

LD
1780
1995
.M478

UNIVERSITY OF FLORIDA
3 1262 08553 7198